

University of Windsor

## Scholarship at UWindor

---

Electronic Theses and Dissertations

Theses, Dissertations, and Major Papers

---

8-1-2021

# Design and Investigation of a Semi-Active Suspension System in Automotive Applications

Behnam Riazi

Follow this and additional works at: <https://scholar.uwindsor.ca/etd>

---

### Recommended Citation

Riazi, Behnam, "Design and Investigation of a Semi-Active Suspension System in Automotive Applications" (2021). *Electronic Theses and Dissertations*. 8683.

<https://scholar.uwindsor.ca/etd/8683>

This online database contains the full-text of PhD dissertations and Masters' theses of University of Windsor students from 1954 forward. These documents are made available for personal study and research purposes only, in accordance with the Canadian Copyright Act and the Creative Commons license—CC BY-NC-ND (Attribution, Non-Commercial, No Derivative Works). Under this license, works must always be attributed to the copyright holder (original author), cannot be used for any commercial purposes, and may not be altered. Any other use would require the permission of the copyright holder. Students may inquire about withdrawing their dissertation and/or thesis from this database. For additional inquiries, please contact the repository administrator via email ([scholarship@uwindsor.ca](mailto:scholarship@uwindsor.ca)) or by telephone at 519-253-3000ext. 3208.

**Design and Investigation of a Semi-Active Suspension System in Automotive  
Applications**

By

**Behnam Riazi**

A Thesis

Submitted to the Faculty of Graduate Studies

through the Department of Mechanical, Automotive, and Materials Engineering

in Partial Fulfillment of the Requirements for

the Degree of Master of Applied Science

at the University of Windsor

Windsor, Ontario, Canada

2021

© 2021 Behnam Riazi

**Design and Investigation of a Semi-Active Suspension System in Automotive  
Applications**

By

**Behnam Riazi**

APPROVED BY:

---

A. Ahmadi

Department of Electrical and Computer Engineering

---

C. Novak

Department of Mechanical, Automotive & Materials Engineering

---

E. Lang, Co-Advisor

Department of Mechanical, Automotive & Materials Engineering

---

L. Oriet, Co-Advisor

Department of Mechanical, Automotive & Materials Engineering

July 5, 2021

## DECLARATION OF ORIGINALITY

I hereby certify that I am the sole author of this thesis and that no part of this thesis has been published or submitted for publication.

I certify that, to the best of my knowledge, my thesis does not infringe upon anyone's copyright nor violate any proprietary rights and that any ideas, techniques, quotations, or any other material from the work of other people included in my thesis, published or otherwise, are fully acknowledged in accordance with the standard referencing practices. Furthermore, to the extent that I have included copyrighted material that surpasses the bounds of fair dealing within the meaning of the *Canadian Copyright Act*, I certify that I have obtained a written permission from the copyright owner(s) to include such material(s) in my thesis and have included copies of such copyright clearances to my appendix.

I declare that this is a true copy of my thesis, including any final revisions, as approved by my thesis committee and the Graduate Studies office and that this thesis has not been submitted for a higher degree to any other University or Institution.

## ABSTRACT

Modern vehicles are equipped with numerous sensors and systems intended to improve performance and ride quality. Suspension systems in vehicles are essential links between the vehicle body and the pavement, and they play a large role in determining ride comfort and handling stability. This is in fact no easy task since these two goals are in conflict. While active suspension systems could help to solve this trade-off, disadvantages such as high costs and high power consumption prevent their widespread adoption in the automotive industry.

On the other hand, a semi-active suspension system can provide desirable performance while providing a more cost-effective solution than a fully active suspension system. Research in this thesis will be conducted on semi-active systems using the MR damper. MR dampers are modelled in MATLAB/Simulink and then their viscoelasticity characteristics are investigated. A quarter-car model is designed in state-space and modelled in MATLAB/Simulink. Two control systems are proposed for a semi-active suspension system using Linear Quadratic Regulator and Fuzzy Logic Controller. Modelled systems are analyzed for four road profiles, including road type C according to international standards ISO/TC108/SC2N67 and the control system's effectiveness will be evaluated by analyzing the RMS values of vertical body acceleration and tire deflection. Results of simulation show that the designed semi-active suspension system can improve vehicle performance regarding both ride comfort and handling stability.

For the following, an additional suspension mechanism has been considered for the seats of vehicles. This suspension system is modelled, which is three degrees of freedom with six state variables in state-space form, and its behaviour is analyzed by using MATLAB/Simulink. It is shown that an additional suspension system can improve the ride quality significantly.

## **ACKNOWLEDGEMENTS**

I would like to express my sincere gratitude towards my research advisor, Dr. Leo Oriet, and Co-advisor, Dr. Edward Lang, for their unyielding guidance, immense knowledge, and support towards the completion of my thesis. I am gratefully indebted towards my parents, and family for their precious support and help throughout my research work. My sincere thanks go to my beloved wife, Sahar, who has always been by my side throughout my studies and life, encouraging me to aim higher and try harder. Without her continuous moral support and love, this would not have been such an amazing journey.

# TABLE OF CONTENTS

<b>DECLARATION OF ORIGINALITY</b> .....	<b>iii</b>
<b>ABSTRACT</b> .....	<b>iv</b>
<b>ACKNOWLEDGEMENT</b> .....	<b>v</b>
<b>LIST OF TABLES</b> .....	<b>viii</b>
<b>LIST OF FIGURES</b> .....	<b>ix</b>
<b>LIST OF ABBREVIATIONS/SYMBOLS</b> .....	<b>xii</b>
<b>CHAPTER 1 INTRODUCTION</b> .....	<b>1</b>
1.1 Background .....	1
1.2 Suspension System Overview.....	4
1.2.1 Passive Suspension System .....	4
1.2.2 Semi-Active Suspension System .....	5
1.2.3 Active Suspension System .....	6
1.3 Research Objectives .....	7
1.4 Thesis Overview .....	9
<b>CHAPTER 2 SEMI-ACTIVE SUSPENSION SYSTEM COMPONENTS</b> .....	<b>10</b>
2.1 Adjustable Dampers .....	10
2.1.1 MR fluids.....	10
2.1.2 MR Dampers .....	15
2.2 Springs .....	18
2.3 Control System .....	23
<b>CHAPTER 3 MATHEMATICAL MODELING OF MR DAMPERS</b> .....	<b>27</b>
3.1 Modeling of MR Fluid Dampers.....	27
3.2 Bouc-Wen Model.....	32
3.3 Modified Bouc-wen: .....	39
3.4 Invers Model of MR Dampers .....	49
<b>CHAPTER 4 ROAD PROFILES</b> .....	<b>54</b>
4.1 Step Road Input .....	54

4.2 Sine Road Input .....	55
4.3 Bump Input.....	56
4.4 Road Type C Input.....	57
<b>CHAPTER 5 MATHEMATICAL MODELLING OF THE SUSPENSION SYSTEM.....</b>	<b>63</b>
5.1 Linearized Quarter Car Model.....	63
5.2 Control-oriented Model.....	68
5.3 State Space Model.....	69
5.4 Seat Suspension System .....	70
<b>CHAPTER 6 CONTROLLER DEVELOPMENT FOR A SEMI-ACTIVE SUSPENSION SYSTEM .....</b>	<b>74</b>
6.1 LQR Controller Design .....	74
6.2 Fuzzy Logic Controller Design.....	77
6.2.1 Fuzzification Module .....	78
6.2.2 Defuzzification Module.....	80
6.2.3 Fuzzy Rules Inference.....	84
6.3 Evaluation of Control Methods.....	86
<b>CHAPTER 7 RESULTS AND CONCLUSION .....</b>	<b>94</b>
7.1 Results:.....	94
7.2 Conclusion.....	99
7.3 Future Work.....	100
<b>REFERENCES .....</b>	<b>101</b>
<b>VITA AUCTORIS .....</b>	<b>102</b>



## LIST OF TABLES

Table 2.1: Properties of MR and ER Fluid [22] .....	15
Table 3.1: Values of parameters used in Bingham Model .....	29
Table 3.2: Values of parameters used in Bouc-Wen Model.....	33
Table 3.3: Value of Parameters used in Spencer Model .....	40
Table 4.1: Eight Degree of Road Roughness .....	62
Table 5.1: Parameters of Suspension System [57].....	65
Table 5.2: Significance of Each State Variable .....	69
Table 5.3: Parameters of Seat Suspension System [57]. .....	72
Table 5.4: Significance State Variable for Seat Suspension System .....	72
Table 6.1: FLC Rules for Calculating the Damping Force.....	85
Table 7.1: RMS Values of Sprung Mass Acceleration and Tire Deflection for Step Input .....	94
Table 7.2: RMS Values of Sprung Mass Acceleration and Tire Deflection for Bump Input.....	95
Table 7.3: RMS Values of Sprung Mass Acceleration and Tire Deflection for Sine Wave Input	95
Table 7.4: RMS Values of Sprung Mass Acceleration and Tire Deflection for Road Type C Input .....	96
Table 7.5: Effectiveness of FLC in Ride Quality .....	96
Table 7.6: RMS Values of the Vehicle's Seats Acceleration and Tire Deflection for Step Input .	97
Table 7.7: RMS Values of the Vehicle's Seats Acceleration and Tire Deflection for Bump Input .....	97
Table 7.8: RMS Values of the Vehicle's Seats Acceleration and Tire Deflection for Sine Wave Input.....	98
Table 7.9: RMS Values of the Vehicle's Seats Acceleration and Tire Deflection for Road Type C Input.....	98
Table 7.10: Effectiveness of FLC with an Additional Suspension System for Seats .....	99

## LIST OF FIGURES

Figure 1.1: Horse Carriage Suspension System [2] .....	1
Figure 1.2: Classical scheme of a wheel-to-chassis suspension in a car [3].....	2
Figure 1.3: Velocity-Force Characteristics of Various Suspension Designs [7] .....	4
Figure 2.1: Activation of MR Fluid [23].....	11
Figure 2.2: Basic operating modes for controllable fluid devices [25].....	12
Figure 2.3: MRF-140BC Magneto-Rheological Fluid Description [26].....	13
Figure 2.4: MRF-140BC Magneto-Rheological Fluid Yield Stress Diagram [26].....	13
Figure 2.5: Cross-section of typical MR fluid damper [26] .....	16
Figure 2.6: Mono-Tube MR Damper [30].....	17
Figure 2.7: Schematic Configuration of the Twin Tube MR Damper Without Accumulator [31]	17
Figure 2.8: Schematic illustration of the Twin Tube MR Damper with Accumulator [32] .....	18
Figure 2.9: Example of a Leaf Spring.....	19
Figure 2.10: Example of a Torsion Bar.....	19
Figure 2.11: Example of a Coil Spring .....	20
Figure 2.12: Schematic representation of a Gas Spring Implemented With Pneumatic Spring [3] .....	21
Figure 2.13: Schematic representation of a gas spring Implemented with Hydro-Pneumatic Spring [3].....	21
Figure 2.14: Schematic Representation of Skyhook Theory (a) and Groundhook Theory (b) [35] .....	24
Figure 3.1: Bingham Model [25] .....	27
Figure 3.2: Bouc-Wen Model [25].....	28
Figure 3.3: Modified Bouc-Wen, Spencer Model [25] .....	28
Figure 3.4: Simulation of the Bingham model in MATLAB/Simulink .....	30
Figure 3.5: Displacement-Force diagram obtained from Bingham Model .....	31

Figure 3.6: Velocity-Force diagram obtained from Bingham Model .....	31
Figure 3.7: Simulink Subsystem for Generating Z1 Based on Equation (3.6) .....	34
Figure 3.8: Simulink Subsystem for Generating Z2 Based on Equation (3.7) .....	35
Figure 3.9: Simulink Subsystem for Generating Z3 Based on Equation (3.8) .....	35
Figure 3.10: Simulink Subsystem for Generating Z Based on Equation (3.5) .....	36
Figure 3.11: Simulink Subsystem for Generating F1 Based on Equation (3.10).....	37
Figure 3.12: Simulink Subsystem for Generating F2 Based on Equation (3.11).....	37
Figure 3.13: Simulink Subsystem for Generating F3 Based on Equation (3.12).....	37
Figure 3.14: Simulation of the Bouc-Wen Model in MATLAB/Simulink .....	38
<i>Figure 3.15: Displacement-Force diagram obtained from Bouc-Wen Model .....</i>	<i>38</i>
Figure 3.16: Velocity-Force diagram obtained from Bingham Model.....	39
Figure 3.17: Simulink Subsystem for Generating C0 Based on Equation (3.18) .....	41
Figure 3.18: Simulink Subsystem for Generating $\alpha$ Based on Equation (3.16) .....	41
Figure 3.19: Simulink Subsystem for Generating C <sub>1</sub> Based on Equation (3.17).....	41
Figure 3.20: Simulink Subsystem for Generating u Based on Equation (3.19).....	42
Figure 3.21: Simulink Subsystem for Generating Z1 Based on Equation (3.21) .....	43
Figure 3.22: Simulink Subsystem for Generating Z2 Based on Equation (3.22) .....	43
Figure 3.23: Simulink Subsystem for Generating Z3 Based on Equation (3.23) .....	44
Figure 3.24: Simulink Subsystem for Generating Z Based on Equation (3.14) .....	44
Figure 3.25: Simulink Subsystem for Generating $y_b$ Based on Equation (3.15) .....	45
Figure 3.26: Simulink Subsystem for Generating the Final $y_b$ and C <sub>1</sub> Based on Equations (3.15) and (3.17) .....	46
Figure 3.27: Simulation of the Modified Bouc-Wen, Spencer Model, in MATLAB/Simulink ....	47
Figure 3.28: Displacement-Force diagram obtained from Modified Bouc-Wen, Spencer Model.	48
Figure 3.29: Velocity-Force diagram obtained from Modified Bouc-Wen, Spencer Model.....	48

Figure 3.30: Displacement-Force and Velocity-Force Diagrams Obtained From Experimental Data [49].....	49
Figure 3.31: Semi-Active Control System for a Vehicle Suspension Integrated With MR Dampers .....	50
Figure 3.32: Dissipative Domain, Graphical Illustration [3].....	51
Figure 3.33: Dissipative Domain, MATLAB Code.....	52
Figure 4.1: Simulink Block to generate Step input.....	54
Figure 4.2: Step Road Input for Plant Model Simulation.....	55
Figure 4.3: Sine Road Input for the Plant Model Simulation and Used Simulink Blocks .....	56
Figure 4.4: Bump Input for the Plant Model Simulation and Used Simulink Blocks.....	57
Figure 4.5: White noise input signal .....	58
Figure 4.6: Simulink Block to generate Step input.....	61
Figure 4.7: Road type c input for the plant model simulation .....	61
Figure 5.1: Quarter-car Representation of a Suspension System in a Vehicle [3].....	63
Figure 5.2: Quarter Car Suspension Model.....	64
Figure 5.3: Passive Suspension System Simulation in MATLAB/Simulink.....	65
Figure 5.4: Response of Passive Suspension System for Step Input .....	66
Figure 5.5: Response of Passive Suspension System for Sine Wave Input.....	66
Figure 5.6: Response of Passive Suspension System for Bump Input.....	67
Figure 5.7: Response of Passive Suspension System for type C Road Input .....	67
Figure 5.8: Control Oriented Model for Suspension System .....	68
Figure 5.9: Three-degree-of-freedom model of the MR damper seat-suspension system.....	71

## LIST OF ABBREVIATIONS/SYMBOLS

MR	Magnetorheological
ER	Electrorheological
LQR	Linear Quadratic Regulator
FLC	Fuzzy Logic Controller
RMS	Root Mean Value
SH	Skyhook
GH	Groundhook
ADD	Acceleration Driven Damper
MF	Membership Function

# CHAPTER 1

## INTRODUCTION

### 1.1 Background

Vehicle suspension systems have existed since the 19th century when the first vehicle equipped with one was an old horse carriage that was mainly operated by a few leaf springs, as shown in Figure 1.1.

In 1903, the Mors brothers invented the first automobile fitted with shock absorbers, which was based on the horse carriage suspension system. This insight led to further enhancements of the suspension system. As technology cultivated, it has become of increasing interest in the automobile industry. [1]

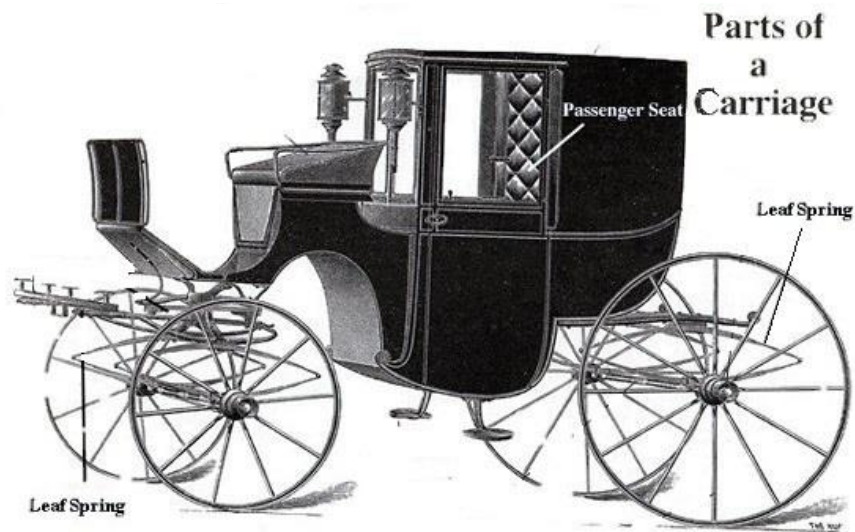


*Figure 1.1: Horse Carriage Suspension System [2]*

Vehicles become excited by road roughness. By cushioning the ride, the suspension system prevents discomfort for passengers as well as excessive fatigue damage to the vehicle's various systems. Suspension systems are dynamic, multi-link systems that absorb energy from the road by means of a spring, then dissipate it through a damper. Figure 1.2 shows a suspension system consisting of three main components:

- An elastic element, like a coil spring, that provides a force proportional to the extension of the suspension. This part also carries the entire static load during operation.
- A damping element which is a mechanism that dissipates force proportional to a suspension's elongation speed. This part produces a negligible force at steady state, but is crucial to the suspension's dynamic behavior.
- An assembly of mechanical components connecting the suspended body to an unsprung mass.

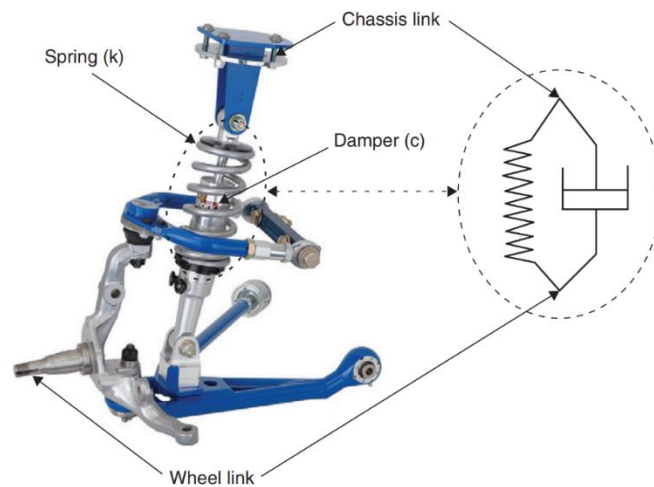


*Figure 1.2: Classical scheme of a wheel-to-chassis suspension in a car [3]*

There are four primary functions of a suspension system:

- 1- To support the vehicle body weight:

The significant purpose of a vehicle suspension system is to carry the static weight of the vehicle, including occupants and cargo, and the elastic element, the coil spring, for example, carries all this static load.

- 2- To improve the ride comfort by effectively isolating road vibrations from the vehicle.

Suspension systems are designed to provide adequate ride quality. A vehicle's ride quality deals with how passengers feel in a moving vehicle when experiencing vibrations. On-board vibration and road surface irregularities are the primary causes of vibration. Vibrations on board can be attributed to imbalances in tire and wheel assemblies, engine vibrations,

aerodynamic forces, and transmission vibrations [4]. Through the engine and transmission mounts, vibrations from the engine and driveline are applied to the vehicle's body. Excitations attributable to wheel placement and tire rotation affect the vehicle's body through the suspension system. However, the main vibration source is the road irregularities transmitted to the vehicle body through the wheel and suspension system [5], [6]. The road vibrations are classified as shocks and vibrations. Compared with shocks such as those caused by potholes and bumps, vibrations include incremental excitations of long duration and low power.

3- To maintain good road holding capacity:

Another function of a suspension system is to maintain sufficient contact force between the tires and the road (road holding ability) with minimal load variation [4]. Different types of forces such as tractive, cornering, and braking forces are generated by the wheel on motion, depending on the wheel's position and motion. It is known that all of these forces are a function of the vertical force acting between the tire and the road [6]. If the suspension system is vibrating, the vertical force will vary in intensity. In turn, tire vibration affects the suspension's road-holding ability and, therefore, affects the handling and stability of the vehicle [4]. Dynamic vertical forces should not exceed static forces in order to maintain contact with the ground. This factor becomes important during cornering due to rapid variation of the vertical load [5]. Although minimizing the unsprung weight is critically important to improving road holding, it has been demonstrated that controllable suspension systems can have a significant effect on vehicle road holding, and designers are trying to improve the vehicle performance regarding road holding and ride handling capacity. To provide good handling stability.

4- To provide good handling stability:

The handling performance of a vehicle depends on the response to steering commands and environmental inputs. The linking of suspension systems has an important influence on the handling and is significant for controlling the direction of the vehicle motion as well as ensuring stability in the presence of external disturbances, including wind gusts and road disturbances. Improvement of handling stability is an important goal in this study. Thus, the controllable suspension system will be designed in such a way that it minimizes tire deflection. Lower tire deflection represents better road holding which in turn, leads to better handling stability.

Suspension systems are generally designed to provide comfortable riding, good handling, and a reasonable range of deflection. Still, these aspects are subjective and based on the vehicle's purpose.



As an example, sports cars often feature stiff suspension systems for better handling but low ride quality. Luxury sedans, by contrast, have softer suspensions as a compromise for comfortable ride quality but suffer from poor road handling capabilities.

## 1.2 Suspension System Overview

Suspension systems have been researched for over a century by many researchers. A suspension system's design and operation are determined by its control function and control principles. Primary segregation of the suspension has been done into passive suspension, semi-active suspension, and active suspension. The main difference between these suspensions is the damping force control mechanism for road disturbances. During the past few decades, technology has made significant progress in both suspension components and system design.

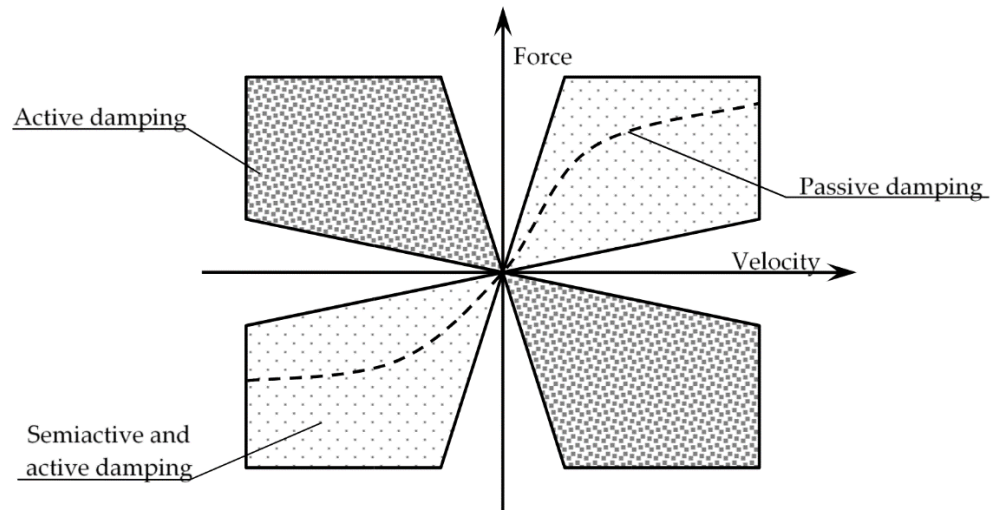


*Figure 1.3: Velocity-Force Characteristics of Various Suspension Designs [7]*

Each system has advantages and disadvantages along with specific operation modes, as shown in Figure 1.3. Detailed characteristics of each suspension technology are discussed in the next section.

### 1.2.1 Passive Suspension System

Passive suspensions can be defined as vibration isolators that are comprised of components with fixed properties. Passive suspensions are the most common type of suspension seen on vehicles because of their high dependability, no energy consumption, simplicity, and they are comparatively less expensive than active and semi-active suspension systems. All passive suspensions are comprised of two main components: a spring and a damping unit. For passive suspension systems,

the effective mode of operation lies in quadrants I & III of Figure 1.3. The spring and damper characteristics are determined according to the performance goals and their intended application. The passive suspension system does not have the capability of controlling suspension stiffness and damping coefficient according to the road roughness or the disturbance amplitude. Schematics of a passive suspension system is depicted in Figure 1.4. The optimal design of passive suspension systems has been the subject of many studies [8], [9].

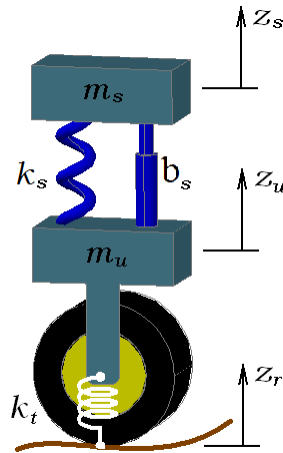


Figure 1.4: Typical passive suspension schematic [10]

### 1.2.2 Semi-Active Suspension System

Unlike passive suspension designs, semi-active suspensions have the ability to adjust the dynamic properties of the system. With this ability, semi-active suspensions can adapt to better dampen forces that are exciting the system. The effective mode of operation in this suspension technology is still restricted to quadrants I & III of Figure 1.3. Figure 1.5 depicts an example of a quarter vehicle model of a semi-active suspension which uses a common spring to support the load and uses an adjustable damper unit to provide the optimal damping for the system.

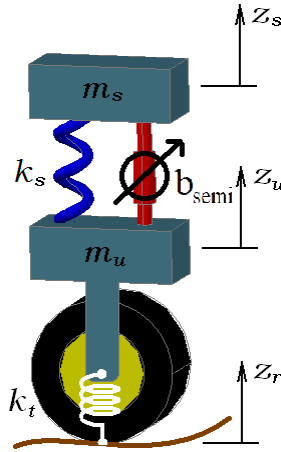


Figure 1.5: Typical semi-active suspension schematics [10]

Semi-active suspensions have advantages over passive suspension in terms of spring stiffness and damping coefficient control. The spring stiffness can be relatively difficult to vary for the specific suspension design, so the semiactive principle mostly focuses on the control of damping coefficient according to road roughness and the disturbances experienced by the unsprung mass of the vehicle [11]. In the automotive industry, unsprung mass refers to the weight of a vehicle's wheels, hubs, brakes, and other components connected to them. A semi-active suspension processes the road roughness/disturbances based on the suspension travel sensor feedback. The particular suspension states are baselined on the signals received from the road disturbances. Semi-active suspension system facilitates better comfort to driver and passenger as compared to the passive one. Also, a controllable damper facilitates the improved handling of the vehicle. This type of suspension can be found in Audi vehicles which feature an electronically controlled gas spring with load-leveling capabilities, and a semi-active damper. Several other car manufacturers such as Audi, VW, Mercedes, Ford, Volvo, and GM manufacturers use this technology in their products as well [12].

### 1.2.3 Active Suspension System

Active suspensions differ from passive and semi-active suspensions in the fact that they do not rely on common springs or dampers but the use of linear actuators. A linear actuator is a device that moves between two points in a linear motion. Linear actuators are available based on a variety of technologies including: Mechanical, Electro-Mechanical, Direct Electric (Linear Motors), Hydraulic & Pneumatic [13]. While there are several different types of linear actuators, hydraulic cylinders have been widely utilized in active suspension design because of their ability to generate

large magnitudes of force within a small package. The Audi A8, Mercedes Benz W222, and Toyota Avalon are among the cars with fully active suspensions [13]. Active suspensions also have a unique dynamic response that depends on the gain value that is set for the actuator's controller. An active suspension is shown in Figure 1.6. Where  $F_A$  is the force provided by the actuator.

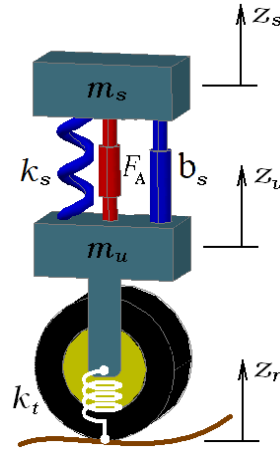


Figure 1.6: Typical active suspension schematics [10]

A force can be provided by active systems based on any number of states. These systems provide the best performance and comfort. However, these actuators commonly consume 5 to 10 kW, while a semi-active suspension system consumes 10 to 20 W [14]. They are expensive to produce and as the actuator is used alongside the regular damper, it causes an increase in the weight of unsprung mass. Consequently, active suspension systems tend to be more expensive, heavy, unreliable, costly and consume more power than semi-active and passive systems [15].

### 1.3 Research Objectives

An effective suspension system eliminates the adverse effects of disturbances (like an irregular road profile) on output variables. The output of the suspension system could be considered vertical body acceleration or tire deflection. When the main goal of our model is improving the ride comfort, the output of the simulation should be vertical body acceleration. However, when the main goal is to provide a good handling stability, the output of the model should be tire deflection.

It is important to note that a decrease in tire deflection translates into better contact between the tire and the road and, which in turn, leads to improved handling stability. on the other hand, a reduced vertical body acceleration means a more comfortable ride for the occupants.

Improving ride comfort and handling stability are two conflicting objectives and suspension designers are always trying to look for possible ways to solve the problem of compromising between opposite goals.

The aim of the research is to deal with the aforementioned trade-off to improve the performance of the semi-active suspension system regarding both ride comfort and handling stability. To achieve this aim, two objectives are specified.

- 1- Developing a proper control system for a semi-active suspension system using Linear Quadratic Regulator (LQR) and Fuzzy Logic, which can provide a high level of performance comparing to passive suspensions.
- 2- considering a suspension system for seats and trying to address a method for improving ride comfort through seat suspension as the second suspension system, while the main suspension's focus will be on improving handling stability.

In accordance with ISO 2631, the root mean square (RMS) value of the outputs is used to evaluate the performance of the suspension system. This study will model semi-active and passive suspension systems in MATLAB/Simulink and will evaluate their performance when excited by a variety of road inputs. The RMS value of the outputs, which are vertical body acceleration and tire deflection, will be measured and compared with each other to find out if the semi active suspension system has been effective in improving the ride quality.

There is a feature in some luxury cars such as Audi that allows the driver to choose between ride damping options like "comfort", "sport", etc. To implement this, each option requires its own control system, but even with comfort driving selected, it is expected that the suspension system be capable of providing the comfort without degrading the handling stability for safety reasons. This is the main goal of this study, designing a semi-active control system that provides good ride comfort as well as an acceptable handling performance.

It should be noted that comfort is a generic and subjective feeling that is difficult to measure, interpret, and related to human physiological homeostasis and psychological wellbeing [16]. As stated in ISO 2631, a particular vibration control may be considered to cause unacceptable discomfort in one situation but may be classified as pleasant or exhilarating in another [17]. One of the goals of this study is to design a suspension system which tries to improve its performance by minimizing the RMS value of the vertical acceleration experienced by the vehicles' occupants

which is called "ride comfort" in this thesis and refers to just the improvement of the proposed semi-active suspension's performance over a passive one.

#### **1.4 Thesis Overview**

This thesis is organized into seven chapters to report the findings of this research. Chapter one is a brief introduction regarding the suspension system and including different types of suspension systems, and also the reason for which this study is focused on the semi-active suspension system is explained. Chapter 1 finishes with the objectives of this research.

In order to determine the design requirements of the suspension, a review of semi-active suspension components is conducted in chapter 2. This chapter starts with an overview of adjustable dampers and proceeds to give a detailed description of the MR fluids and MR dampers. The next section of this chapter discusses the different types of springs, and the final part is devoted to the control system.

Chapter 3 demonstrates the mathematical modelling of the MR dampers. Three mathematical models of an MR damper are introduced and simulated to be compared with the simulated experimental data. This chapter continues with an explanation about the inverse model of dampers and the specific approach which will be employed in this study for studying control systems.

Chapter 4 presents different types of road profiles, which will be used to find out if proposed ideas would be helpful in improving the performance of the suspension system.

In Chapter 5, The suspension system will be simulated using mathematical equations and prediction models. An evaluation of a passive suspension will be conducted in this chapter. The results will be used to measure the improvement of the semi-active control systems, which will be discussed in the following chapter.

Chapter 6 presents the theory and the design of two control systems, Linear Quadratic Regulator and Fuzzy Logic, and will validate the effectiveness of the proposed ideas through comparing the simulation results of a semi-active suspension system with that of a passive one.

Chapter 7 presents the concluding remarks and the suggestions for future areas of research.

## CHAPTER 2

### SEMI-ACTIVE SUSPENSION SYSTEM COMPONENTS

The semi-active suspension benefits from factors such as good performance, cost-effectiveness, safety, and low power consumption compared to fully active, which make it superior to passive and fully active suspension systems as they combine the advantages of both of them. Hence, this study opted to investigate a semi-active suspension system. Springs, Dampers, and control systems are three main topics regarding a semi-active suspension that need to be studied and researched.

The semi-active suspension offers advantages over passive suspension for desirable performance while also providing a more cost-effective solution than full-active suspensions [15]. During the past decade, semi-active suspension has been investigated by a number of researchers as used in automotive and vibration control applications [18].

#### 2.1 Adjustable Dampers

There are three main technologies in adjustable dampers: One classical electrically operated damper is an electrohydraulic one that uses solenoid valves installed inside or outside the damper body. By changing the orifice size, the damping ratio can be changed. Research on variable orifice dampers was done in the early days of semi-active suspension, but due to mechanical motion restrictions, speed adjustment was difficult. On the other hand, magnetorheological and electrorheological technologies, which is usually referred to as ER fluids, are based on fluids that can change their viscosity when exposed to magnetic fields and electric fields.

##### 2.1.1 MR fluids

MR fluids stand for magnetorheological fluids that were first discovered by the inventor Willis Winslow [19], who achieved a US patent regarding these fluids in 1947 [20] and were developed by Jacob Rabinow in 1948 [21]. Fluid yield stresses can be determined by changing the field intensity in a continuous manner, resulting in a continuous damping force. These fluids have found several successful applications in the field of vibration control. This thesis is focused on MR fluid dampers, which are considered more suitable than ER fluid dampers for automotive applications for the reasons given below.

The MR fluid is composed of microscopic bits of magnetically polarizable metal, such as iron particles, suspended in a liquid carrier, such as mineral oil, synthetic oil, water or glycol. A typical MR fluid will contain 20 to 40 percent by volume of relatively pure iron particles around 3-to-10-

micron diameter in size [22] and commonly, some additives, similar to those in commercial lubricants, are added to keep the metal particles from clustering. The fluid encapsulates each metal particles and keeps them separated from each other so they do not clump up together. These additives prevent particles from gravitating and promote particle suspension. Additionally, they improve lubricity and viscosity, as well as inhibit wear of components of the damper. The rheological behavior of MR fluids is dramatically affected by a magnetic field. When subjected to a magnetic field, MR fluids can reversibly and instantaneously transform from free-flowing liquids into semisolids within a few milliseconds [23]. Without an applied field, MR fluids are roughly equivalent to Newtonian liquids. A Newtonian fluid is defined as one with constant viscosity, with zero shear rate at zero shear stress, that is, the shear rate is directly proportional to the shear stress [24]. As shown in Figure 2.1(a), it is free-flowing and has a consistency similar to motor oil. The iron particles in this state are amorphous. Magnetic fields cause ferrous particles to align along the flux path, as shown in Figure 2.1(b), and finally form particle chains in the fluid, as shown in Figure 2.1(c). Such chains resist and restrict fluid movement. As a result, yield stress develops in the fluid. Magnetic fields are responsible for varying the amount of change, and research has shown that this change can occur within 1 millisecond [25]. MR dampers can have a viscosity ranging from 1000 to 15000, although in the automotive industry, dampers with a viscosity range of 1000 to 5000 are commonly used [26].

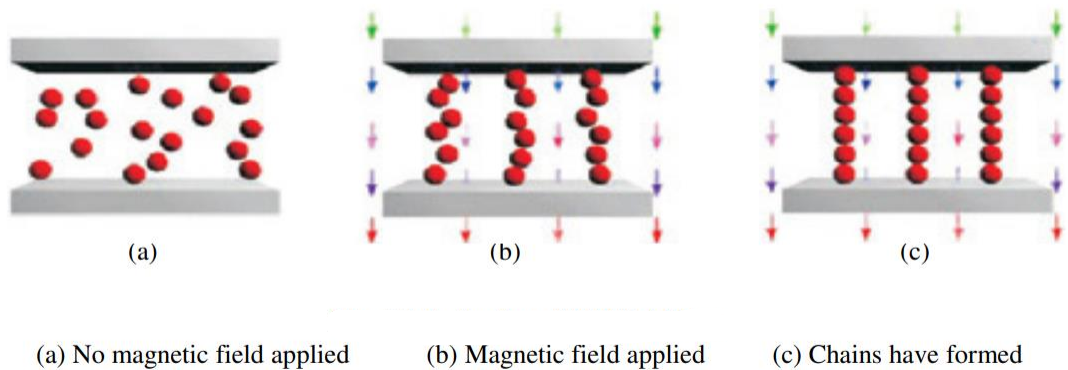


*Figure 2.1: Activation of MR Fluid [25]*

This controllable yield stress is exploited at MR fluid devices that feature different modes of operation based on how they make the MR fluid flow. There are three basic operating modes for these devices: (a) valve mode, (b) direct shear mode, and (c) squeeze mode. The basic operating modes are illustrated in Figure. 2.2. Servo-valves, dampers and actuators are examples of a valve mode device. The list of shear mode devices includes clutches, brakes, dampers and composites.



Despite its limited understanding, the squeeze mode is used in some low-amplitude vibration dampers [27].

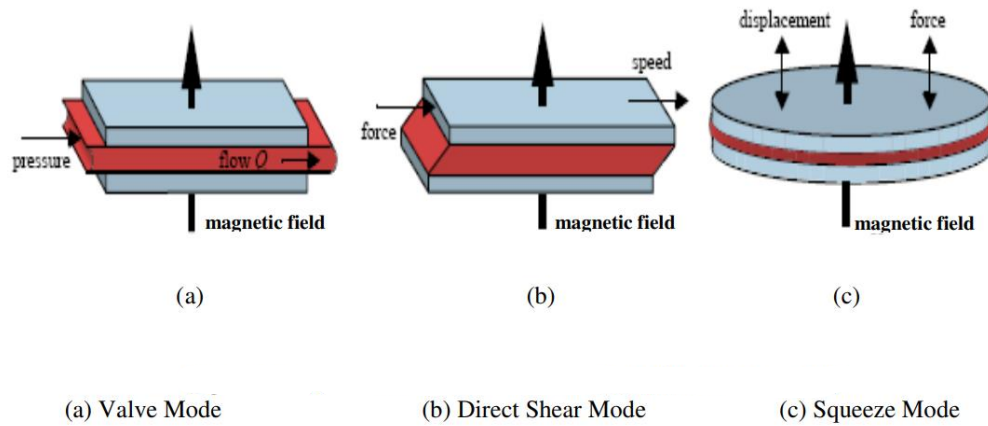


*Figure 2.2: Basic operating modes for controllable fluid devices [27]*

Figure 2.3 and 2.4 show the specification of an MR fluid produced by Lord company which is named MRF-140BC, and based on its description, it can be used in valve mode which the fluid flows through an orifice. As it is demonstrated in the diagram, yield stress can rise from about 5 KPa to more than 70 KPa when it is exposed to a magnetic field.

# MRF-140BC Magneto-Rheological Fluid

## Description

LORD MRF-140BC fluid is a hydrocarbon-based magneto-rheological (MR) fluid formulated for general use in controllable, energy-dissipating applications such as brakes, clutches and rotary knobs.

MRF-140BC fluid is a suspension of micron-sized, magnetizable particles in a carrier fluid. When exposed to a magnetic field, the rheology of MRF-140BC fluid reversibly and instantaneously changes from a free-flowing liquid to a semi-solid with controllable yield strength. Altering the strength of the applied magnetic field precisely and proportionally controls the consistency or yield strength of the fluid.

MRF-140BC fluid can be used in *valve mode* (fluid flowing through an orifice) or in *shear mode* (fluid shearing between two surfaces), but is typically better suited for shear mode. In the absence of a magnetic field, MRF-140BC fluid flows freely. Upon application of a magnetic field, the fluid's particles align with the direction of the field in chain-like fashion, thereby restricting the fluid's movement within the gap in proportion to the strength of the magnetic field.

## Features and Benefits

**Fast Response Time** – responds instantly and reversibly to changes in a magnetic field.

**Dynamic Yield Strength** – provides high yield strength in the presence of a magnetic field and very low yield strength in the absence of a magnetic field; allows for a wide range of controllability.

**Temperature Resistant** – performs consistently throughout a broad temperature range.

**Non-Abrasive** – formulated to not abrade the devices in which the MR fluid is used.

## Application

**Mixing** – Under common flow conditions, no separation is observed between particles and the carrier fluid. However, a degree of separation may eventually occur under static conditions. If needed, use a paint shaker to redisperse the particles into a homogeneous state prior to use.

## Storage

Keep container tightly closed when not in use.

Figure 2.3: MRF-140BC Magneto-Rheological Fluid Description [28]

## Yield Stress vs. Magnetic Field Strength

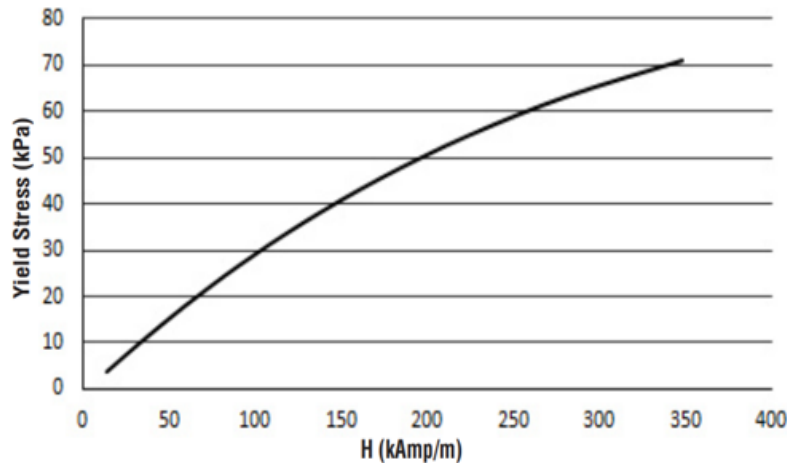


Figure 2.4: MRF-140BC Magneto-Rheological Fluid Yield Stress Diagram [28]

MR fluids are considered to be an attractive alternative to ER fluids for use in controllable fluid dampers [29]. This can be seen in Table 2.1, which compares the physical properties of both MR and ER fluids [30]. In contrast to ER fluids, MR fluids are 20 to 50 times stronger. Furthermore, because the magnetic polarization mechanism is unaffected by temperature, the performance of MR-based devices is relatively insensitive to temperature over a broad temperature range

(including the range for automotive use) [31]. In fact, MR fluids can operate at temperatures from - 40 to 150 °C with only slight variations in the yield stress [1], in contrast to ER fluids (restricted to a range of 10 to 90°C). MR fluids are significantly less sensitive to impurities or contaminants, such as are commonly encountered during manufacturing and usage [27]. MR technology can provide flexible control capabilities in designs that are far less complicated and more reliable than those based on ER technology [30]. Moreover, as can be seen from Table 2.1, in contrast to ER fluids, MR fluids can be readily operated from a low voltage (e.g., ~12–24V), current-driven power supply outputting only ~1–2 amps.

The advantages of MR technology relative to conventional and electro-mechanical solutions are summarized as follows [28]:

- Quick response time (less than 10 milliseconds).
- Continuously variable control of damping.
- Simple design of MR devices (few or no moving parts).
- Consistent efficiency across extreme temperature variations.
- High dissipative force and low-velocity dependence compared to passive dampers.
- Greater energy density.
- Minimal power usage (typically 12V., 1 A).
- Inherent system stability (no active forces generated).

Table 2.1: Properties of MR and ER Fluid [30]

Property	MR Fluid	ER Fluid
Max. yield Stress	50 to 100 kPa	2 to 5 kPa
Max. field	~250 kA/m	~4 kV/mm
Plastic Viscosity	0.1 to 1.0 Pa.s	0.1 to 1.0 Pa.s
Operable Temperature Range	-40 to 150 0C	+10 to 90 0C
Stability	Unaffected by Most Impurities	Cannot Tolerate Impurities
Response Time	ms	ms
Density	3 to 4 g/cm <sup>3</sup>	1 to 2 g/cm <sup>3</sup>
Dynamic Viscosity/Yield Stress	5e-11 s/Pa	5e-8 s/Pa
Max. Energy Density	0.1 J/cm <sup>3</sup>	0.001 J/cm <sup>3</sup>
Power Supply (typical)	2 to 25 V & 1 to 2 A	2000 to 5000 V & 1 to 10 A

### 2.1.2 MR Dampers

An MR damper basically includes a piston, magnetic coils, accumulators, seals, and a reservoir of MR fluid. Figure 2.5 shows a Lord RD-1005-3 MR fluid damper [28]. Through orifices in the piston head, the piston rod is pushed into the housing, causing MR fluid to flow from the high pressure chamber to the low pressure chamber. The accumulator contains compressed gas (usually nitrogen), and its piston acts as a barrier between the MR fluid and the gas. The accumulator serves three purposes:

- 1- It softens the piston rod by providing an extra allowance for the volume changes when it enters the housing.
- 2- It accommodates the thermal expansion of the fluid.
- 3- It prevents the cavitation that could occur during piston motions in the MR fluid.

The magnetic field generated in the activation regions by the magnetic coils changes the characteristics of the MR fluid. As a result, the MR damper's physical characteristics are determined by the magnitude of the magnetic coil input current. An MR damper's maximum force varies according to its characteristics, fluid flow patterns, and size [28].

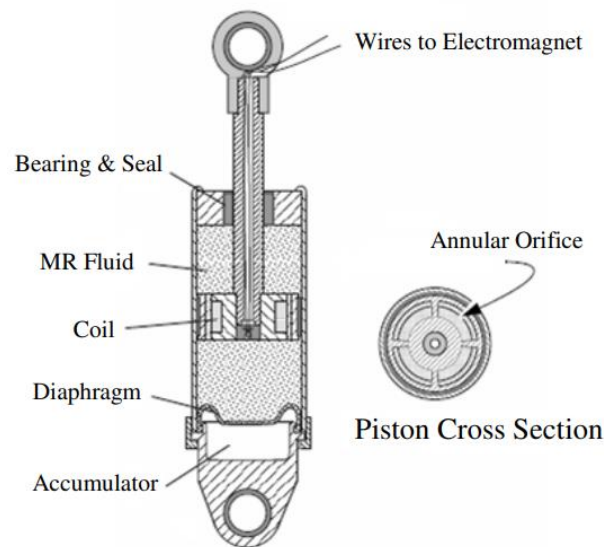


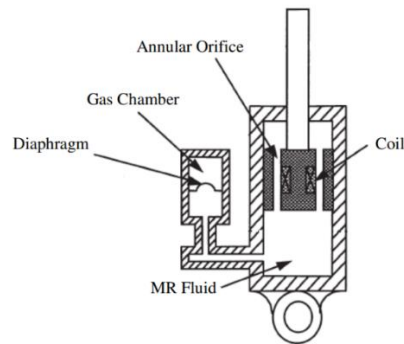
*Figure 2.5: Cross-section of typical MR fluid damper [28]*

Two major types of MR fluid dampers are commonly used in vehicle suspensions:

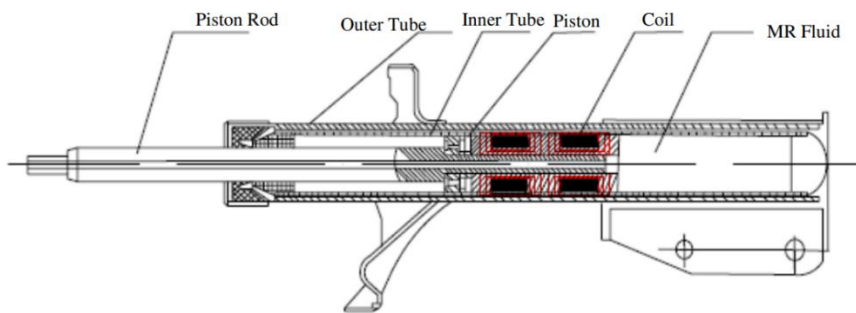
- Monotube
- Twin tube

Figure 2.6 illustrates a monotube MR fluid damper with a single reservoir and accumulator that is commonly used in car seat suspensions [32]. The twin tube MR damper, illustrated in Fig. 2.7, is commonly used in suspension systems for vehicles [33]. It consists of two fluid reservoirs, one inside the other. These dampers consist of an inner and outer tube. The inner tube guides the piston, similar to a monotube damper. The inner reservoir is the volume enclosed by the inner tube. The outer reservoir is the volume that lies between the inner and outer tubes. In the inner reservoir, MR

fluid is fully injected so that no air pockets exist. As the piston moves, changes in volume are accommodated by an outer reservoir partially filled with MR fluid.



*Figure 2.6: Mono-Tube MR Damper [32]*



*Figure 2.7: Schematic Configuration of the Twin Tube MR Damper Without Accumulator [33]*

In other designs the outer reservoir is completely filled and separated by a diaphragm from a gas filled accumulator as shown in Fig. 2.8 [34].

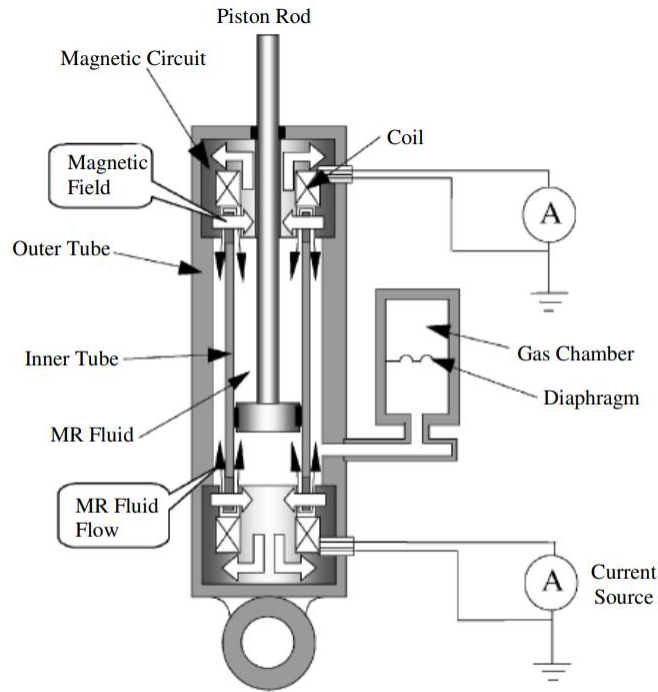


Figure 2.8: Schematic illustration of the Twin Tube MR Damper with Accumulator [34]

It should be noted that MR dampers are designed such that MR fluid passes through an orifice and a magnetic field surrounds the orifice and is not propagated throughout the entire damper.

## 2.2 Springs

The automotive industry uses four different types of springs:

- Leaf springs
- Torsion Bars
- Coil Springs
- Air Springs

In the design of leaf springs, a set of blades cascades down into each other. Leaf springs are made up of a slender coil of steel, rectangular in cross-section, with a U-bolt joining them together. Most commonly, the arc's center is used to locate the axle, and ends of the arc form loops that attach to the vehicle's chassis. Several leaves of different lengths, such as those shown in Figure 2.9, can be stacked on top of each other to form a leaf spring for very heavy vehicles.

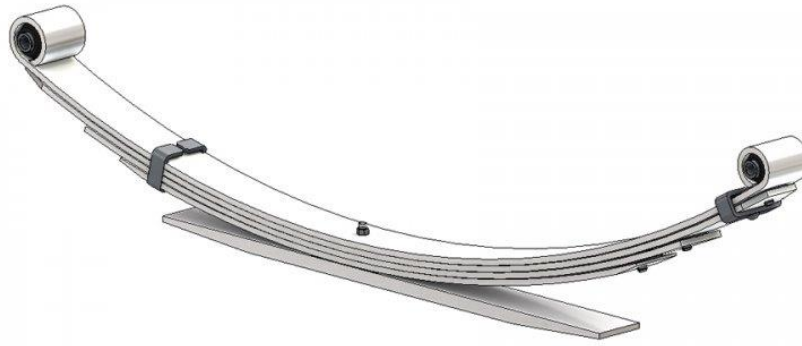


*Figure 2.9: Example of a Leaf Spring*

Torsion Bar is basically a length of metal rod which is attached one end to the vehicle chassis and the other end to the suspension link. When the car passes over a bump, for instance, the bar twists and returns to its original position, restoring the drive height. Length, Cross section, shape, material, and manufacturing process are the factors which determines the effective spring rate of the bar. A torsion bar is depicted in Figure 2.10.

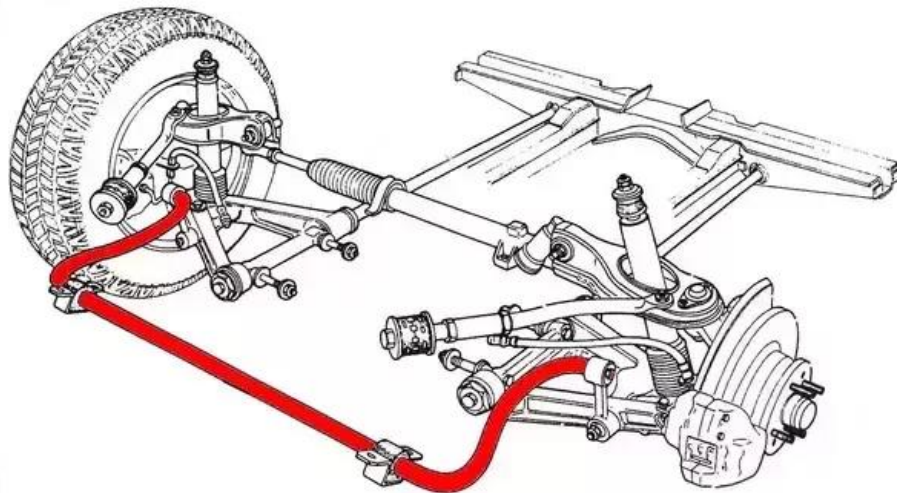


*Figure 2.10: Example of a Torsion Bar*

Coil springs are elastic elements assumed to be subject only to vertical forces and displacements. The force is delivered as a result of the torsion of the coils, while other effects are ignored. And the stiffness of the spring is determined by the rigidity modulus of the material of coils, the wire diameter, the mean of the internal radius of the coil, and the number of active coils. It should be noted that due to the static load of the suspended mass, a suspension works "pre-compressed" around a steady-state condition. Coil springs are responsible for the static load, and they are



designed to carry this load and also allow movement around the steady position both in the compression and rebound phase.



*Figure 2.11: Example of a Coil Spring*

Another type of springs with improved performance, compared to those mentioned, is air springs or gas springs. Their obvious advantages have made them increasingly popular in recent years. Air springs are designed to perform the same function as mechanical springs, although they operate off of different dynamic principles. Air springs generate force from compressing air that is enclosed in the spring volume. As a result, an air spring with a fixed mass of air can only increase its reaction force in compression. Air spring's ability to generate a given force depends on the effective area and internal pressure of the spring. The effective area is a fictitious area that is equivalent to the load applied divided by the internal pressure of the spring. Depending on the construction of the spring, the change of effective area can have a large effect on the generated forces.

Figure 2.12 and Figure 2.13 portray two suspension frameworks in which gas springs are typically implemented. A pneumatic suspension implements the spring by enclosing the shock absorber in an air chamber. The second is hydro-pneumatic suspension, where an accumulator is attached to the shock absorber and the gas in it is compressed by movements of the fluid.

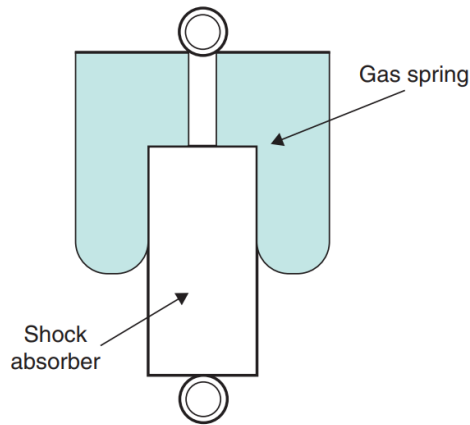


*Figure 2.12: Schematic representation of a Gas Spring Implemented With Pneumatic Spring [3]*

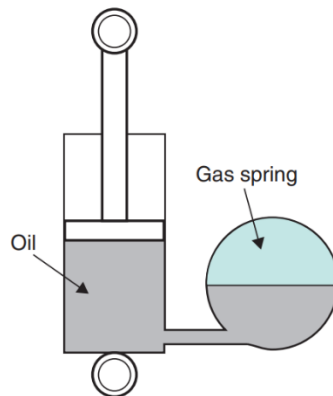


*Figure 2.13: Schematic representation of a gas spring Implemented with Hydro-Pneumatic Spring [3]*

The following assumptions need to be considered when studying the force-deflection characteristic of a gas spring:

- It is supposed that the gas is ideal. Note that air is a close approximation to an ideal gas.
- The gas is subjected to an adiabatic transformation during normal use of the suspension so that no thermal energy is exchanged with the ambient. Note that the dynamics involving suspension are relatively much faster than those involving thermal exchanges [3].

The force delivered by the gas spring is derived from the pressure applied to the active area of the gas chamber. For any suspension deflection, the variation in the active area is supposed to be negligible.

$F_k$  is the force delivered by a gas spring which is proportional to the difference between the internal pressure  $P$  and the external pressure, which is actually the ambient pressure  $P_{atm}$ , as follows:

$$F_k = A(P - P_{atm}) \quad (2.1)$$

Where  $A$  is the active area of the air chamber. Linear stiffness associated with the air spring can be approximated by the following equation:

$$k = \frac{P_0 \gamma A L_0}{(L_0 - x)^{\gamma+1}} \quad (2.2)$$

Where  $L_0$  and  $p_0$  are the spring length and the pressure when the suspension is fully expanded;  $\gamma$  is the adiabatic constant of the gas which is 1.4 for air; the suspension deflection is represented by  $x$  which is always positive, so that  $x$  would be zero when the suspension is fully compressed, while when the suspension is fully expanded,  $x$  would be  $L_0$ .

Proof of Equation (2.2):

to verify equation (2.6), Consider the adiabatic transform of an ideal gas:

$$PV^\gamma = P_0 V_0^\gamma \quad (2.3)$$

where  $V$  is the gas volume in the chamber. By differentiating, the following holds:

$$\begin{aligned} \partial PV^\gamma + P\gamma V^{\gamma-1} \partial V &= 0 \\ \Rightarrow \quad \partial P &= - \frac{P\gamma \partial V}{V} \end{aligned} \quad (2.4)$$

The variations of deflection are supposed to have no effect on the active area of the spring, consequently, the gas volume  $V$  might be expressed as follow:

$$V = (L_0 - x)A \quad (2.5)$$

Which results to the following equation:

$$\partial V = -A\partial x. \quad (2.6)$$

By differentiating relation (2.1) and taking into account equation (2.4) the following holds:

$$\partial F = \partial A(P - P_{atm}) = A\partial P = A \left( -\frac{P\gamma\partial V}{V} \right) = A \left( -\frac{P\gamma(-A\partial x)}{V} \right) = \frac{P\gamma A^2}{V} \partial x \quad (2.7)$$

The stiffness of a spring is defined as  $k = \frac{\partial F}{\partial x}$ , so Equation (2.2) might be verified by algebraic manipulations:

$$k = \frac{\partial F}{\partial x} = \frac{P\gamma A^2}{V} = P_0 \frac{V_0^\gamma}{V^{\gamma+1}} \gamma A^2 \quad (2.8)$$

$$\Rightarrow k = \frac{P_0 \gamma A L_0}{(L_0 - x)^{\gamma+1}} \quad (2.2)$$

### 2.3 Control System

Suspension control is not a new concept; development began around the 1950s and '60s [35]. The first vehicle to be manufactured with a semi-active electronically controlled suspension system was the Mitsubishi Gallant in 1987. However, many advances in control theory, as well as practical implementations, have been made since then. The applications for suspension control include improved performance in terms of handling, comfort, and safety. This is not an easy task since comfort and performance are in direct conflict with each other [36].

During the past decade, various semi-active control strategies have been proposed for improving the performance of semi-active suspension systems for automotive and vibration control applications. The initial semi-active suspension system was proposed by Karnopp [35] using the skyhook control strategy. The skyhook strategy improves the ride quality with a virtual damping term proportional to the sprung mass velocity by setting an imaginary damper between the vehicle body and the imaginary sky. The skyhook strategy is the simplest control but very effective in a semi-active control system. On the other hand, ground hook is a control system which is basically a road-holding oriented semi-active approach as its objective is to minimizing tire-road forces.

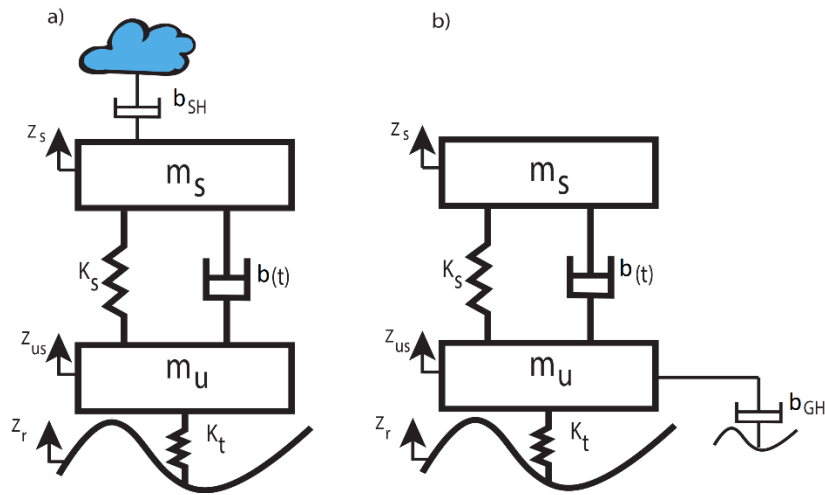


Figure 2.14: Schematic Representation of Skyhook Theory (a) and Groundhook Theory (b) [37]

Where  $m_s$  and  $m_u$  are sprung and unsprung mass, respectively;  $K_s$  is the stiffness of the spring and  $b(t)$  represents the damping coefficient;  $K_t$  is the stiffness of the tire and  $Z_r$ ,  $Z_{us}$ , and  $Z_s$  are the vertical displacement of the road, unsprung mass and the sprung mass, respectively. Skyhook control is generally classified as continuous skyhook control or on-off skyhook control [38]. On-off Skyhook control is typically simpler and is more appropriate for industrial applications. The control law can be described as follows:

$$b_{in} = \begin{cases} b_{min} & \text{if } v_r v_b \geq 0 \\ b_{max} & \text{if otherwise} \end{cases} \quad (2.9)$$

Where  $v_b$  is considered to be the absolute velocity of the body and  $v_r$  is the relative velocity of the body and wheel across the suspension.  $b_{min}$  and  $b_{max}$  are the minimal and maximal damping coefficients which could be achieved by the damper. This control system suggests that when relative velocity and the absolute velocity of the suspended mass are both positive or negative, the damping factor should be maximum; otherwise the damping factor should be minimum.

The Skyhook (SH) strategy is to improve the ride comfort for the passengers and is not intended to improve road holding performance because the sprung mass vibration is not considered in its control law. The control strategy known as Groundhook (GH) focuses on improving the road holding. This controller follows a similar principle to the SH, but it is oriented to the dynamic tire forces reduction to guarantee the desired level of road holding.

Acceleration Driven Damper (ADD) control system was introduced in 2005 by Savaresi [39] and was also investigated in 2006 by Golnaraghi [14]. This was based on the measurement of the absolute vertical acceleration of the vehicle body rather than the absolute velocity. damping factor, in this method, is determined as follows:

$$b_{in} = \begin{cases} b_{min} & \text{if } a_b v_r \leq 0 \\ b_{max} & \text{if } a_b v_r > 0 \end{cases} \quad (2.10)$$

Where  $a_b$  is considered to be the absolute vertical acceleration of the body and  $v_r$  is the relative velocity of the body and wheel across the suspension.  $b_{min}$  and  $b_{max}$  are the minimal and maximal damping coefficients which could be achieved by the damper. Analytical and experimental results confirm that this method reduces both the acceleration and relative displacement of the sprung mass by a significant amount. Some linear feedback control methods and intelligent strategies have also been investigated in the semi-active suspension system [40]. More recently, many control strategies, including fuzzy logic control [41], skyhook, ground-hook and hybrid control [42], neural network predictive control algorithm [43], semi-active fuzzy control [40], and adaptive vibration control [44], have been explored.

In general, the performance of a semi-active control system is highly dependent on the control strategy, which is the core of the system controller. Various control strategies, such as classical and advanced control strategies, have been proposed to improve the performance of semi-active

vibration control systems. Experimental trials have been conducted on a wide range of them for vehicles with semi-active suspension in order to improve ride quality.

## CHAPTER 3

### MATHEMATICAL MODELING OF MR DAMPERS

#### 3.1 Modeling of MR Fluid Dampers

(MR) fluids are multiphase materials that exhibit properties typical of a viscoelastic material. In the post-yield regime, MR fluids typically exhibit viscous properties, while in the Pre-Yield regime, MR fluids typically exhibit elastic properties [45]. The evaluation of the magnetorheological properties and the development of a model are essential for the improvement of the performance and the design of a damper utilizing MR fluids. In order to develop control algorithms that utilize the damper's unique features, models must be developed that adequately characterize its nonlinear viscoelastic behaviour.

There are a number of mathematical models that have been published to simulate the behaviour of MR dampers. The most basic model is a Bingham model, illustrated in Figure 3.1, which was introduced first to study the dynamical behaviour of ER dampers [46] and then used for MR dampers in [47]. The Bouc-Wen model, shown in Figure 3.2, is an extremely versatile model that is able to emulate a variety of viscoelastic behaviours, specifically hysteretic behaviours. By "hysteretic," it meant that the output is dependent not just on the instantaneous values of the inputs but also on the history of the output [48], i.e., such a system has "memory." Spencer proposed a modified Bouc-Wen model, illustrated in Figure 3.3, which modified the Bouc-Wen representation through the introduction of an extra internal degree of freedom [47]. The experimental validation showed that the modified Bouc-Wen model is able to accurately predict the response of a typical MR damper over a wide range of operating conditions under various input voltage levels [47].

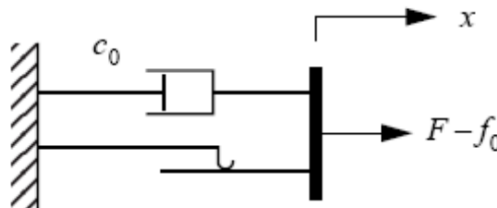


*Figure 3.1: Bingham Model [27]*



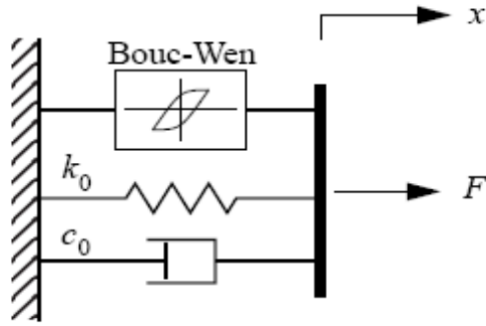


Figure 3.2: Bouc-Wen Model [27]

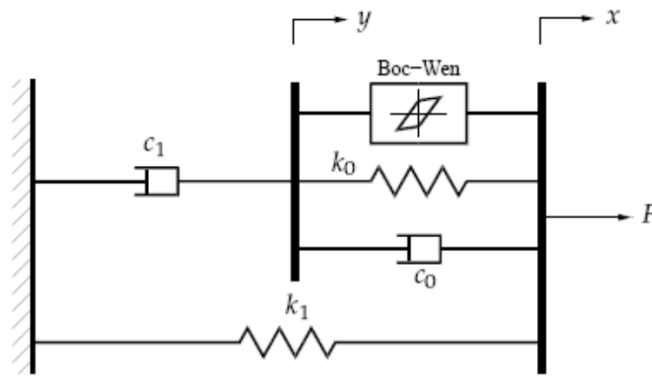


Figure 3.3: Modified Bouc-Wen, Spencer Model [27]

The Bingham viscoelastic model is often employed to explain the behaviour of MR (and ER) fluids [49]. For this model, the plastic viscosity is determined by the slope of the shear stress,  $\tau$ , versus the shear strain rate,  $\dot{\gamma}$ , data. Thus, the total stress for values of  $\dot{\gamma}$  greater than 0 is given by the following equation:

$$\tau = \tau_{y(field)} \operatorname{sgn}(\dot{\gamma}) + \eta \dot{\gamma} \quad (3.1)$$

Where  $\tau_{y(field)}$  is the yield stress induced by magnetic (or electric) field;  $\eta$  is the viscosity of the fluid;  $\dot{\gamma}$  is the shear rate, and  $\operatorname{sgn}(\dot{\gamma})$  represents the sign of the shear rate.

On the basis of this rheological model of ER fluids, Stanway proposed an idealized mechanical model of the behaviour of an ER damper, denoted the Bingham model [46]. Figure 3.1 illustrates a Bingham friction model with a coupled friction element and a viscous damper adjacent to it. With

this model, the force generated by the device for nonzero piston velocities,  $\dot{x}$ , can be calculated as follows:

$$F = f_c \operatorname{sgn}(\dot{x}) + c_0 \dot{x} + f_0 \quad (3.2)$$

Where  $c_0$  is the damping coefficient; and  $f_c$  is the frictional force, which is related to fluid yield stress, and  $\dot{x}$  is the velocity of displacement in damper piston. Due to the presence of the accumulator, a nonzero mean in the measured force is included to account for it. Note that if the piston's velocity is zero at any point, the frictional force is equal to the applied force. For testing its ability to predict the behaviour of the MR damper, Bingham model was fit to the 2.5 Hz sinusoidal response data for the case when the command voltage to the current driver is a constant 1.5 V. The parameters chosen as shown in Table 3.1.

*Table 3.1: Values of parameters used in Bingham Model [22]*

<b>Parameter</b>	<b>Value</b>
$f_c$	670 N
$c_0$	50 N.s/cm. V
$f_0$	-95 N.

Using represented equations and parameters shown in table 3.1, the Bingham model is simulated by MATLAB/Simulink that is depicted in Figure 3.2.

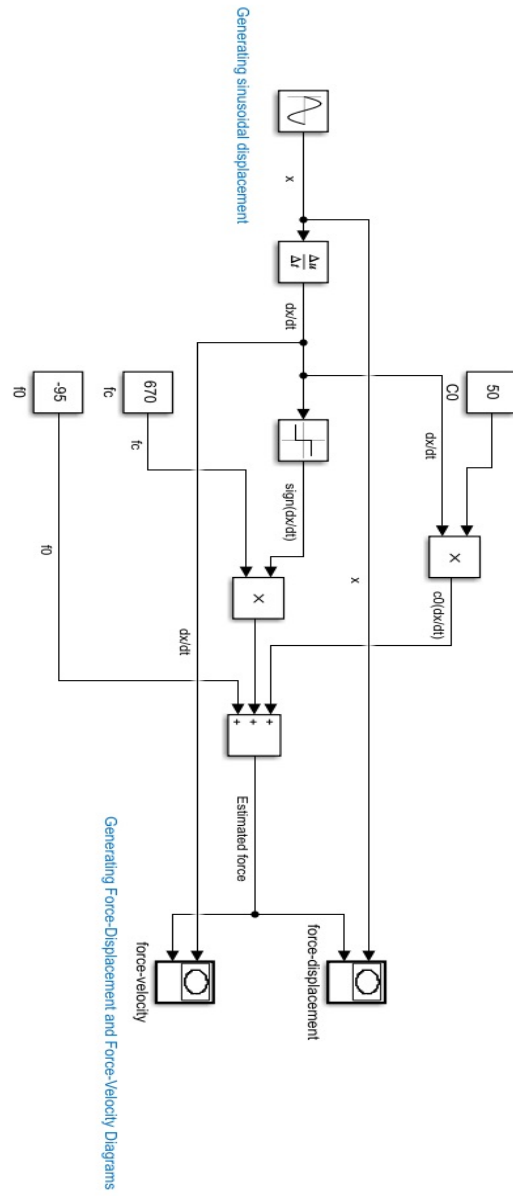


Figure 3.4: Simulation of the Bingham model in MATLAB/Simulink

Figure 3.3 shows the results obtained from simulation model.

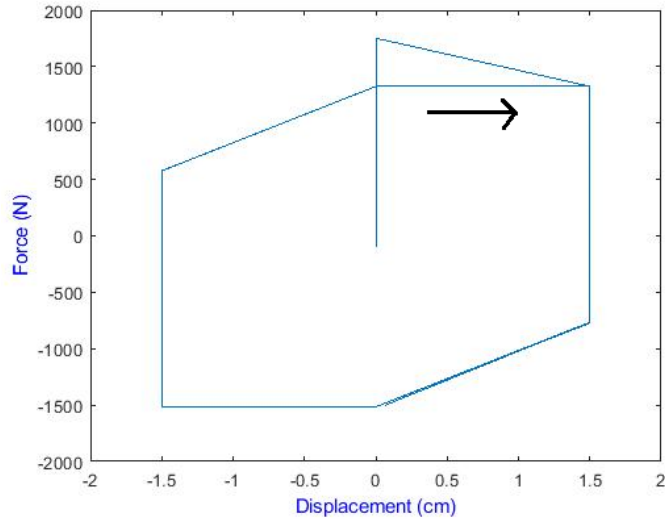


Figure 3.5: Displacement-Force diagram obtained from Bingham Model

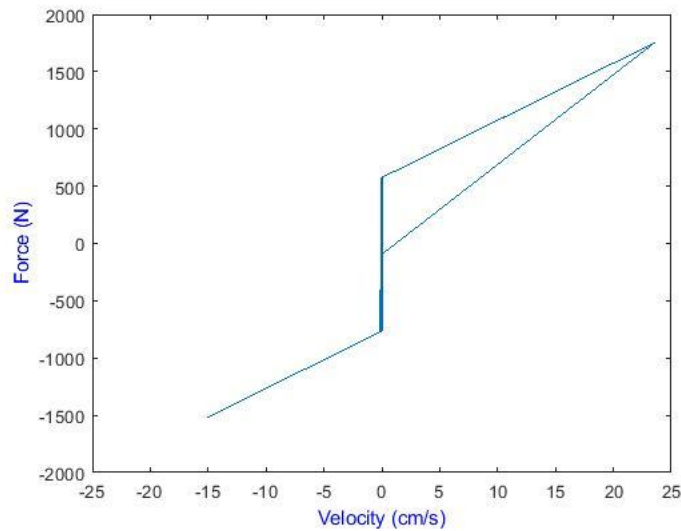


Figure 3.6: Velocity-Force diagram obtained from Bingham Model

In Figure 3.5, we can observe the hysteresis effect of the MR damper: when the displacement is positive, the generated force is different from when the displacement is negative. In fact, when MR fluids are subjected to an external shear stress in the perpendicular direction to the magnetic field, those polarization chains can resist the shear stress to some extent, and the MR fluids behave in a viscoelastic way. This region is referred to as the pre-yield region. When the external shear stress is increased and exceeds a certain value, the polarization chains will be broken, and MR fluids becomes in regular Newtonian fluids; this region is referred to as the post-yield region. The

gradually decreasing shear stress links up the polarization chains, but the stress value to do the link is less than before the polarization chains break happens, producing the hysteresis. [50]

It is shown that the predicted results differ from experimentally obtained data, and although the force-displacement behaviour seems to be reasonably captured, the force-velocity response indicates that the damper's behaviour is not captured, especially when velocities are near zero. Specifically, when the acceleration and velocity have opposite signs (or alternatively, when the velocity and displacement have the same sign) and the magnitude of the velocity is small, the model does not exhibit the nonlinear force-velocity relationship observed in the data. Despite its suitability for response analysis, this model is not suitable for control analysis. The model predicts that force and velocity are one-to-one, but the experimentally obtained results are not one-to-one.

When the velocity is zero, the measured force has a positive value, when the acceleration is negative (a positive displacement) and has a negative value when the acceleration is positive (a negative displacement). This behaviour must be accurately represented in a mathematical model to characterize the device for control applications.

### 3.2 Bouc-Wen Model

There has been extensive use of The Bouc-Wen model for modelling viscoelastic systems because it is numerically tractable [47]. The Bouc-Wen model is very versatile, and it is capable of exhibiting a wide variety of viscoelastic behaviour. A schematic of this model is shown in Figure 3.2. The force in this system is given by

$$F = c_0\dot{x} + k_0(x - x_0) + \alpha z \quad (3.3)$$

Where the evolutionary variable,  $z$ , is an internal variable which helps to simulate the behaviour of the MR damper and is governed by

$$\dot{z} = -\gamma|\dot{x}|z|z|^{n-1} - \beta\dot{x}|z|^n + A\dot{x} \quad (3.4)$$

Where  $x$  is the displacement in MR damper as shown in Figure 3.2.

By adjusting the parameters  $\gamma$ ,  $\beta$ , and  $A$  of the model, one can control the linearity in the unloading and the smoothness of the transition from the preyield to the postyield region. In addition, the force

$f_0$  due to the accumulator can be directly incorporated into this model as an initial deflection  $X_0$  of the linear spring  $k_0$ .

A set of parameters was determined to fit the response of the Bouc-Wen model to the experimentally measured response of the MR damper (2.5 Hz sinusoidal displacement and a constant applied voltage of 1.5 V). The parameters for the model in Equation (3.3) and Equation(3.4) were chosen to be as illustrated in table 3.3.

*Table 3.2: Values of parameters used in Bouc-Wen Model [51]*

Parameter	Value	Parameter	Value
$\alpha$	880 N/cm	$\beta$	100 cm <sup>-2</sup>
$C_0$	50 N.s/cm	n	2
$K_0$	25 N/cm	A	120 N/cm
$\gamma$	100 cm <sup>-2</sup>	$X_0$	3.8 cm

The Bouc-Wen model could be simulated in MATLAB/Simulink using given equations and parameters. Since this model is a bit complicated, subsystems are employed so that the simulation would be cleaner and easier to understand.

The evolutionary variable,  $z$ , is comprised of three elements as follow:

$$\dot{Z} = Z1+Z2 +Z3 \quad (3.5)$$

Where

$$Z1 = -\gamma|\dot{x}|z|z|^{n-1} \quad (3.6)$$

$$Z2 = \beta \dot{x} |z|^n \quad (3.7)$$

$$Z3 = A \dot{x} \quad (3.8)$$

Z1 could be simulated as shown in Figure 3.7, in which two inputs of the subsystem are z and the displacement, x, and the output is the first part of the equation (3.5), Z1.

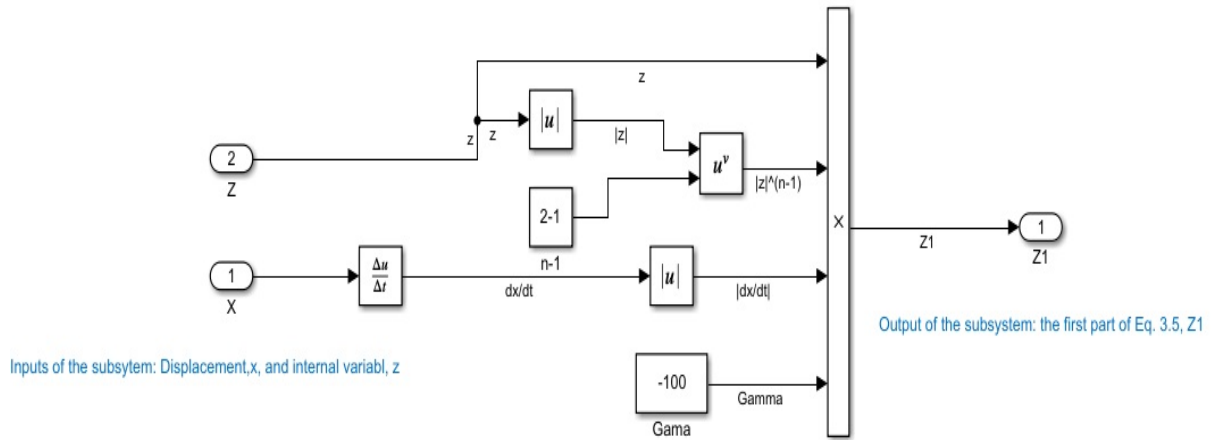


Figure 3.7: Simulink Subsystem for Generating Z1 Based on Equation (3.6)

Z2 could be simulated as shown in Figure 3.8, in which two inputs of the subsystem are z and displacement, x, and the output is the second part of the equation (3.5), Z2.

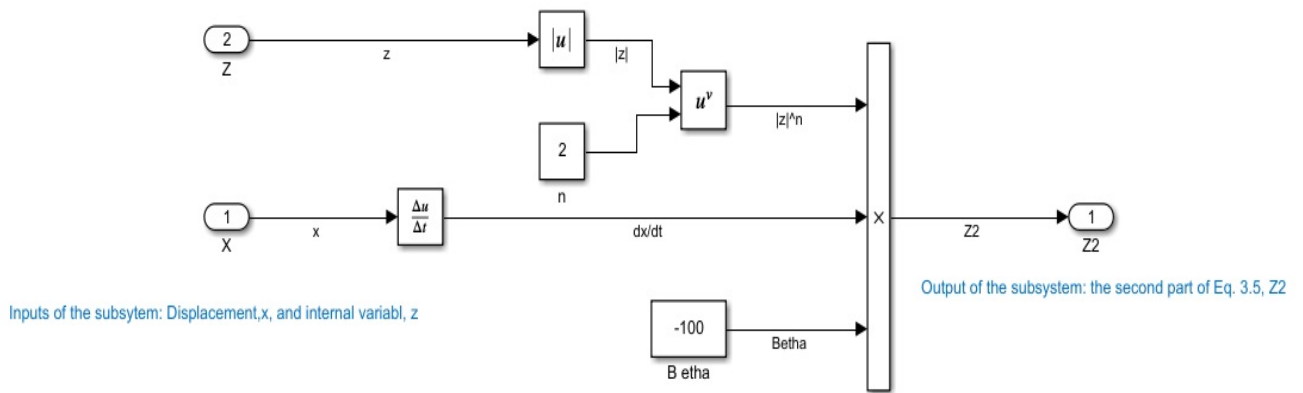


Figure 3.8: Simulink Subsystem for Generating  $Z_2$  Based on Equation (3.7)

$Z_3$  could be simulated as shown in figure 3.9, in which the input of the subsystem is the displacement,  $x$ , and the output is the first part of the equation (3.5),  $Z_3$ .

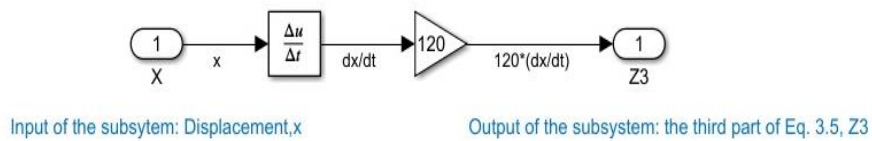


Figure 3.9: Simulink Subsystem for Generating  $Z_3$  Based on Equation (3.8)

Using these three subsystems, we can calculate the value of  $z$  by the simulation shown in Figure(3.10). The input of this subsystem is displacement,  $x$ , and the output is  $Z$ .



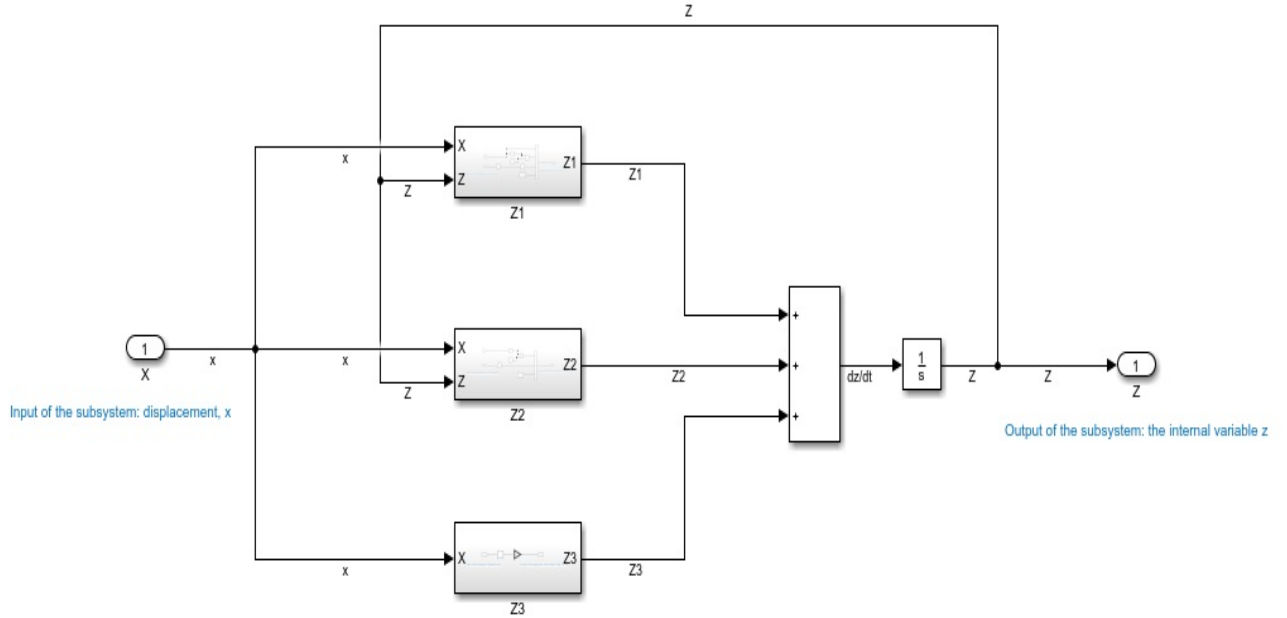


Figure 3.10: Simulink Subsystem for Generating Z Based on Equation (3.5)

likewise, the delivered force includes three parts as follows:

$$F = F1 + F2 + F3 \quad (3.9)$$

Where

$$F1 = c_0 \dot{x} \quad (3.10)$$

$$F2 = k_0(x - x_0) \quad (3.11)$$

$$F3 = \alpha z \quad (3.12)$$

F1, F2, and F3 could be calculated by the simulation subsystems shown in Figure (3,11), Figure(3.12), and Figure (3.13) respectively.

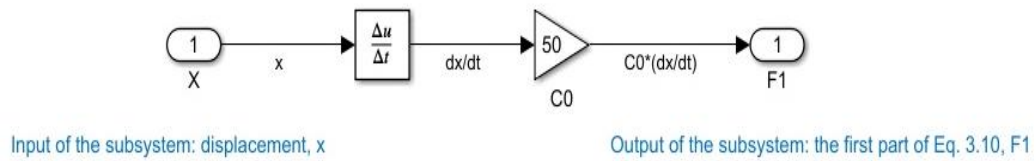


Figure 3.11: Simulink Subsystem for Generating  $F1$  Based on Equation (3.10)

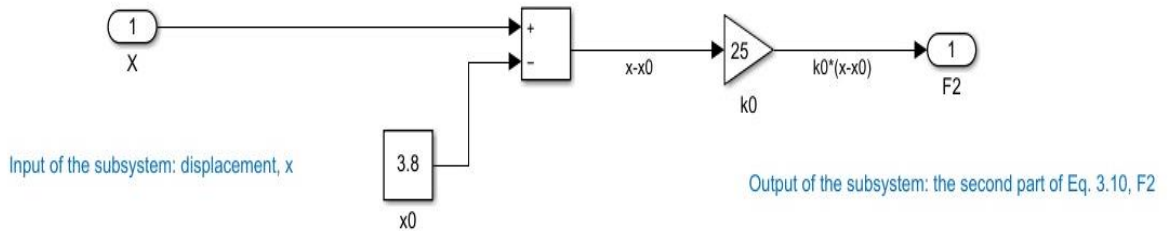


Figure 3.12: Simulink Subsystem for Generating  $F2$  Based on Equation (3.11)

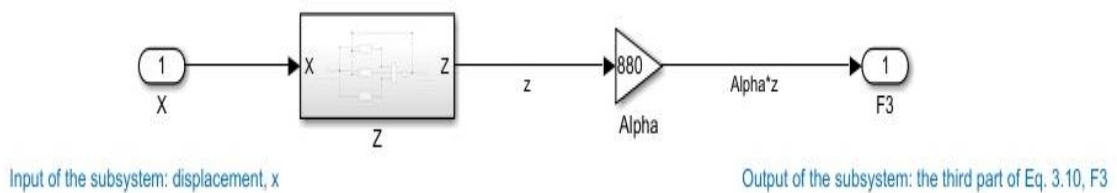


Figure 3.13: Simulink Subsystem for Generating  $F3$  Based on Equation (3.12)

Finally, the Bouc-Wen model could be modeled as illustrated in Figure (3.14).

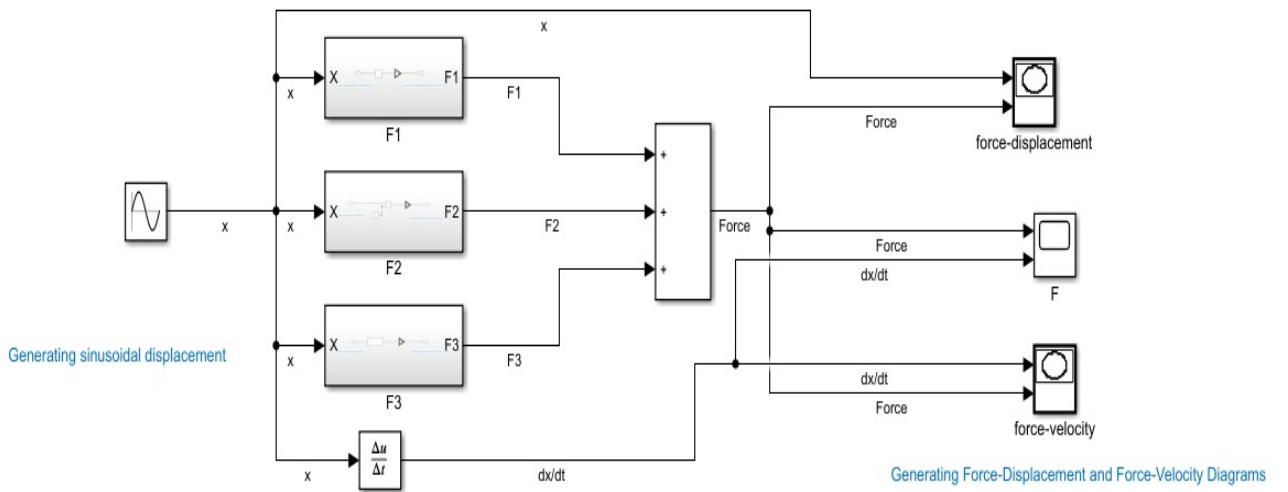


Figure 3.14: Simulation of the Bouc-Wen Model in MATLAB/Simulink

The results of the simulated Bouc-Wen model are shown in Figure (3.15) and Figure (3.16).

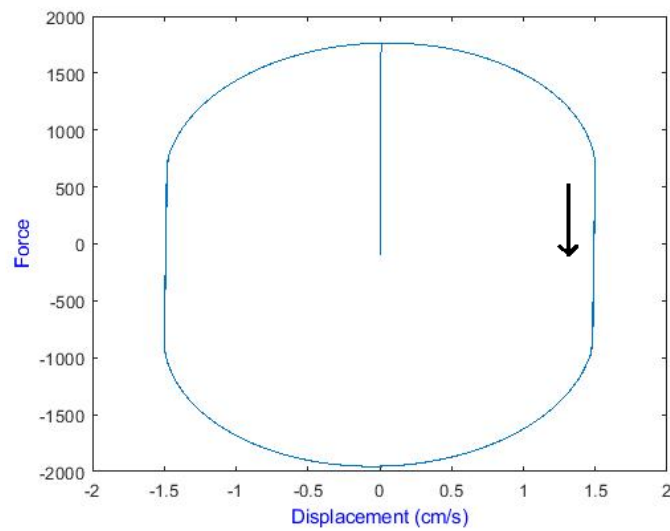


Figure 3.15: Displacement-Force diagram obtained from Bouc-Wen Model

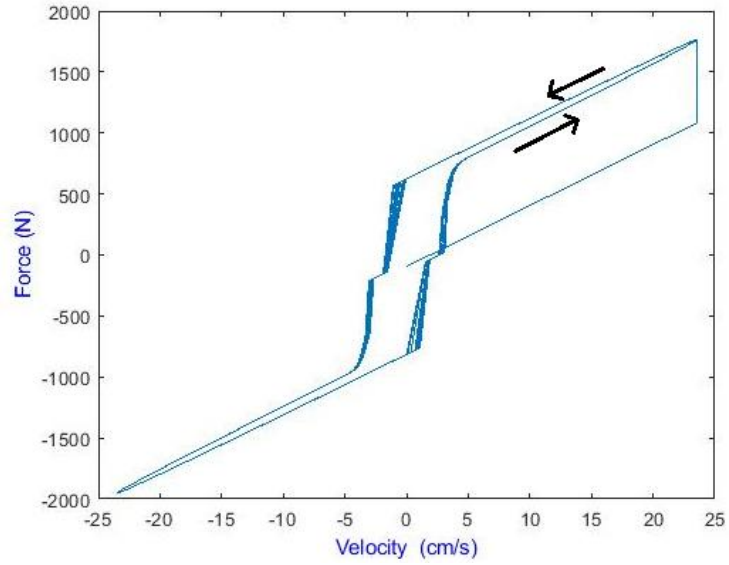


Figure 3.16: Velocity-Force diagram obtained from Bingham Model.

Compared to the experimental data, the Bouc-Wen model predicts the force-displacement behavior of the damper well and displays force-velocity behavior that is more in line with the experimental data. However, the BoucWen model behaves similarly to the Bingham model in the region where the velocity and acceleration are opposite and the magnitude of the velocity is small, as it does not roll off in this region.

### 3.3 Modified Bouc-wen:

Modified Bouc-Wen model was proposed by Spencer [51]. The force in this system is given by  $F_{MR}$  which represents the damping force and is predicted as follows:

$$f_{MR} = c_1 \dot{y}_b + k_{1B}(x_d - x_0) \quad (3.13)$$

$$\dot{z} = -\gamma |\dot{x}_b - \dot{y}_b| |z|^{n-1} - \beta (\dot{x}_b - \dot{y}_b) |z|^n + A(\dot{x}_b - \dot{y}_b) \quad (3.14)$$

$$\dot{y}_b = \frac{1}{c_0 + c_1} \{ \alpha z + c_0 \dot{x}_d + k_1(x_d - y_d) \} \quad (3.15)$$

Where  $y_b$  is the internal displacement of the MR damper;  $x_d$  is the damper displacement in the x-direction;  $x_0$  is the initial deflection of the damper;  $z$  is a variable that accounts for the historical dependence of the response, and  $\gamma$  is the constant for the model. The model parameters are given as:

$$\alpha = \alpha_a + \alpha_b u \quad (3.16)$$

$$c_1 = c_{1a} + c_{1b} u \quad (3.17)$$

$$c_0 = c_{0a} + c_{0b} u \quad (3.18)$$

where  $u$  is the output of the first-order filter as:

$$\dot{u} = -\eta(u - v) \quad (3.19)$$

There are 14 parameters in this model, which could be determined by comparing experimental data and results from the model. Spencer evaluated the performance of a fixed-orifice damper filled with an MR fluid. The MR fluid was VersaFlo MRX-135GD developed by Lord Corp. The MR damper was excited by a 2.5 HZ sinusoid with an amplitude of 1.5 cm with different voltage levels and used a constrained nonlinear optimization to obtain the parameters, which are shown in Table 3.3.

*Table 3.3: Value of Parameters used in Spencer Model [51]*

Parameter	Value	Parameter	Value
$\alpha_a$	140 N/cm	$\beta$	363 cm <sup>-2</sup>
$C_{0a}$	21 N.s/cm	$n$	2
$C_{0b}$	3.5 N.s/cm.V	$A$	301 N/cm
$C_{1a}$	283 N.s/cm.V	$X_0$	14.3 cm
$C_{1b}$	2.95 N.s/cm.V	$\eta$	190 s <sup>-1</sup>
$K_1$	5.00 N/cm	$\alpha_b$	695 N/cm.V
$\gamma$	363 cm <sup>-2</sup>	$K_0$	46.9 N/cm

To simulate the Spencer model, first, we simulate  $\alpha$ ,  $c_1$ ,  $c_0$ , and  $u$  by using four subsystems shown in Figure (3.7), Figure (3.8), Figure (3.9), and Figure (3.10), respectively.

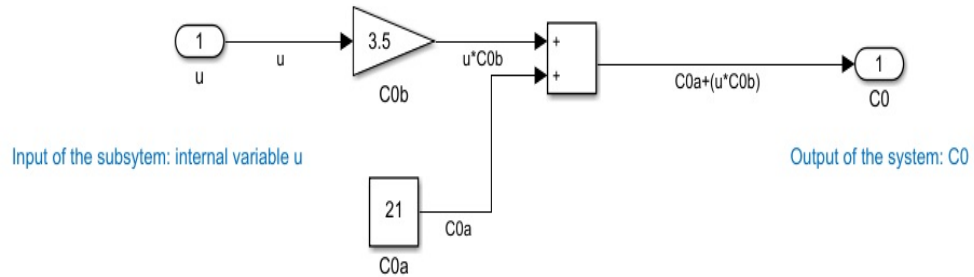


Figure 3.17: Simulink Subsystem for Generating  $C_0$  Based on Equation (3.18)

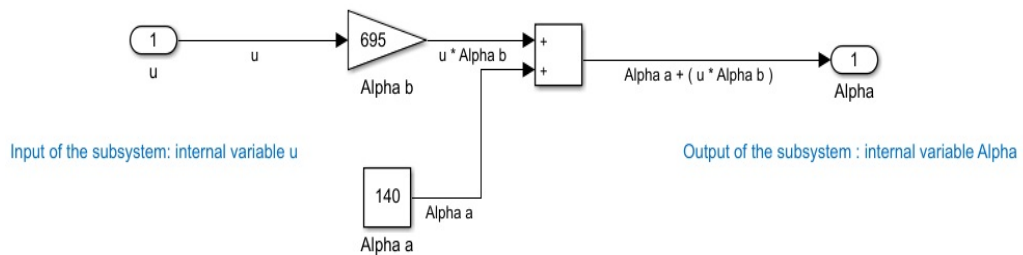


Figure 3.18: Simulink Subsystem for Generating  $\alpha$  Based on Equation (3.16)

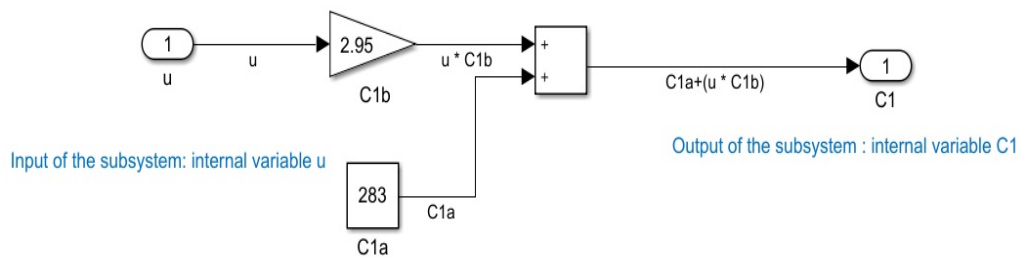


Figure 3.19: Simulink Subsystem for Generating  $C_1$  Based on Equation (3.17)

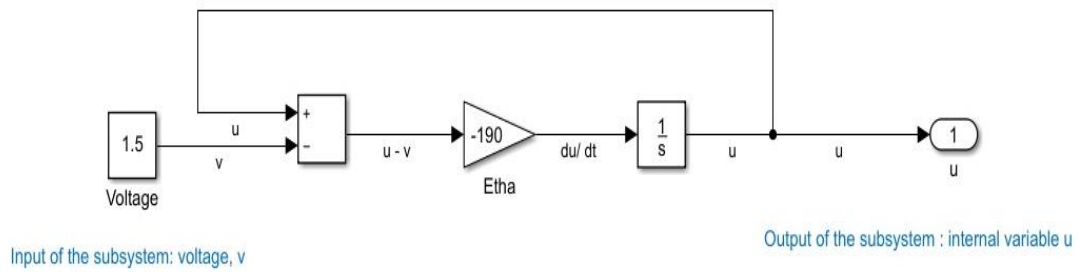


Figure 3.20: Simulink Subsystem for Generating  $u$  Based on Equation (3.19)

Just like the bouc-wen model, the variable evolution,  $z$ , needs to be simulated for the Spencer model which consists of three parts and will be simulated as shown in Figure (3.21), Figure (3.22), and Figure (3.23), respectively.

$$Z = Z1 + Z2 + Z3 \quad (3.20)$$

Where

$$Z1 = -\gamma|\dot{x}_b - \dot{y}_b|z|z|^{n-1} \quad (3.21)$$

$$Z2 = -\beta(\dot{x}_b - \dot{y}_b)|z|^n \quad (3.22)$$

$$Z3 = +A(\dot{x}_b - \dot{y}_b) \quad (3.23)$$

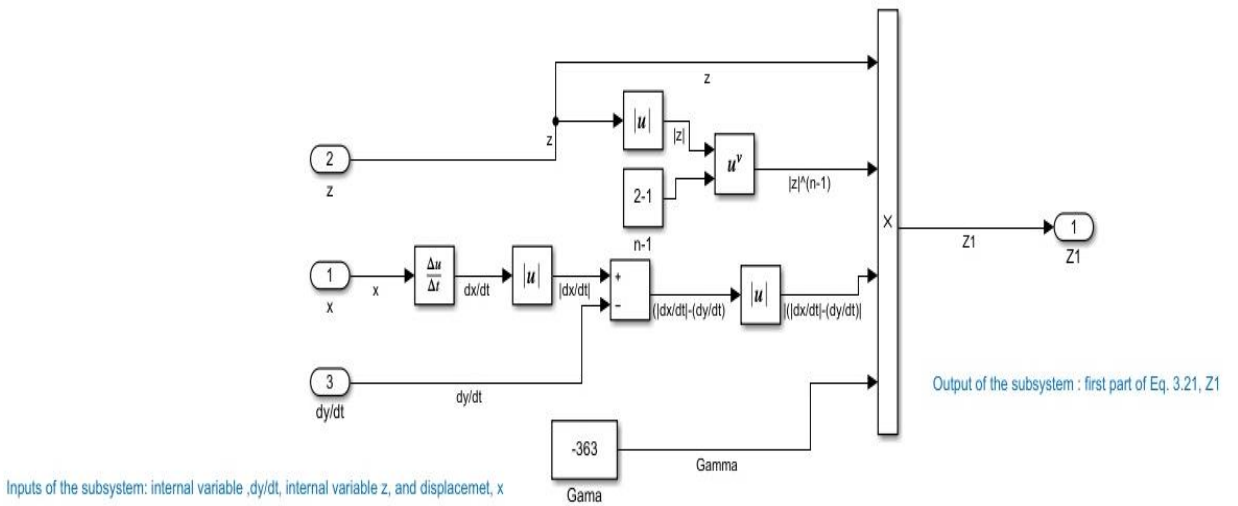


Figure 3.21: Simulink Subsystem for Generating  $Z_1$  Based on Equation (3.21)

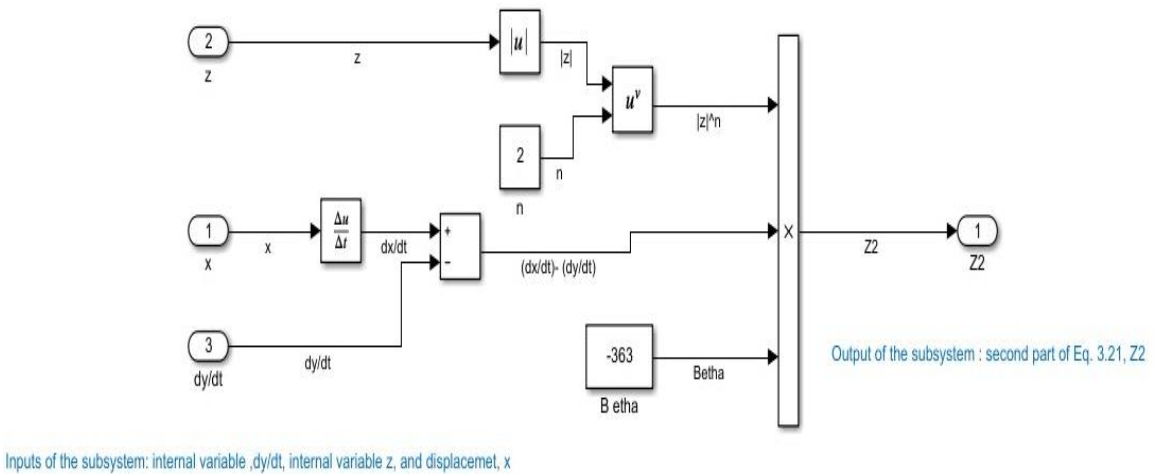


Figure 3.22: Simulink Subsystem for Generating  $Z_2$  Based on Equation (3.22)



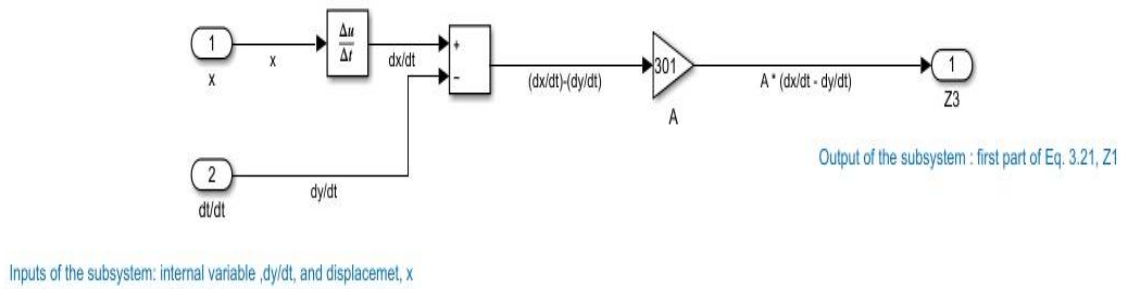


Figure 3.23: Simulink Subsystem for Generating Z3 Based on Equation (3.23)

Inputs are displacement,  $x$ ,  $\dot{y}$ , and  $z$ . and the outputs are three parts of the variable  $z$  which will be simulated based on equation (3.14) as show in the figure (3.24).

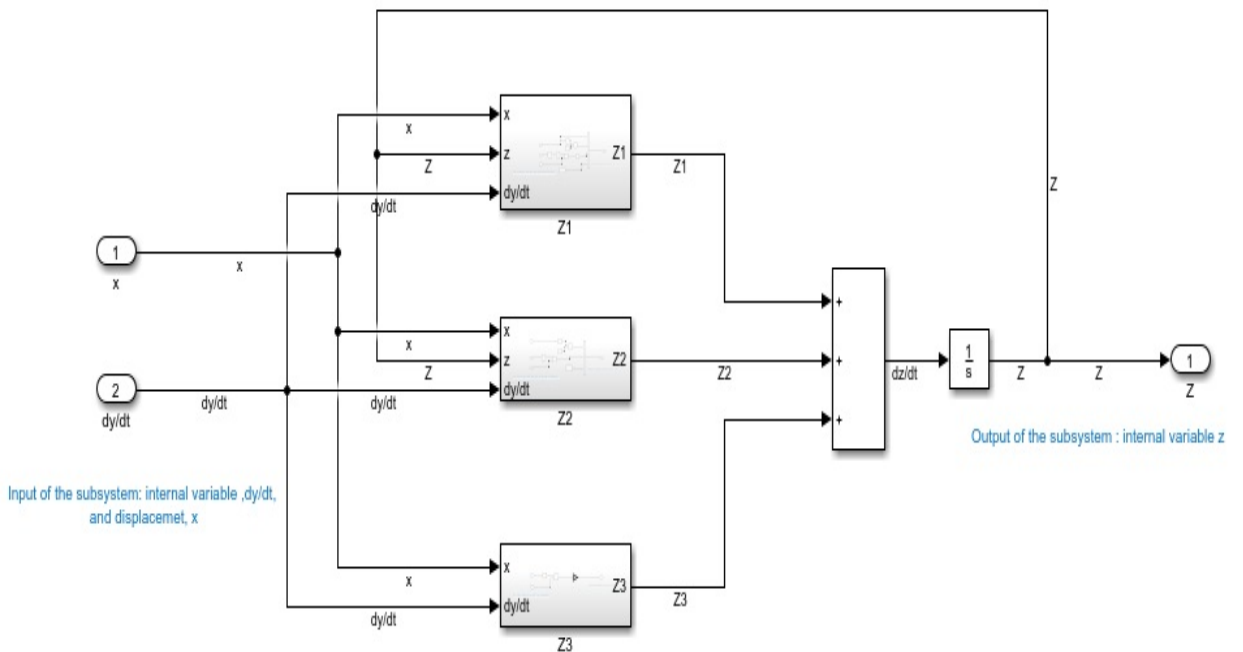


Figure 3.24: Simulink Subsystem for Generating Z Based on Equation (3.14)

Equation (3.15) is simulated in another subsystem which is depicted in figure (3.25)

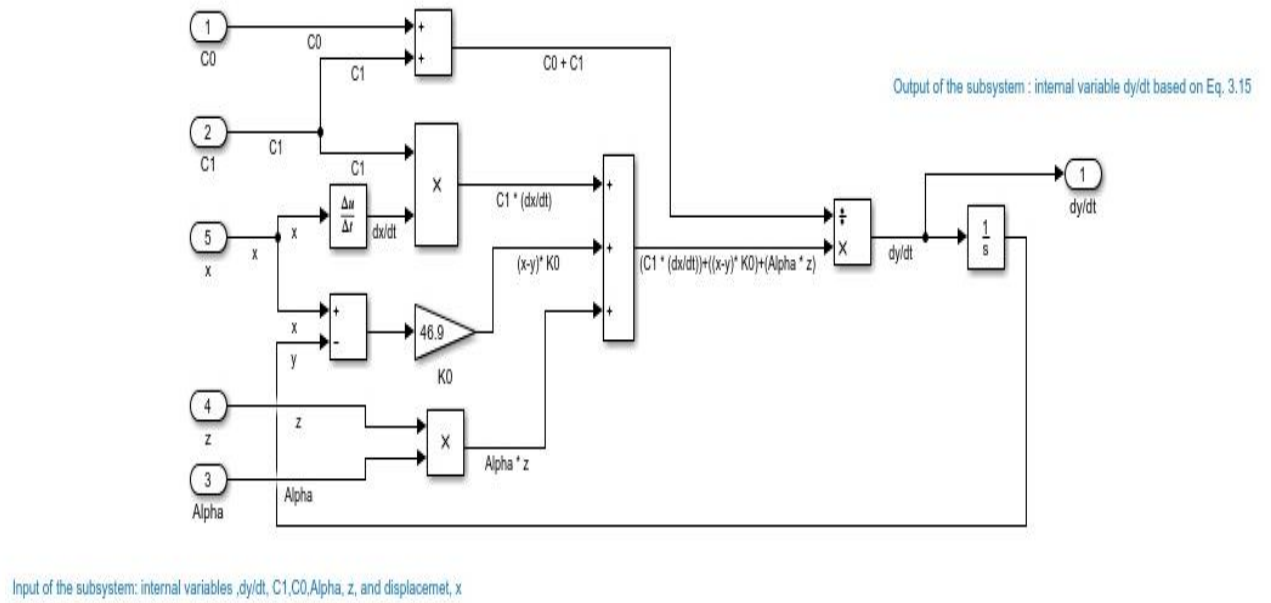


Figure 3.25: Simulink Subsystem for Generating  $\dot{y}_b$  Based on Equation (3.15)

The last subsystem includes reviewed subsystems to calculate the  $\dot{y}_b$ , and  $c_1$ , which will be used to evaluate the delivered force based on equation (3.13), illustrated in Figure (3.26).

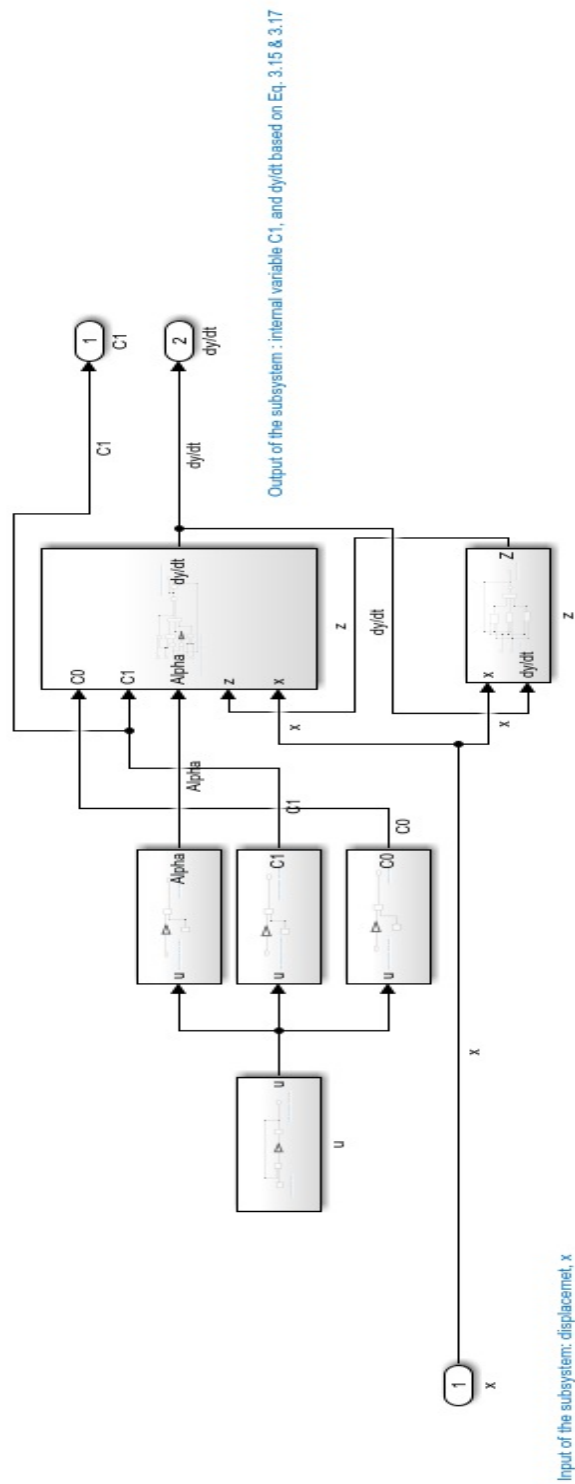


Figure 3.26: Simulink Subsystem for Generating the Final  $\dot{y}_b$  and  $C_1$  Based on Equations (3.15) and (3.17)

The final simulation of the Modified Bouc-Wen model, which is known as the “Spencer model”, is illustrated in figure (3.27) and the final results are shown in Figure (3.28) and Figure(3.29).

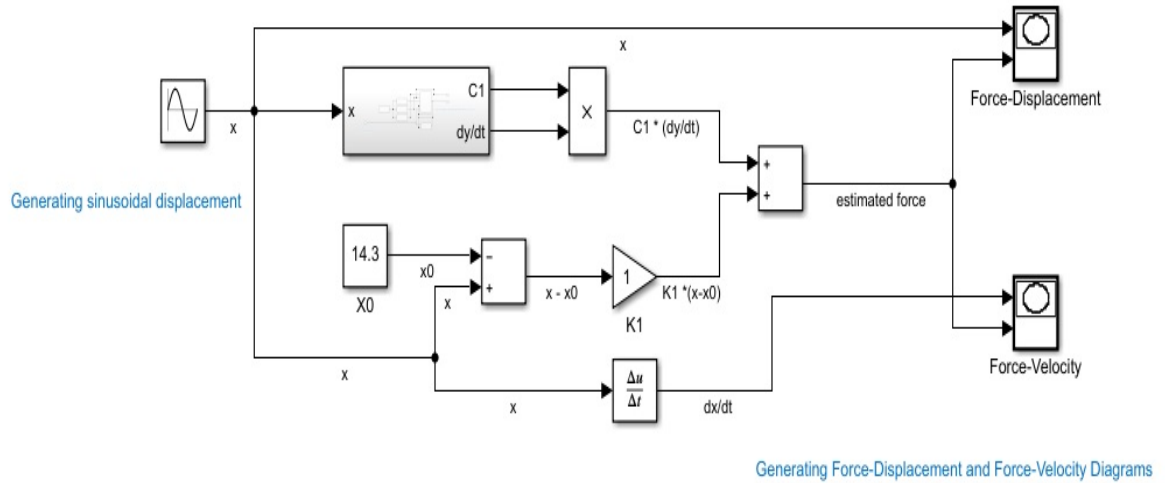


Figure 3.27: Simulation of the Modified Bouc-Wen, Spencer Model, in MATLAB/Simulink

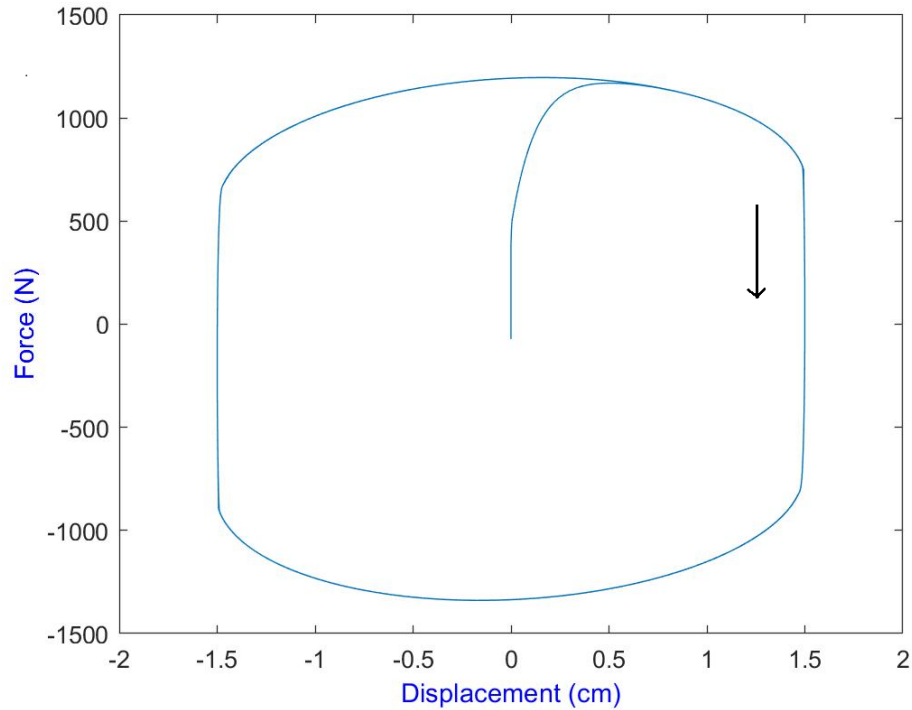


Figure 3.28: Displacement-Force diagram obtained from Modified Bouc-Wen, Spencer Model

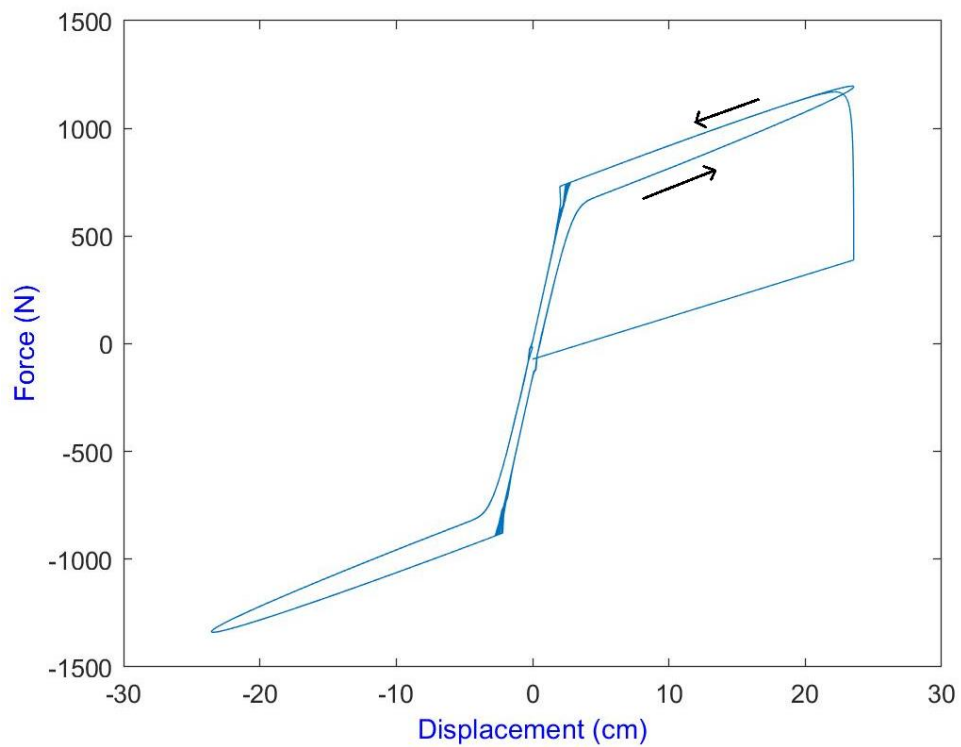
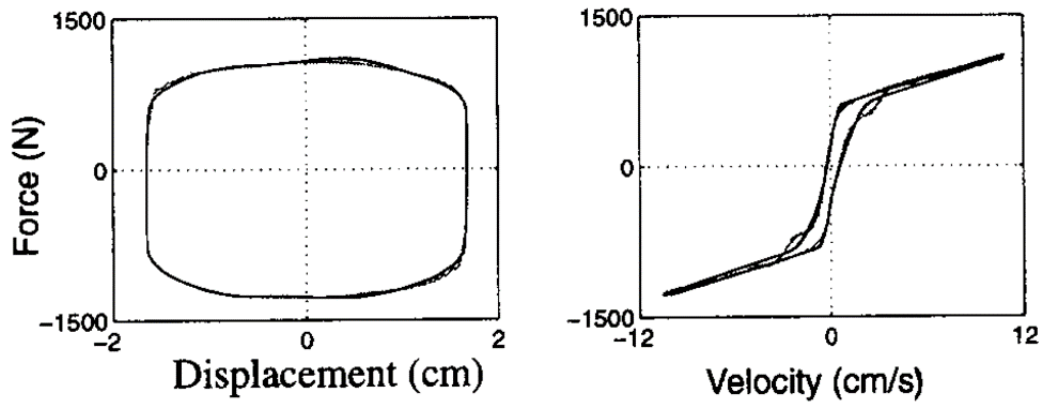


Figure 3.29: Velocity-Force diagram obtained from Modified Bouc-Wen, Spencer Model

Force-Displacement and Force-Velocity diagrams obtained from the experimental data are shown in Figure (3.30), which are quite similar to the diagrams obtained from the Spencer model, illustrated in Figure (3.28) and Figure (3.29).



*Figure 3.30: Displacement-Force and Velocity-Force Diagrams Obtained From Experimental Data [51]*

Consequently, by obtaining the parameters through experimental data for each MR damper, the Spencer model could be used to simulate nonlinear viscoelastic behaviour of the damper.

### **3.4 Invers Model of MR Dampers**

When it comes to designing a control system for a semi-active suspension system, an inverse model of the damper is commonly being employed. In this approach, as shown in Figure (3.31), a control algorithm is used to generate the demanded damping force, and the inverse model of the MR damper will generate the input voltage to emulate the demanded damping force.

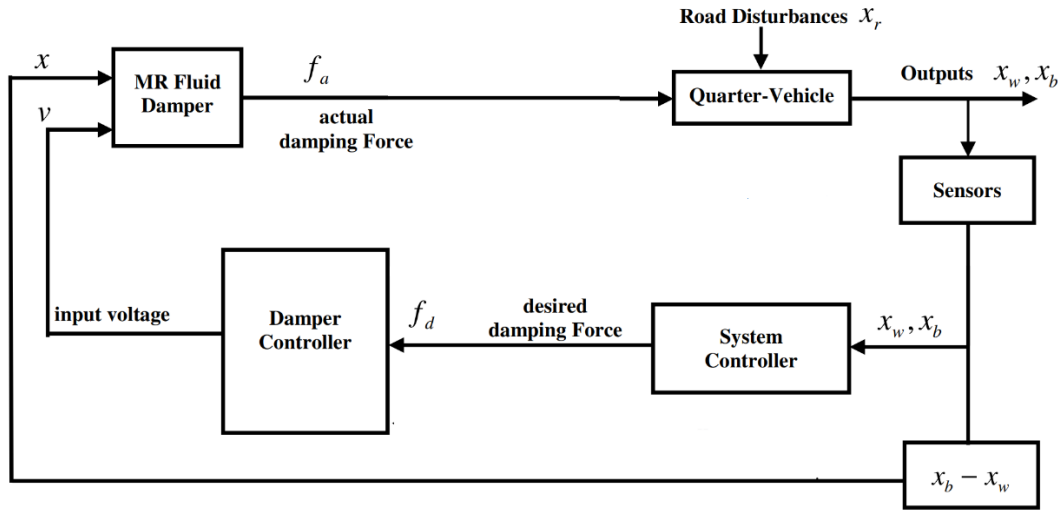


Figure 3.31: Semi-Active Control System for a Vehicle Suspension Integrated With MR Dampers

It is also critical to remember that MR dampers can only produce a dissipative control force, and this should be considered in the simulation. Besides, the provided damping coefficient of each damper is limited, which varies based on properties of the damper like size, fluid, and etc. With these limitations in mind, an inverse dynamics model can develop the required input voltage or current, so the MR damper can produce the forces as close to the demanded ones as possible. These limitations are illustrated in Figure (3.32), where  $b_{min}$  and  $b_{max}$  are the minimal and maximal damping coefficients of the MR damper. [46]

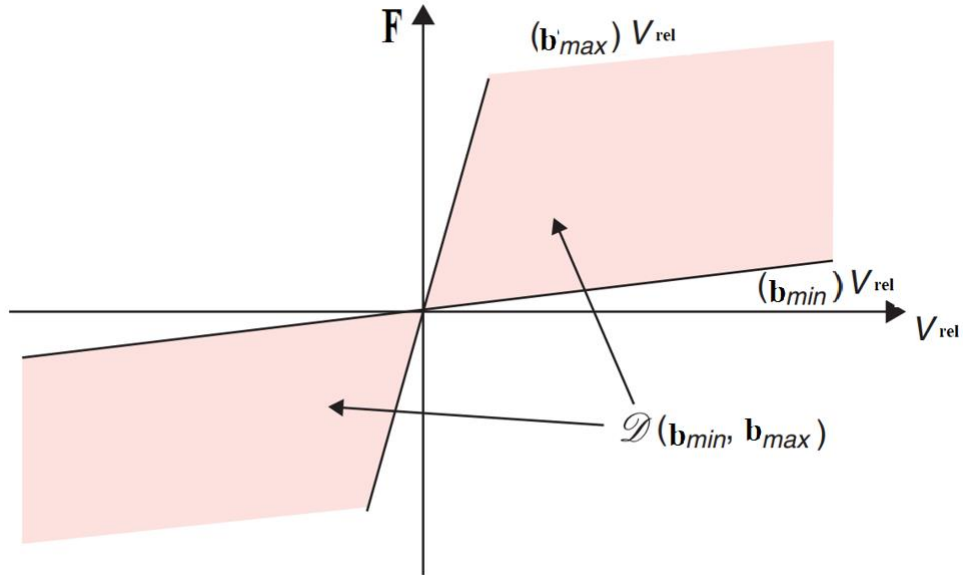


Figure 3.32: Dissipative Domain, Graphical Illustration [3]

As the focus of this study is to design a control system that can improve the performance of a semi-active suspension system, optimal damping force will be achieved by the control algorithm, and then dissipative constraints of an MR-damper will be taken into account to ensure that the required damping force is achievable through adjusting the input voltage to the MR-damper. In fact, when the required damping force does not fall within the dissipative domain, shown in Figure (3.32), it should be considered the minimum for simulation process. A MATLAB code, shown in Figure (3.33), will be used to fit the semi-active control constraints. It needs to be noted that the minimum damping force of the damper is considered a fixed one that cannot be adjusted, and the controllable damping force would be adjusted within the range of zero and the difference between the maximum and the minimum amount of damping factor. This is the approach that is commonly being used in the literature in which the main focus is to design a control system, like [52, 53, 54].



```

function fsemi = fcn(u,vrel)
% fsemi is the actual damping force
% u is desired damping force
% vrel is relative velocity of body and wheel across the suspension
% bsemi is the damping coefficient
% fsemi and bsemi will be zero at zero relative velocity
if (vrel == 0)
    fsemi = 0;
    bsemi = 0;
% if vrel and u are both positive, delivered damping force will be zero
elseif (vrel > 0)
    if (u >= 0)
        fsemi = 0;
        bsemi = 0;
% calculating the damping force, when vrel is positive and u is negative
    else
        bsemi = abs(u/vrel);
        if bsemi >= 4000
            bsemi = 4000;
        end
        fsemi = -bsemi * vrel;
    end
% if vrel and u are both negative, delivered damping force will be zero
else
    if (u <= 0)
        fsemi = 0;
        bsemi = 0;
    else
% calculating the damping force, when vrel is negative and u is positive
        bsemi = abs(u/vrel);
        if bsemi >= 4000
            bsemi = 4000;
        end
        fsemi = -bsemi * vrel;
    end
end
end

```

*Figure 3.33: Dissipative Domain, MATLAB Code*

Where  $v_{rel}$  is the relative velocity of the body and wheel across the suspension;  $u$  is desired damping force;  $f_{semi}$  is the actual damping force;  $b_{semi}$  is the damping coefficient, and  $b_{max}$  is the maximum possible damping coefficient. As illustrated in the matlab code, at zero relative velocity, an MR damper cannot produce any damping force and, therefore,  $f_{semi}$  and  $b_{semi}$  will be zero. Additionally, when desired damping force,  $u$ , and relative velocity,  $v_{rel}$ , are both positive, or negative, they will be outside the dissipative domain, shown in Figure 3.32, and the  $f_{semi}$  and

$b_{semi}$  will be zero. Therefore, the controllable damping force will be generated if the  $u$  and  $v_{rel}$  have different signs, but the maximum damping coefficient must be considered. For this reason, damping coefficient is determined by dividing absolute damping force by relative velocity,  $abs(u/v_{rel})$ , and if the result is greater than the maximum damping coefficient, the value would be assumed to be  $b_{max}$ . The final damping force will be calculated by multiplying the relative velocity by the damping coefficient with a negative sign because the  $b_{semi}$  is calculated by dividing the absolute value of  $u$  by  $v_{rel}$ .

## CHAPTER 4

### ROAD PROFILES

The road is the most powerful source of excitation for the vehicle. The vertical behaviour of the vehicle is dependent on many factors, many of them associated with the road: length, angle, shape, frequency of irregularities, etc. Every road is characterized by irregularities (small ups and downs) that may be random or periodic [55]. In reality, most roads have a random profile or irregularities. Therefore, to study the suspension system behaviour accurately, this research uses four different road signals. These include Step signal, sinusoidal signal, bump signal, and road type C profile input according to international standards ISO/TC108/SC2N67 [56], which represent the real road profiles.

#### 4.1 Step Road Input

Step input signal is a basic input to simulate the response of the suspension system. It simulates a very intense force for a very short time. The suspension system simulation has been carried out for on-road as well as off-road conditions. The maximum excitation that a vehicle may undergo is during an off-roading activity. Therefore, 70 mm (0.07 m) step is considered for this project, which is the acceptable limit of displacement for an automotive suspension system [57]. As the derivative of a step unit is infinitive, a filter has been employed to prevent this issue which is illustrated in Figure 4.1. The resulted step unit which is considered for the simulation of modelled suspension system in this study, is depicted in Figure 4.2.



*Figure 4.1: Simulink Block to generate Step input*

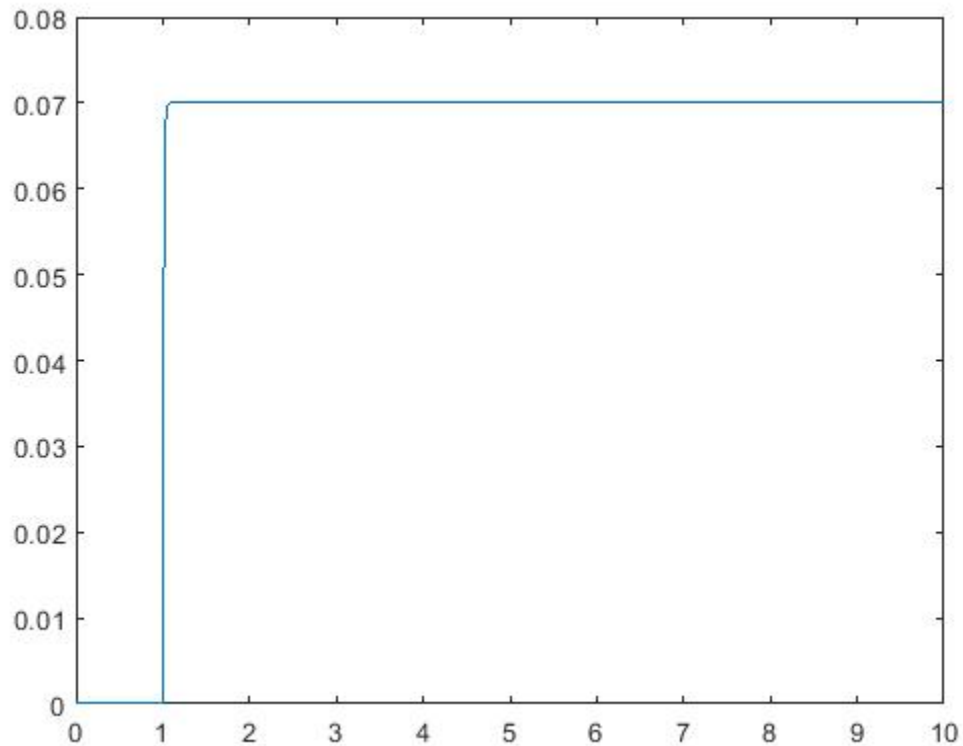


*Figure 4.2: Step Road Input for Plant Model Simulation*

## **4.2 Sine Road Input**

Periodic pavement fluctuations can be simulated using a sine wave input signal. By this input, the car's suspension elastic resilience can be tested while it drives on a periodic-wave surface.

Sine input pavement test is made by every automotive industry before a new vehicle drives on the road [58]. This type of input is commonly used in the literature to evaluate the performance of the suspension system like [59], [60]. Sine wave input of amplitude 70 mm (0.07 m) and frequency 6.28 rad/sec (1 HZ) is given as road input. Figure 4.3 shows the sine road input considered for the simulation of the modelled suspension system.

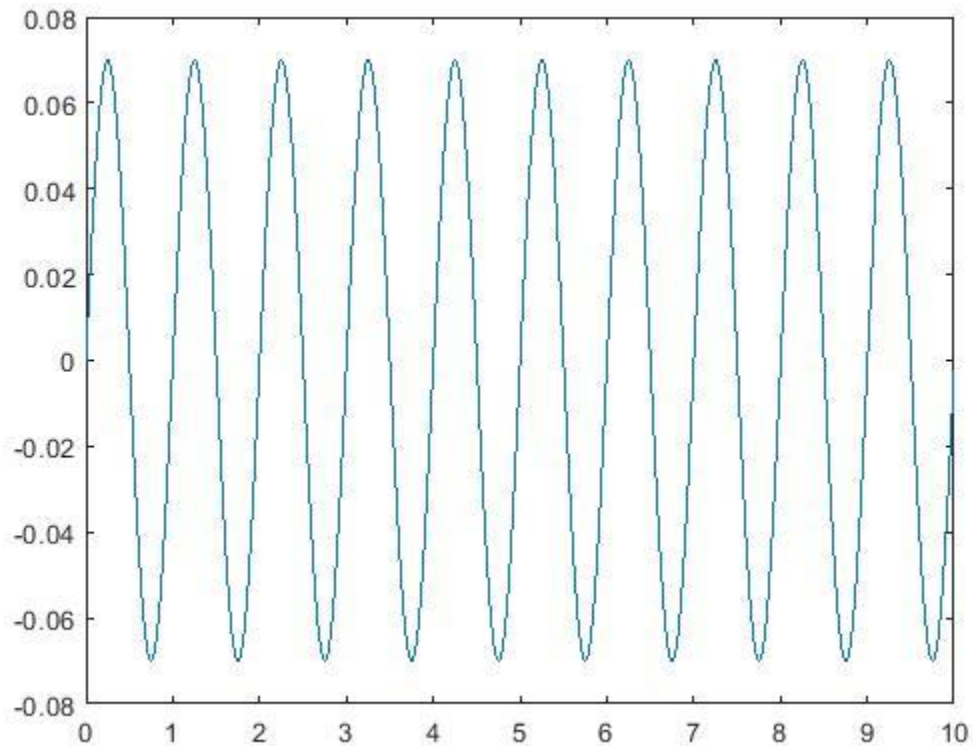


*Figure 4.3: Sine Road Input for the Plant Model Simulation and Used Simulink Blocks*

### **4.3 Bump Input**

The bump input refers to a bump on the road which might be viewed by a vehicle's suspension system. The interest of this time input is that it is very likely to realize in practice and to interpret, and since it can represent a range of suspension behaviours. Figure 4.4 illustrates a typical bump test profile.

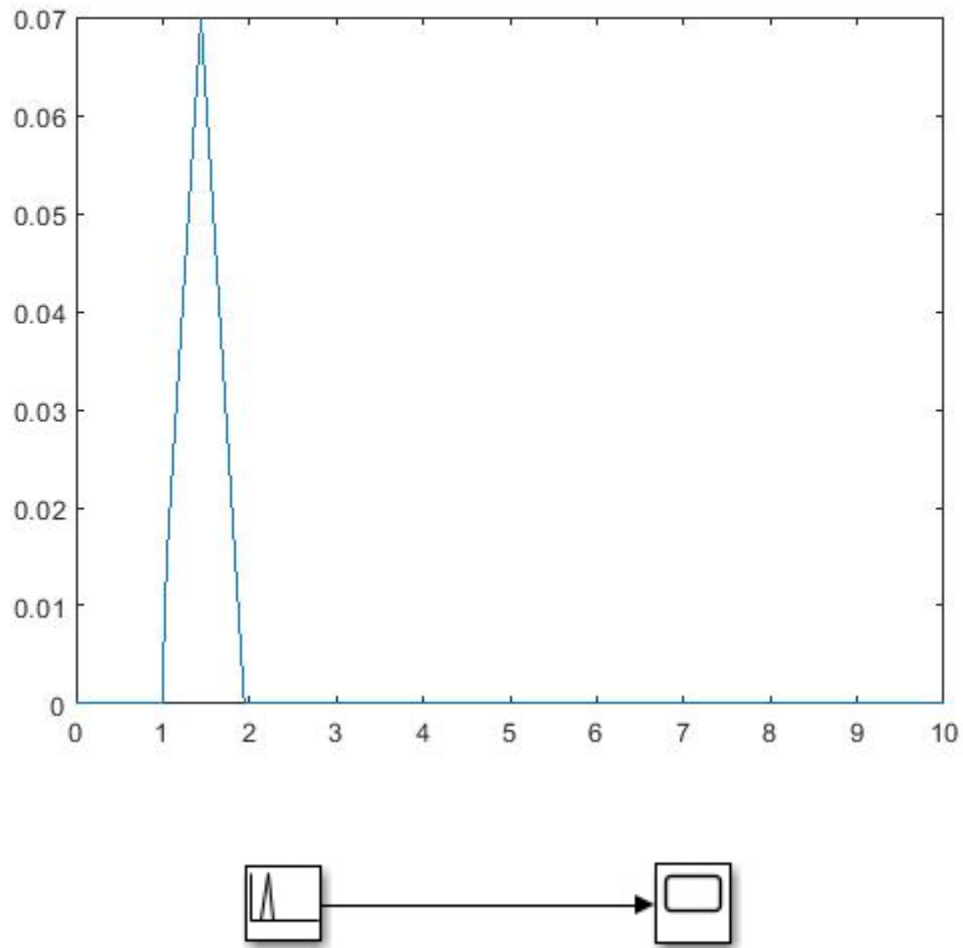


Figure 4.4: Bump Input for the Plant Model Simulation and Used Simulink Blocks

#### 4.4 Road Type C Input

The road roughness of vehicles at constant speeds is considered as a stochastic process that follows Gaussian distribution, and it is not possible to accurately model it with mathematical relations. The vehicle speed power spectral density is a constant, so it can be simply transformed to the road roughness time domain model by using the definition and statistical characteristic of white noise. A number of studies have used this method, such as [59]. An example for the creation of white noise by using MATLAB/ Simulink is shown as below: (noise power is 1, sample time is 0.1)

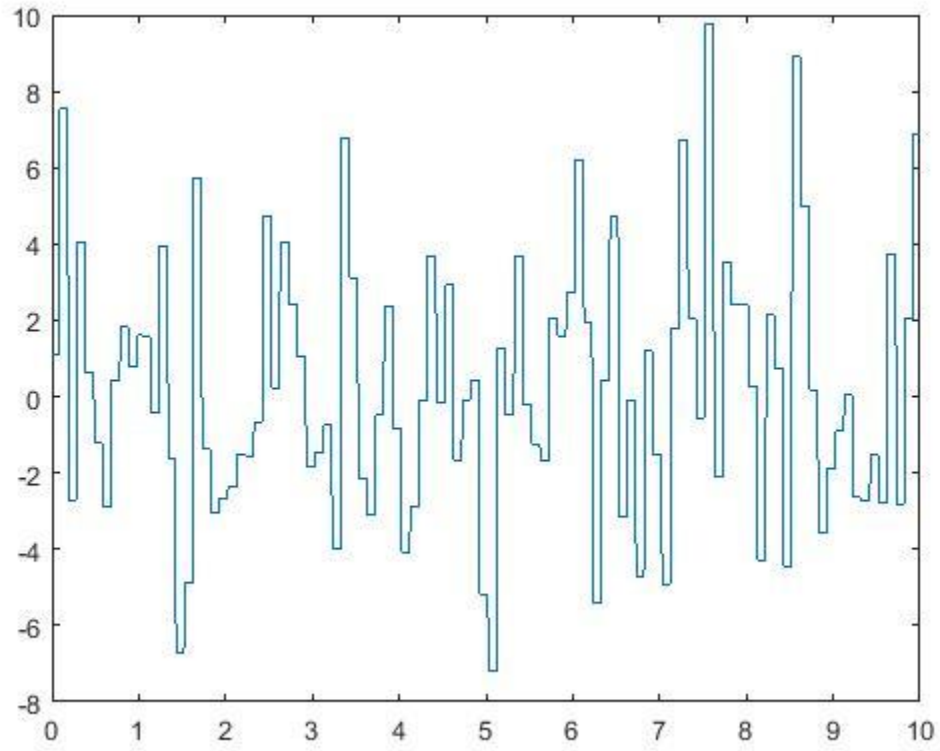


Figure 4.5: White noise input signal

The transformation of white noise road input signal can perfectly simulate the actual pavement condition. When the road power spectral density is used to describe its statistical properties, the input can have a random character.

Power spectral density (PSD) is a very useful tool for analyzing stationary road roughness. Road roughness can be viewed as a static process in the space domain when a car moves at a constant velocity  $u$ , and the PSD of the road disturbance input can be expressed by:

$$G_q(n) = G_q(n_0) \left( \frac{n}{n_0} \right)^{-w} \quad (4.1)$$

Where  $G_q(n)$  is the road PSD;  $n$  is the spatial frequency. The reference spatial frequency  $n_0$  can be defined by:

$$n_0 = 0.1 \left( \frac{\text{cycle}}{m} \right) \quad (4.2)$$

$G_q(n)$  is the road roughness coefficient, which is the value of PSD at the reference spatial frequency  $n_0$ , and represent different grades of road,  $w$  is called waviness and indicates whether the road has more long wavelengths ( $w$  is large) or short wavelengths ( $w$  is small). The waviness  $w$  is found within the range  $1.75 \leq w \leq 2.25$ , generally  $w = 2$ . When introduce spatial angular frequency  $\Omega$ :

$$\Omega = 2\pi n \quad (4.3)$$

Equation (4.1) can be written as:

$$G_q(W) = G_q(W_0) \left( \frac{W}{W_0} \right)^{-w} \quad (4.4)$$

Where  $G_q(W)$  is the road PSD,  $\Omega$  is the spatial angular frequency (rad/m).  $W_0$  is the reference spatial angular frequency and is defined by:

$$W_0 = 2\pi n_0 \quad (4.5)$$

$G_q(W_0)$  is also the road roughness coefficient, which is the value of PSD at the reference spatial angular frequency  $\Omega_0$ .  $w$  has been mentioned before and has the same definition.

When the vehicle drives at a constant velocity  $u$ , the relationship between the time frequency  $f$  and the vehicle forward velocity  $u$  is defined by:

$$f = u \times n \quad (4.6)$$

Derived from Equation (4.6), the PSD of ground displacement has the following general form:

$$G_q(f) = \frac{G_q(n_0) n_0^2 u}{f^2} \quad (4.7)$$

From the equation (4.7), we can get theoretic ground PSD under different frequencies.

The relationship between the spatial angular frequency  $\Omega$  (rad/m) and the angular velocity  $\omega$  (rad/s) can be defined as follows:

$$\omega = u\Omega \quad (4.8)$$

So, the road roughness in frequency domain can be described as the follow.



$$G_q(\omega) = G_q(\Omega)/u = G_q(\Omega_0)u/\omega^2 \quad (4.9)$$

However, it may be troubles at  $\omega = 0$ ,  $G_q(\omega) = \infty$ . An improved equation for PSD of road roughness in frequency domain is shown as

$$G_q(\omega) = G_q(\Omega_0)u/(\omega^2 + \omega_0^2) \quad (4.10)$$

Where  $\omega_0$  is the lowest cut-off angular frequency.

$$\Omega_0 = 2\pi f_0 = 2\pi un_0 \quad (4.11)$$

Equation (4.10) can be considered as a response of a first order linear system to white noise excitation.

Based on the theory of random vibration, the following relationship can be obtained.

$$G_q(\omega) = |H(\omega)|^2 S_w(\omega) \quad (4.12)$$

Where  $H(\omega)$  is the transfer function, and  $S_w$  is the PSD of white noise, where normally  $S_w(\omega) = 1$ . So from the equation (4.10) and (4.12) the transfer function  $H(\omega)$  can be described as:

$$H(\omega) = \frac{\sqrt{G_q(\Omega_0)u}}{\omega_0 + j\omega} \quad (4.13)$$

According to Laplace transform, the above equation can be written as:

$$H(s) = \frac{\sqrt{G_q(\Omega_0)u}}{\omega_0 + s} \quad (4.14)$$

The equation (4.14) can be viewed as the transfer function from white noise signal to road roughness. From the above equation, we can get the following equation:

$$\dot{z}_r(t) + \omega_0 z_r(t) = \sqrt{G_q(\Omega_0)u} w(t) \quad (4.15)$$

Where  $z_r(t)$  is the road roughness,  $w(t)$  is a white noise signal. Because  $\omega_0 = 2\pi f_0 = 2\pi un_0$ , the above equation can be shown as:

$$\dot{z}_r(t) + 2\pi n_0 z_r(t) = \sqrt{G_q(\Omega_0)} u_w(t) \quad (4.16)$$

From equation (4.16), the road roughness can be obtained. The numerical calculation for the road roughness was carried out by MATLAB/Simulink, as can be seen in Figure (4.6).

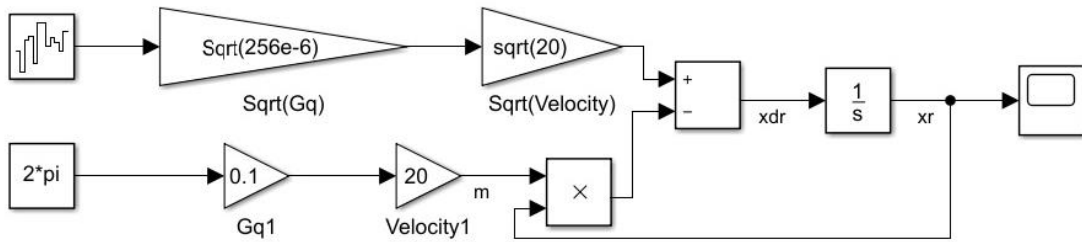


Figure 4.6: Simulink Block to generate Step input

Figure 4.7 shows the road input when vehicle drives at 20 m/s on Grade C road.

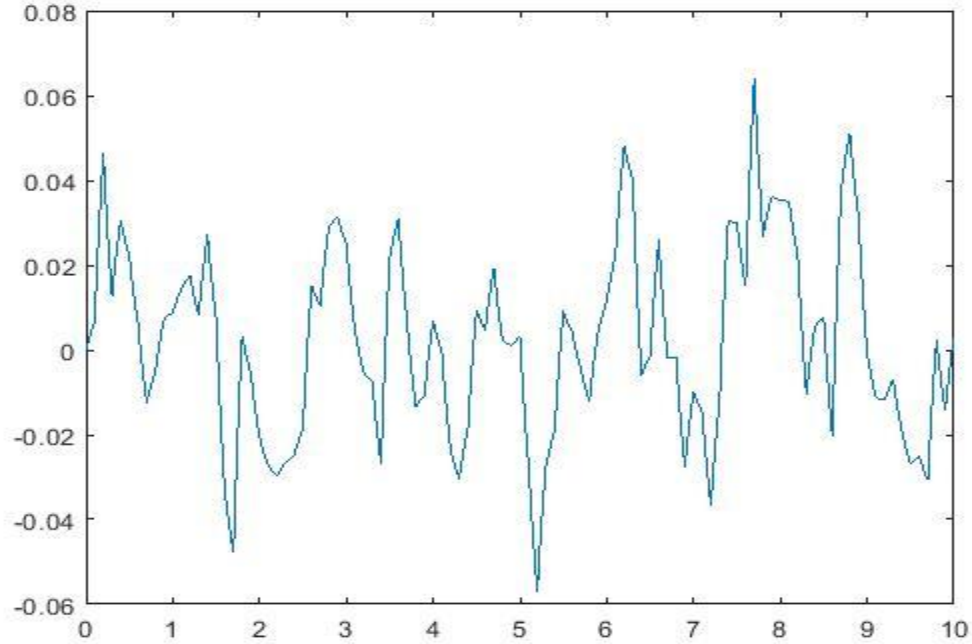


Figure 4.7: Road type c input for the plant model simulation

According to the international standard, there are eight road levels, which is from A to H, which A level is the best road level and H is the worst. The following form shows the reference changing with different road level.

Table 4.1 shows different road level's  $G_q(n_0)$

*Table 4.1: Eight Degree of Road Roughness [61]*

Road Level	$G_q(n_0)/(10^{-6}m^3)$ $(n_0 = 0.1 m^{-1})$
A	3.81
B	7.61
C	15.23
D	30.45
E	60.90
F	121.80
G	243.61
H	487.22

In this thesis, class C road is used as the road surface, but we can easy change road class by changing parameters used in the simulation.

## CHAPTER 5

### MATHEMATICAL MODELLING OF THE SUSPENSION SYSTEM

#### 5.1 Linearized Quarter Car Model

Since passive vehicle suspensions are inherently nonlinear, linearizations are often performed to ease in the modelling of components. A common method of modelling a simplified vehicle suspension utilizes a quarter vehicle model. Quarter vehicle models are typically comprised of linearized component dynamics and block masses.

Shown in Figure (5.1) is a conventional quarter car model. This model provides information on bounce mode only (vertical deflection). The majority of the current research studies on this topic utilize the quarter car model due to its simplicity and its ability to provide useful insight into the dynamics of the vehicle [62].

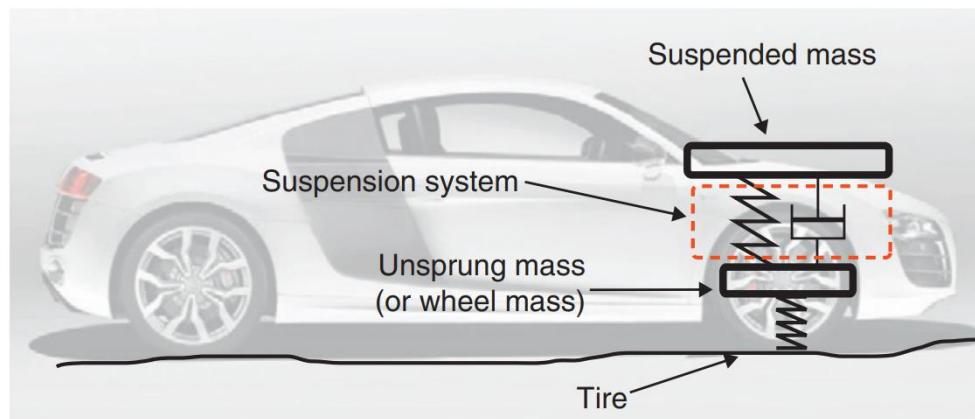


*Figure 5.1: Quarter-car Representation of a Suspension System in a Vehicle [3]*

Following assumptions need to be taken into account for modelling of suspension system:

- This system is a two-degree-of-freedom suspension system, as depicted in Figure 5.2, and assumed to be a linear system for a quarter car.
- The effect of minor forces is neglected to reduce complexity due to their minimal magnitude, for example, backlash in the body and movement, and flex in the several linkages, joints, and gear systems.
- This model assumes that the vehicle tire does not leave the ground.

- Vertical displacement of both the vehicle body and the tire are measured from their respective equilibrium positions.

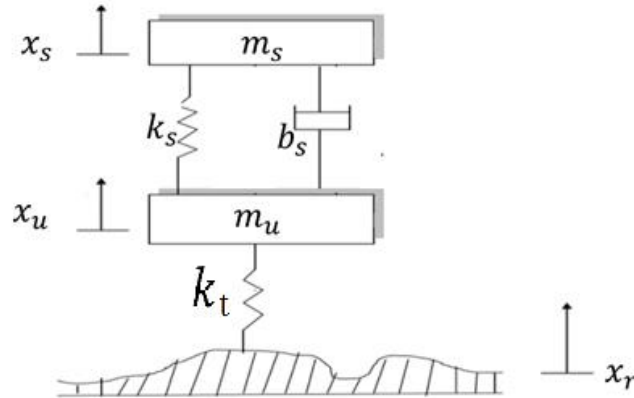


Figure 5.2: Quarter Car Suspension Model

The sprung mass, denoted by  $m_s$ , represents the mass of the vehicle body; in this case, it will equal  $\frac{1}{4}$  of the total vehicle body mass. The position of the sprung mass is indicated by  $x_s$ . The unsprung mass, denoted by  $m_u$ , represents the mass of the wheel, hub and the brake assembly and its position is indicated by  $x_u$ . The suspension is modeled by using a spring damper combination ( $k_s$  and  $b_s$ ). The road profile is given by  $x_r$ , which is considered to be the only input in this model, since no control is involved. The tire has stiffness, but the damping is very minimal and is taken to be zero. The stiffness of the tire is denoted by  $k_t$ .

Basic laws of mechanics are employed to carry out the mathematical modelling of a two-degree-of-freedom quarter car body for a suspension system which is shown as:

$$m_s \ddot{x}_s = k_s (x_u - x_s) + b_s (\dot{x}_u - \dot{x}_s) \quad (5.1)$$

$$m_u \ddot{x}_u = -k_s (x_u - x_s) - b_s (\dot{x}_u - \dot{x}_s) + k_t (x_u - x_r) \quad (5.2)$$

As shown in Figure 5.3, MATLAB/Simulink could be used to simulate a vehicle suspension system using the derived mathematical equation and provided parameters in Table 5.1.

Table 5.1: Parameters of Suspension System [63]

$m_s$	Sprung Mass (kg)	400
$m_u$	Unsprung Mass (kg)	45
$k_s$	Stiffness Coefficient of the spring for $m_s$ (N/m)	26500
$k_u$	Stiffness Coefficient of the spring for $m_u$ (N/m)	175000
$b_s$	Damping Coefficient of the damper for $m_s$ (N.s/m)	1000

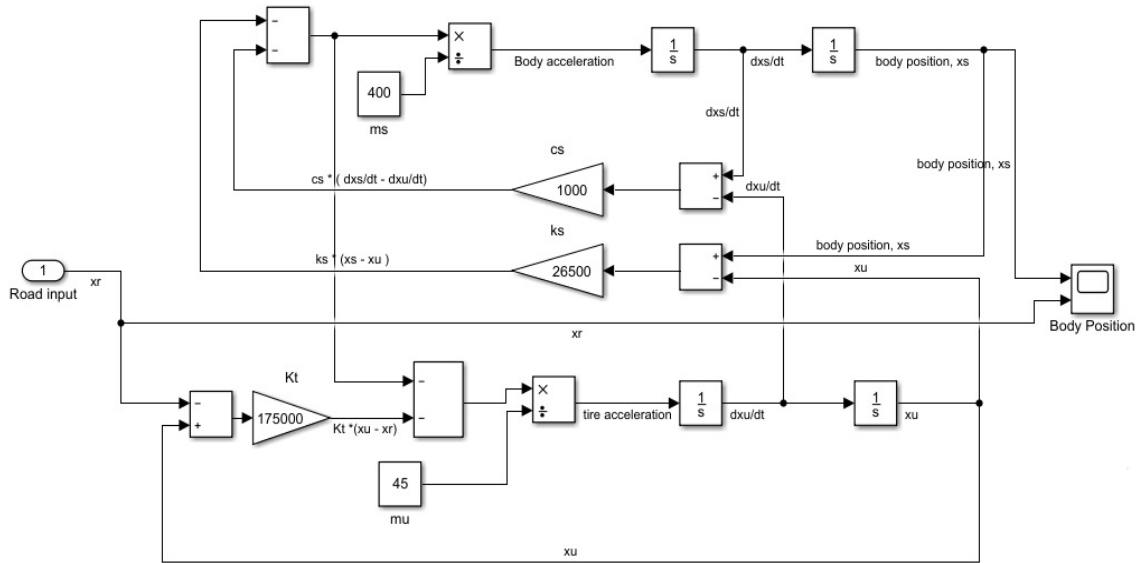


Figure 5.3: Passive Suspension System Simulation in MATLAB/Simulink

The Simulated suspension system is excited by four types of inputs, which were introduced in the previous chapter, to evaluate the performance of the system. The output of the simulated system is body position,  $x_s$ , which is illustrated in Figure 5.4, Figure 5.5, Figure 5.6, and Figure 5.7 when it is excited by the step unit, sine wave, bump, and road type C, respectively.

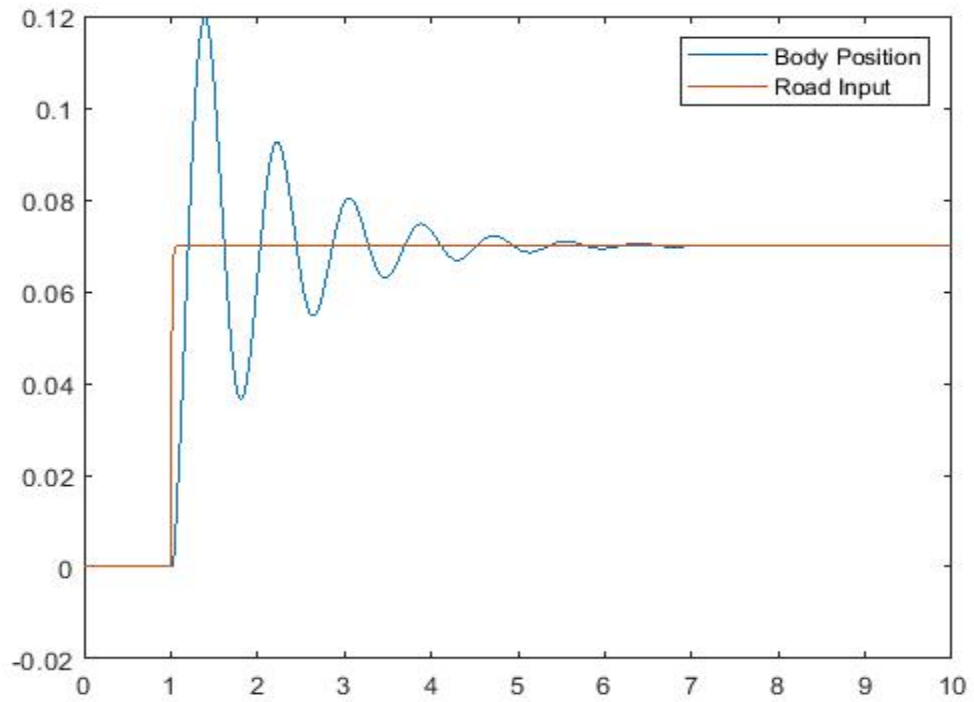


Figure 5.4: Response of Passive Suspension System for Step Input

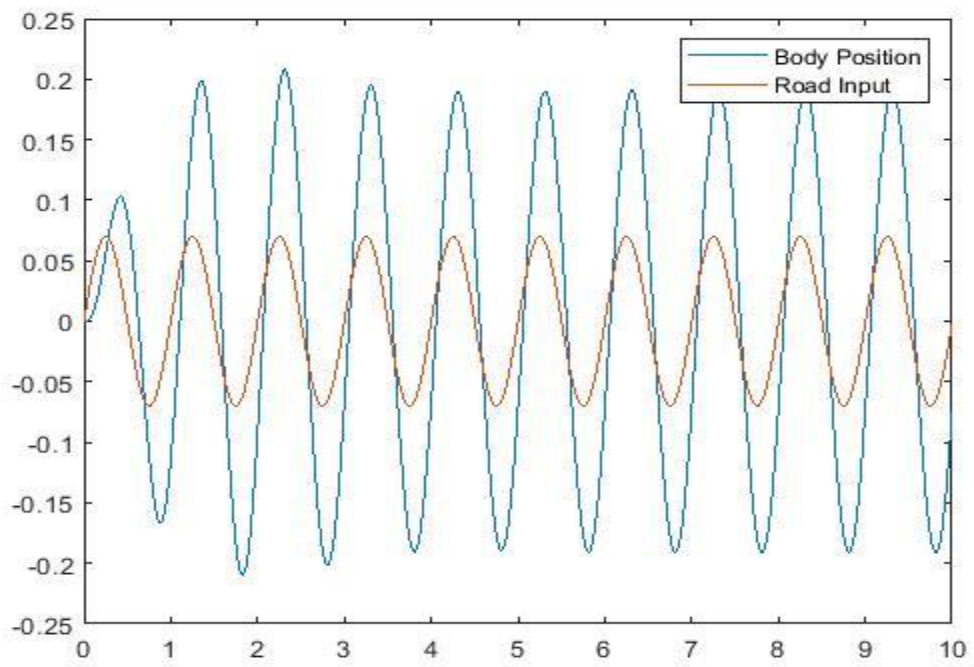


Figure 5.5: Response of Passive Suspension System for Sine Wave Input

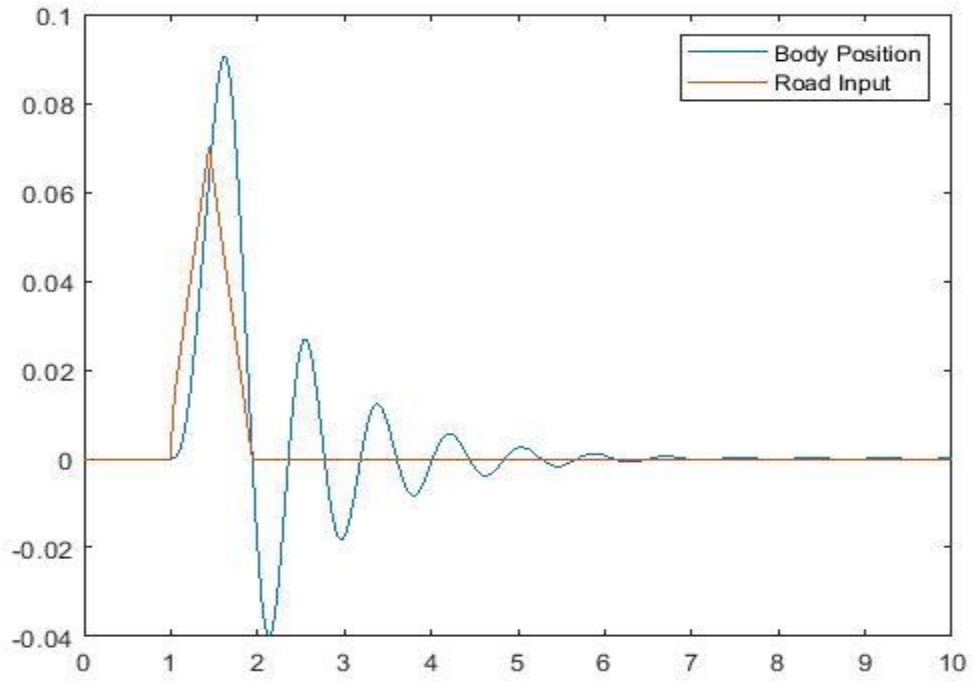


Figure 5.6: Response of Passive Suspension System for Bump Input

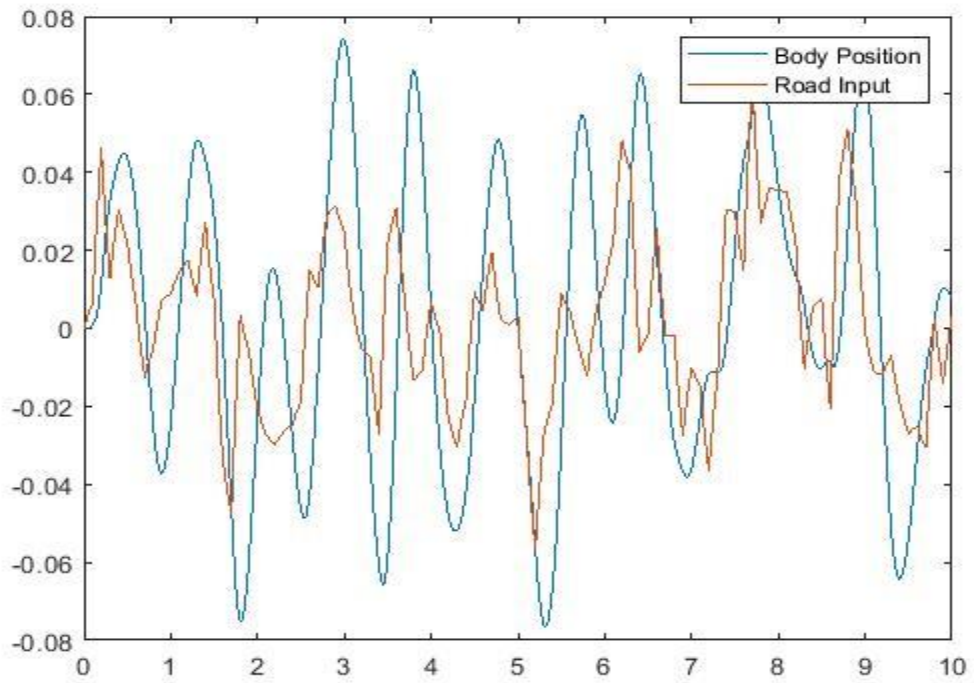


Figure 5.7: Response of Passive Suspension System for type C Road Input



## 5.2 Control-oriented Model

Shown in Figure 5.8 is the semi-active quarter car control model. The damping force input is now denoted by  $u(t)$ . MR damper consists of viscous damping force, friction force, and controllable damping force, which is represented by  $u(t)$ . Even in the absence of magnetic fields, viscous damping and friction forces persist. The controllable damping force can be varied by different input currents. In the absence of input current, the MR damper can still control vibration through viscous damping. MR dampers are considered fail-safe, so they can provide vibration control with or without control systems. Furthermore, as a semi-active suspension can be controlled, a control algorithm should be utilized to determine the appropriate damping force required.

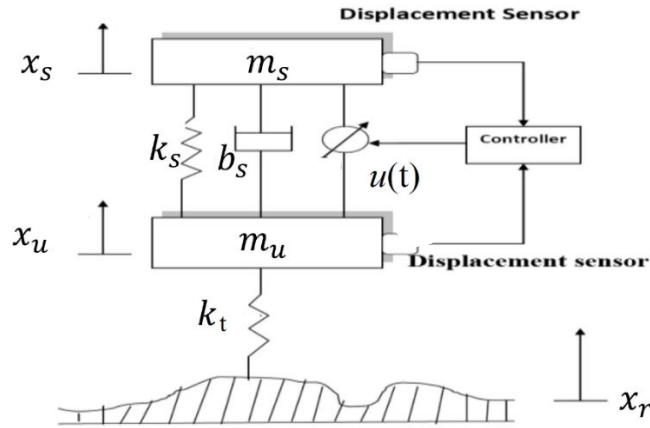


Figure 5.8: Control Oriented Model for Suspension System

The equations of motion for the quarter car control model shown in Figure 2 are equations (5.3) and (5.4).

$$m_s \ddot{x}_s = k_s (x_u - x_s) + b_s (\dot{x}_u - \dot{x}_s) + u \quad (5.3)$$

$$m_u \ddot{x}_u = -k_s (x_u - x_s) - b_s (\dot{x}_u - \dot{x}_s) + k_t (x_u - x_r) - u \quad (5.4)$$

### 5.3 State Space Model

In order to provide a controller for the system, it is imperative that the system is represented in state-space form. The state-space model helps us to tackle a first-order differential equation instead of a second order, and there are many studies on it like in [64]. To represent the model in the state-space model, first, states of interest need to be determined. The determination of the states depends upon the designer of the controller. The designer should choose states that are important to the system as well as states that are of interest to the designer. Shown in Table 5.2 are the chosen states and the variables they represent. In the state-space formulation,  $X$  is a vector representing the system state.

*Table 5.2: Significance of Each State Variable*

STATE	SIGNIFICANCE
$x_1$	$x_s$
$x_2$	$\dot{x}_s$
$x_3$	$x_u$
$x_4$	$\dot{x}_u$
Disturbance	$x_r$

The state-space form for equations (5.3) and (5.4) takes the general form shown in equation (5.5).

$$\dot{X}(t) = A * X(t) + B * u(t) + L * x_r(t) \quad (5.5)$$

where  $A$  is an  $n*n$  constant coefficient matrix, and  $n$  is equal to the number of states.  $B$  and  $L$  are  $n*1$  constant coefficient vectors.  $X(t)$  is the state and is a  $n*1$  vector,  $u(t)$  is the control force which is a scalar input and  $x_r(t)$  is the road profile which is a scalar value. Matrices  $A$ ,  $B$ , and  $L$  are as follow:

$$A = \begin{bmatrix} 0 & 1 & 0 & 0 \\ \frac{-k_s}{m_s} & \frac{-b_s}{m_s} & \frac{k_s}{m_s} & \frac{b_s}{m_s} \\ 0 & 0 & 0 & 1 \\ \frac{-k_s}{m_u} & \frac{b_s}{m_u} & \frac{-k_s-k_t}{m_u} & \frac{-b_s}{m_u} \end{bmatrix} \quad (5.6)$$

$$B = \begin{bmatrix} 0 \\ 1 \\ \frac{1}{m_s} \\ 0 \\ -1 \\ \frac{1}{m_u} \end{bmatrix} \quad (5.7)$$

$$L = \begin{bmatrix} 0 \\ 0 \\ 0 \\ \frac{k_t}{m_u} \\ 0 \\ 0 \end{bmatrix} \quad (5.8)$$

#### 5.4 Seat Suspension System

One of the common methods to obtain increased vibration isolation is to add additional isolator systems that separate the operator from the chassis and is extensively studied in the literature [65]. With the implementation of new technology, there have been advancements in suspension systems to allow suspensions to adapt to changing road conditions. Off-road and commercial vehicles are more likely to suffer from this problem as the driver is exposed to longer and stronger excitation from the road roughness. Additional suspension system for the seats will be studied in this research, and for this reason, a three-degree-freedom model should be developed, which is shown in Figure 5.9.

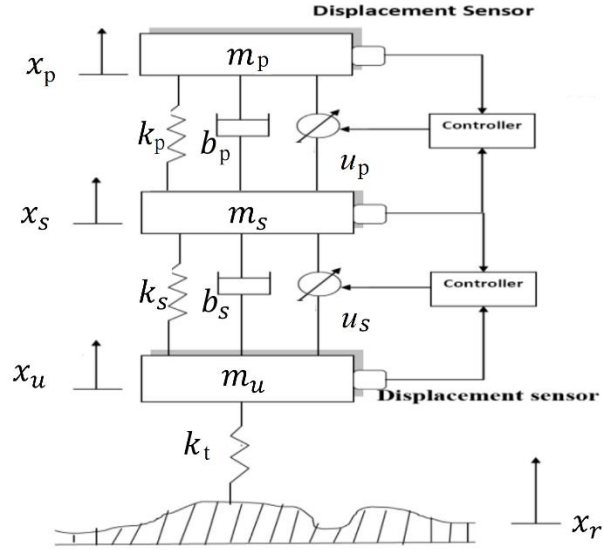


Figure 5.9: Three-degree-of-freedom model of the MR damper seat-suspension system

The equations of motion for this model are equations (5.9), (5.10) and (5.11).

$$m_p \ddot{x}_p = k_p (x_s - x_p) + b_p (\dot{x}_s - \dot{x}_p) + u_p \quad (5.9)$$

$$m_s \ddot{x}_s = -k_p (x_s - x_p) - b_p (\dot{x}_s - \dot{x}_p) - u_p + k_s (x_u - x_s) + b_s (\dot{x}_u - \dot{x}_s) + u_s \quad (5.10)$$

$$m_u \ddot{x}_u = -k_s (x_u - x_s) - b_s (\dot{x}_u - \dot{x}_s) - u_s + -k_t (x_r - x_u) \quad (5.11)$$

Where the position of the vehicle's seat is indicated by  $x_p$  and the seat's mass denoted by  $m_p$ .  $k_p$  and  $b_p$  represent stiffness and damping factor for seats. Future simulations will be based on these parameters, which are shown in Table 5.3.

Table 5.3: Parameters of Seat Suspension System [57].

$m_p$	Mass of Seat and Driver (kg)	100
$k_p$	Stiffness Coefficient of the spring for $m_p$ (N/m)	2500
$b_p$	Stiffness Coefficient of the spring for $m_p$ (N.s/m)	200

State variables are determined according to Table 5.4 to represent Equations (5.9), (5.10), and (5.11) in state-space form.

Table 5.4: Significance State Variable for Seat Suspension System

STATE	SIGNIFICANCE	STATE	SIGNIFICANCE
$x_1$	$x_p$	$x_5$	$x_u$
$x_2$	$\dot{x}_p$	$x_6$	$\dot{x}_u$
$x_3$	$x_s$	Disturbance	$x_r$
$x_4$	$\dot{x}_s$		

The state-space form for a three-degree-of-freedom system is shown in equation (5.12).

$$\dot{X}(t) = A2 * X(t) + \dot{B}2 * u(t) + L2 * x_r(t) \quad (5.12)$$

This representation of the system is the same as that of Equation (5.5), but the matrices are different from what has been shown previously.  $u(t)$  is not a scalar input as it includes two forces,  $u_p(t)$  and  $u_s(t)$ , and matrices  $A2$ ,  $B2$ , and  $L2$  are as follow:

$$A2 = \begin{bmatrix} 0 & 1 & 0 & 0 & 0 & 0 \\ -k_p & -b_p & k_p & b_p & 0 & 0 \\ m_p & m_p & m_p & m_p & 0 & 0 \\ 0 & 0 & 0 & 1 & 0 & 0 \\ k_p & b_p & -k_p - k_s & -b_p - b_s & k_s & b_s \\ m_s & m_s & m_s & m_s & m_s & m_s \\ 0 & 0 & 0 & 0 & 0 & 1 \\ 0 & 0 & k_s & b_s & -k_s - k_t & -b_s \\ & & m_u & m_u & m_u & m_u \end{bmatrix} \quad (5.13)$$

$$B = \begin{bmatrix} 0 & 0 \\ 1 & 0 \\ m_p & 0 \\ -1 & 0 \\ m_s & 0 \\ 0 & 1 \\ 0 & m_s \\ 0 & -1 \\ 0 & m_u \end{bmatrix} \quad (5.14)$$

$$L = \begin{bmatrix} 0 \\ 0 \\ 0 \\ 0 \\ 0 \\ k_t \\ m_u \end{bmatrix} \quad (5.15)$$

## CHAPTER 6

### CONTROLLER DEVELOPMENT FOR A SEMI-ACTIVE SUSPENSION SYSTEM

#### 6.1 LQR Controller Design

As discussed in chapter 3, the goal of the controller system is to find the optimal damping force which falls within the dissipative domain of an MR damper.

Linear quadratic regulator (LQR) theory has been studied and used by many researchers in an attempt to design an optimal controller for active and semi-active suspension systems [66]. This type of controller works towards generating an optimal actuator force that leads to the minimization of the performance index. The performance index is user-defined criteria based upon the dynamics of the model and the states of interest [36].

In this method, the control force is given by:

$$u(t) = -Kx(t) \quad (6.1)$$

LQR is actually an optimization procedure that involves determining the input control such that the performance index  $J$  is minimized.  $J$  denotes the controller input limit as well as the performance requirement. According to this definition, the optimal controller for a given system minimizes the following performance index:

$$J = \frac{1}{2} \int_0^t (x^t Q x + u^t R u) dt \quad (6.2)$$

The matrix gain  $K$  is represented by:

$$K = R^{-1} B^T P \quad (6.3)$$

The matrix  $P$  must satisfy the reduced-matrix equation given as:

$$A^T P + P A - P B R^{-1} B^T P + Q = 0 \quad (6.4)$$

Then the feedback regulator  $u(t)$  is as follow:

$$u(t) = -(R^{-1} B^T P)x(t) \quad (6.5)$$

$$u(t) = -K x(t) \quad (6.6)$$

The selection of  $Q$  and  $R$  determines the optimality in the optimal control law [58]. These matrices are chosen by the designer. This matrix's values are usually determined by trial and error in simulation.  $Q$  and  $R$  matrices are chosen as diagonals as a rule of thumb. In general, when a state is important, and it is to be small in magnitude, the corresponding diagonal element should be large. For a fixed  $Q$  matrix, a decrease in  $R$  matrix values will reduce the transition time and overshoot but increase the rise time and steady-state error. Under the other condition, where  $R$  is fixed but  $Q$  decreases, the transition time and overshoot will increase, whereas the rise time and steady-state error will decrease. In this thesis, the values are chosen to reduce the sprung mass acceleration without significantly penalizing the other performance aspects.

A suspension system controlled by LQR is simulated by MATLAB/Simulink, in which  $K$  is calculated using the MATLAB command,  $K = \text{lqr}(A,B,Q,R)$ , and then different weighting factors were tested. The performance of the system is evaluated, with the specified weighting factor, regarding ride comfort and handling stability to determine which factors lead to the best performance. According to the simulation results, the best performance weighting factors are selected as follows:

$$Q = 1e6 * [10 \quad 5 \quad 7 \quad 3] \quad (6.7)$$

$$R = [1] \quad (6.8)$$

When  $Q$  and  $R$  are determined, the gain values are found by using MATLAB's built-in function. Shown in equation (6.9) is the MATLAB command, where  $A$  and  $B$  are the matrices shown in Equations (5.6) and (5.7).

$$K = \text{lqr}(A, B, Q, R) \quad (6.9)$$

Based on Equation (5.5), The quarter car model in state-space form could be employed to simulate the suspension system as shown in Figure 6.1:



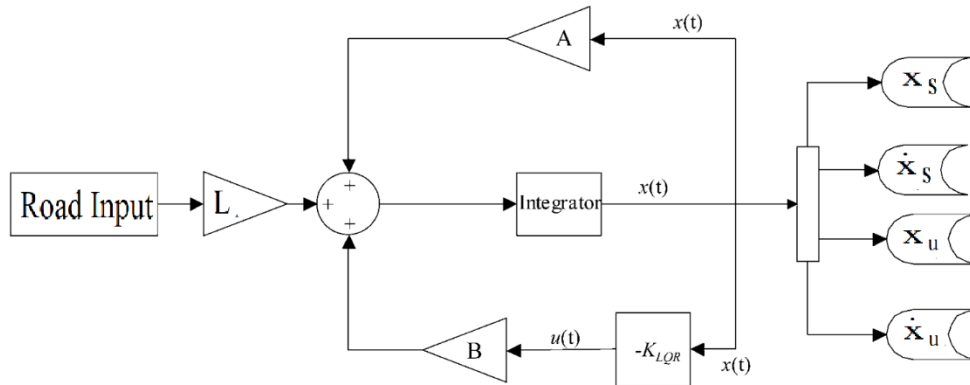


Figure 6.1: The Block Diagram of Semi-Active Control System [67]

In addition, damping force needs to be in the dissipative domain, which is addressed by a MATLAB code introduced in chapter 3. Consequently, an LQR control system could be simulated as shown in Figure 6.2:

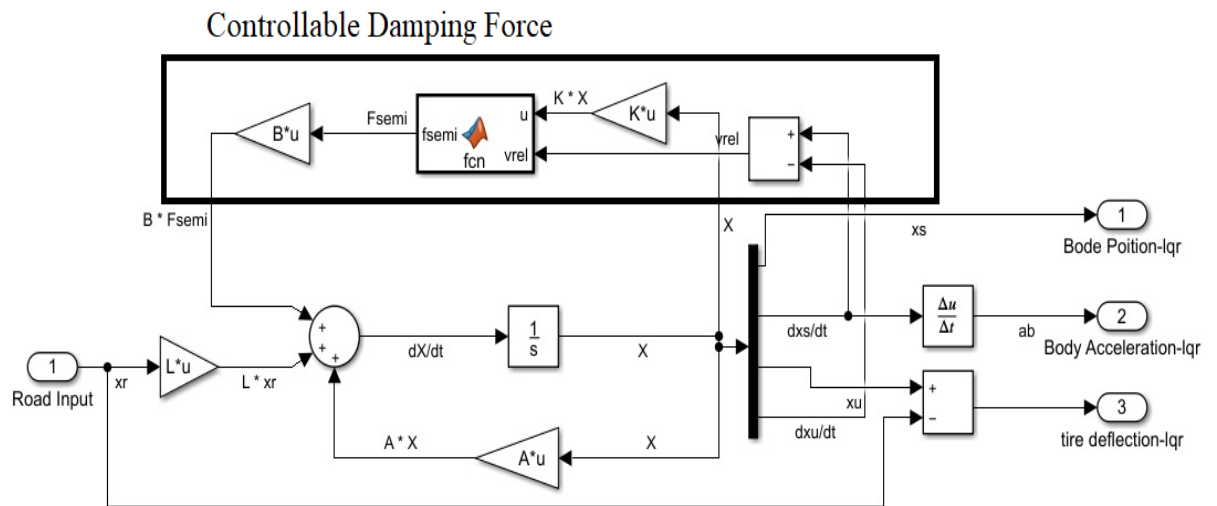


Figure 6.2: Simulink Block of Suspension System using LQR Control System

R and Q need to be determined when an additional suspension system for the vehicle's seat is added, there will be three-degree-of-freedom suspension system with six state variables. In this case, weighting factors are named Q2 and R2 and, based on simulation results are selected as follow:

$$Q2 = 1e9 * [10 \ 5 \ 1 \ 1 \ 7 \ 2] \quad (6.7)$$

$$R2 = \begin{bmatrix} 1 & 0 \\ 0 & 1 \end{bmatrix} \quad (6.8)$$

A Three-degree-of-freedom suspension system using LQR control system could be simulated as depicted in Figure 6.3:

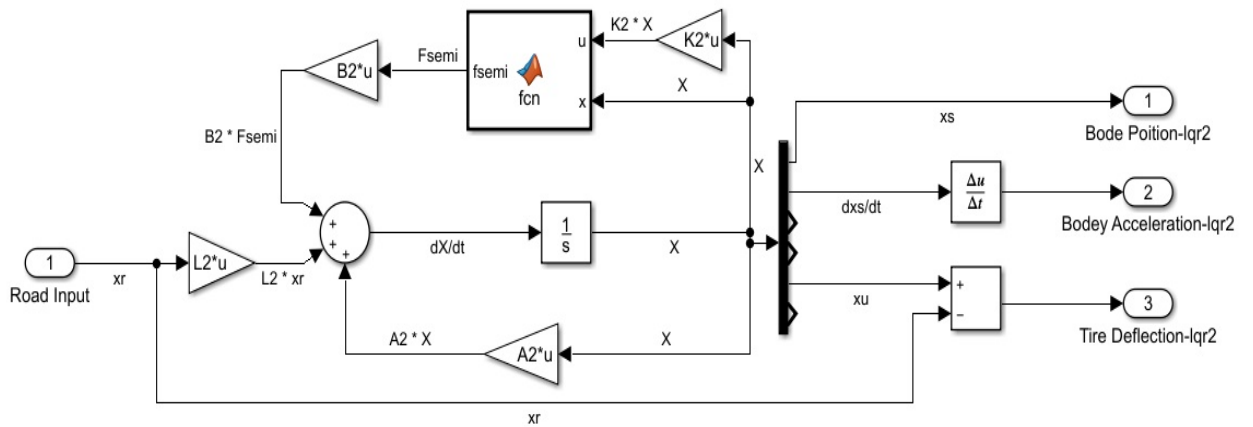


Figure 6.3: Simulink Block of a Three-degree-of-freedom Suspension System Using LQR Control System

## 6.2 Fuzzy Logic Controller Design

Since controlling the semi-active suspension requires various sensor readings for the controller to generate the required damping coefficient by the system, Fuzzy logic control (FLC) has been gaining a lot of attention from researchers in recent years due to its effectiveness at controlling real-time (RT) systems with inexact system model and inaccurate sensor readings.

The basic fundamental concept of FLC is to describe a relationship between the system inputs and output in terms of degrees of membership and a set of IF-THEN fuzzy rules. These parameters are referred to as the knowledge base of the fuzzy controller. Using the knowledge base the fuzzy controller is able to stabilize the controlled system. Generally, the FLC uses a set of fuzzy stages to implement the control system as shown in Figure 6.4, which are: Fuzzification, Fuzzy Inference, and Defuzzification.

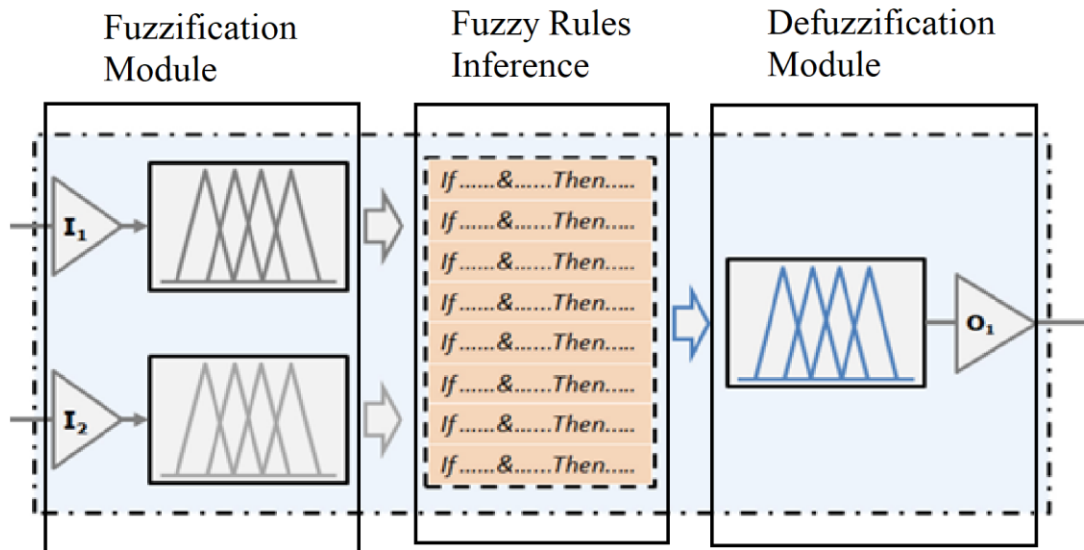


Figure 6.4: Fuzzy Logic Control Block [68]

### 6.2.1 Fuzzification Module

Fuzzy logic control employs a number of different membership functions in the control process, such as the Triangular, Gaussian, and Singleton. These membership functions define the relationship between the "crisp" sensor and its corresponding fuzzy values. In this thesis, the membership functions used to perform the input conversion process are the Gaussian Membership Function with the following linguistic variables: Negative Big (NB), Negative Medium (NM), Negative Small (NS), Zero (ZR), Positive Small (PS), Positive Medium (PM), as Positive Big (PB). Figures 6.5 and 6.6 illustrate these membership functions.

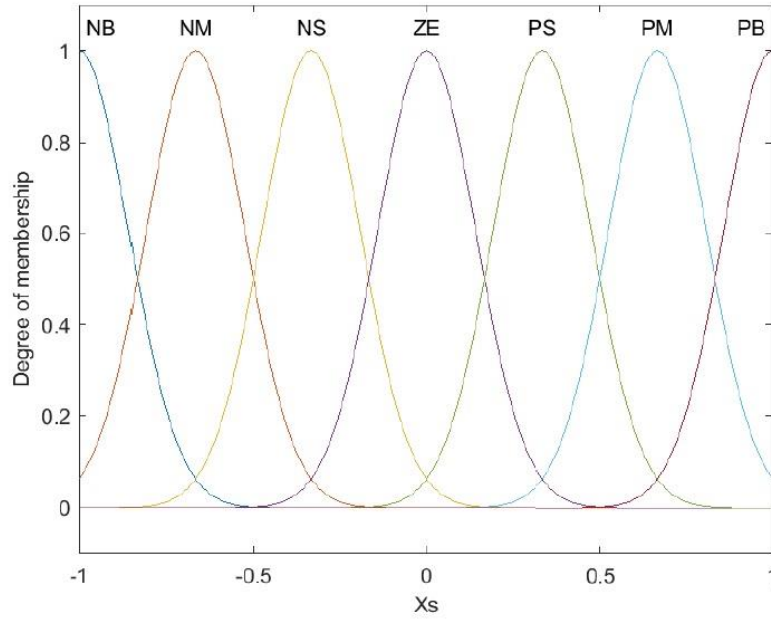


Figure 6.5: Membership Function for the Fuzzy Logic Controller,  $X_s$

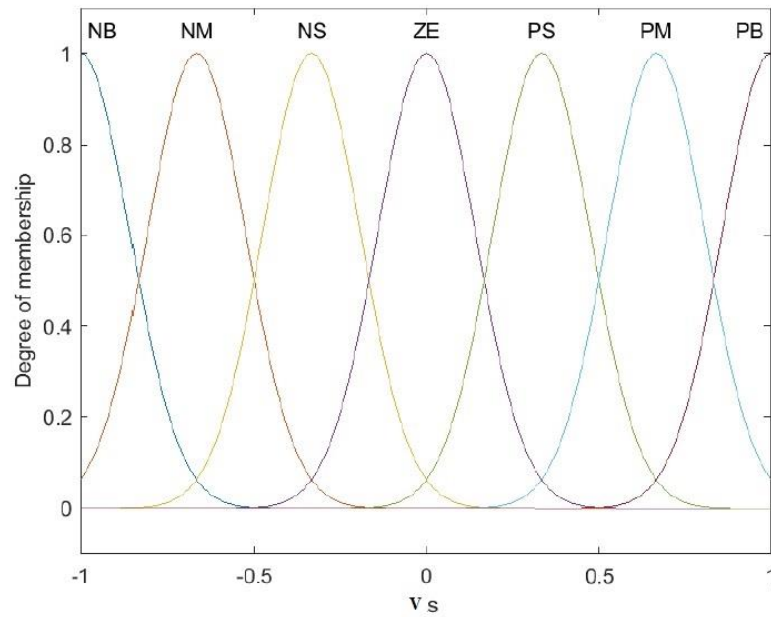


Figure 6.6: Membership Function for the Fuzzy Logic Controller,  $V_s$

The inputs of the proposed FLC in this study are sprung body position,  $x_s$ , and sprung body velocity,  $\dot{x}_s$ . A key factor in FLC is the determination of the input range for the membership function. According to simulation results, when the inputs are within the determined range for the membership function, the performance of the controller is significantly better. In order to address this problem, the FLC input range is designed between -1, and 1, and we use normalized values for

inputs Fig. 6.7 shows the block diagram for dividing  $x_s$  and  $\dot{x}_s$  by their maximum value, which results in an output range of [-1,1]. A controller with this feature could have better performance in a variety of input types.

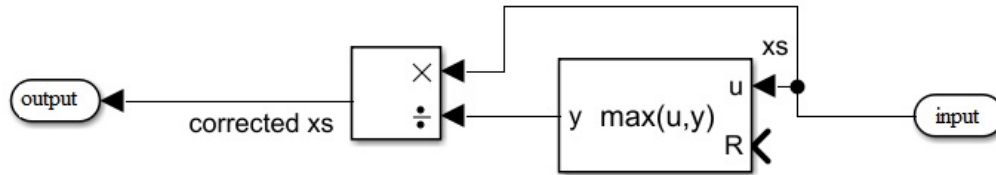


Figure 6.7: Simulink Block to generate the normalized value

### 6.2.2 Defuzzification Module

Rule inference creates 'conclusions' that indicate the degrees of membership. Before the output can be passed to the plant, it must be converted to a real crisp output value. Hence the defuzzification stage is required by the controller. In this study, the output is designed as nine Gaussian membership functions with the linguistic variables: Negative Big (NB), Negative Medium (NM), Negative Small (NS), Zero (ZR), Positive Small (PS), Positive Medium (PM), as Positive Big (PB). Just as with inputs, FLC outputs are within [-1,1], and the maximum damper force is multiplied by [-1,1] to achieve the required damping force.

Another way to improve FLC performance is to adjust the shape and position of each membership function. Simulation results suggest that performance would be enhanced by focusing membership functions near zero. In other words, the output membership functions are better to be as shown in Figure 6.9 rather than 6.8.

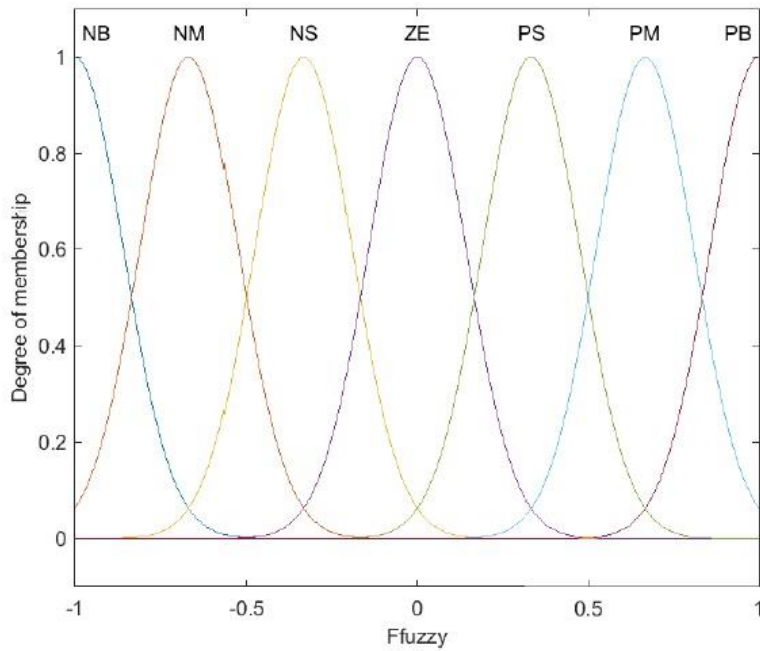


Figure 6.8: Membership Function for Output

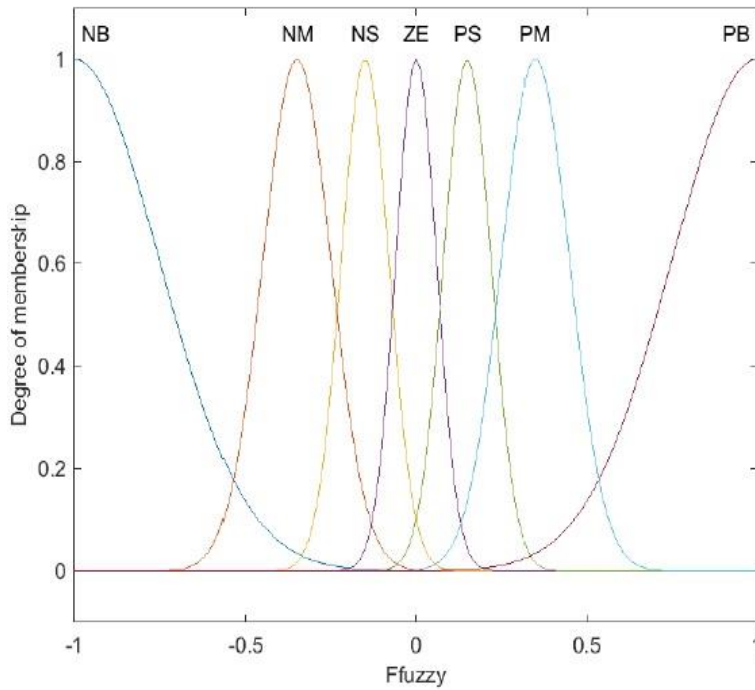


Figure 6.9: Membership Function for Output

A fuzzy logic controller with two degrees of freedom can be simulated in MATLAB/Simulink using Equation (5.5). The simulation is shown in Figure 6.10.

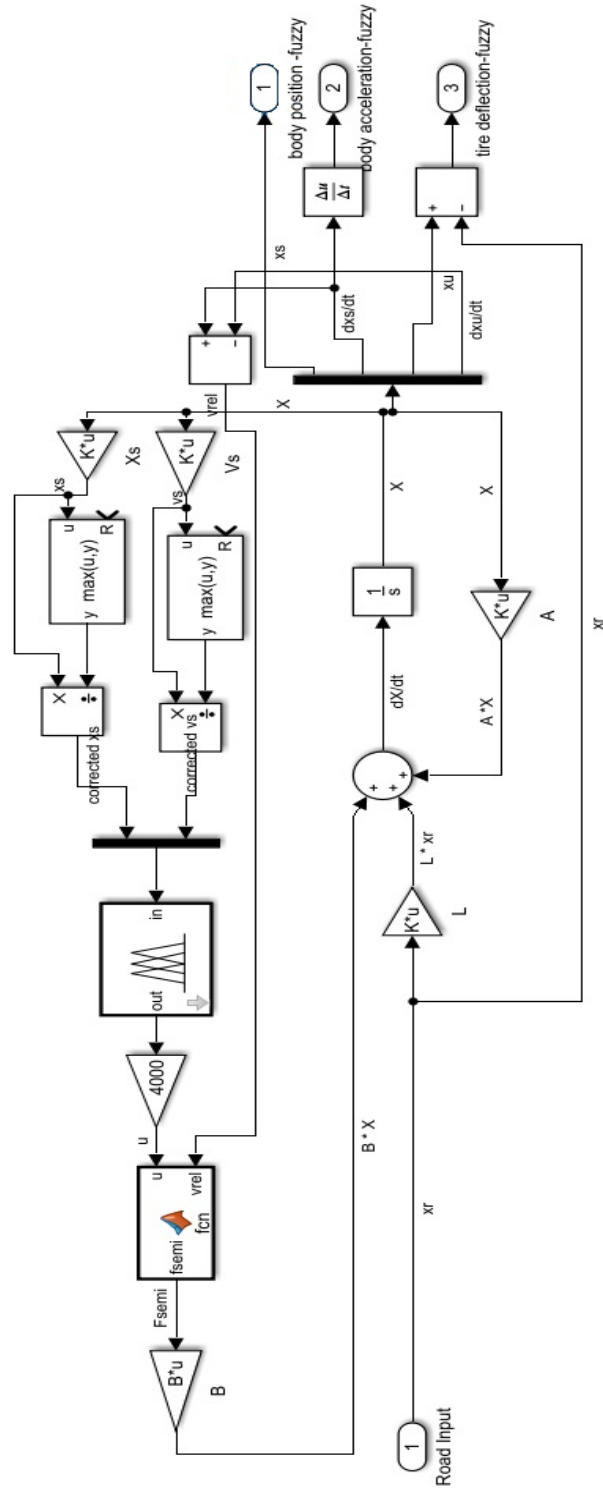


Figure 6.10: Simulink Block of a Semi-Active Suspension System using Fuzzy Logic Controller

Figure 6.11 illustrates the simulated FL controller at three degrees of freedom suspension system when modeled by Equation (5.12).

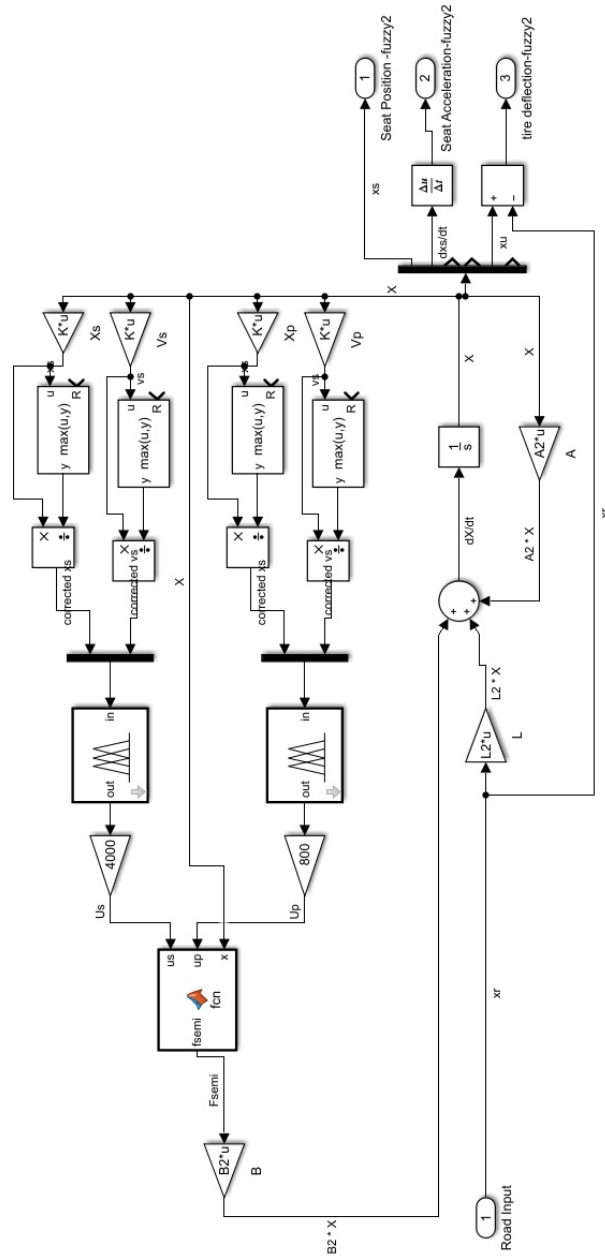


Figure 6.11: Simulink Block of a Three-degree-of-freedom Suspension System Using Fuzzy Logic Control System



### 6.2.3 Fuzzy Rules Inference

In FLC, the rules are considered as the knowledge of the expert in the plant dynamics. The fuzzy control rules take the form of an IF-THEN statement as follows:

$$IF\ x\ is\ A\ AND\ y\ is\ B,\ THEN\ z\ is\ C \quad (6.9)$$

The example fuzzy rule described in Equation (6.9) describes a condition that the plant can exhibit at a given point using linguistic variables (x and y) and fuzzy sets (A and B). The "AND" operator in the fuzzy rule above is the minimum operation between the two fuzzy sets. This rule is used in the rule inference stage of the FLC to compute the degree to which the input data matches the condition of a given rule. The number of fuzzy control rules present in an FLC depends on the number of membership functions for each input. This relationship ensures that there is an active rule for every state that the plant can exhibit. Table 6.1 shows the fuzzy rules implemented in the proposed controller.

Table 6.1: FLC Rules for Calculating the Damping Force

Rule #	Sprung Body Position	Sprung Body Velocity	Damping Force	Rule #	Sprung Body Position	Sprung Body Velocity	Damping Force
1	NB	NB	PB	26	ZE	PS	NS
2	NB	NM	PB	27	ZE	PM	NM
3	NB	NS	PB	28	ZE	PB	NM
4	NB	ZE	PM	29	PS	NB	PS
5	NB	PS	PM	30	PS	NM	PM
6	NB	PM	PS	31	PS	NS	ZE
7	NB	PB	ZE	32	PS	ZE	NS
8	NM	NB	PB	33	PS	PS	NM
9	NM	NM	PB	34	PS	PM	NM
10	NM	NS	PM	35	PS	PB	NB
11	NM	ZE	PM	36	PM	NB	PS
12	NM	PS	PS	37	PM	NM	ZE
13	NM	PM	ZE	38	PM	NS	NS
14	NM	PB	NS	39	PM	ZE	NM
15	NS	NB	PB	40	PM	PS	NM
16	NS	NM	PM	41	PM	PM	NB
17	NS	NS	PM	42	PM	PB	NB
18	NS	ZE	PS	43	PB	NB	ZE
19	NS	PS	ZE	44	PB	NM	NS
20	NS	PM	NS	45	PB	NS	NM
21	NS	PB	NM	46	PB	ZE	NM
22	ZE	NB	PM	47	PB	PS	NB
23	ZE	NM	PM	48	PB	PM	NB
24	ZE	NS	PS	49	PB	PB	NB

The output surface in the input-output space of the fuzzy logic controller is shown in Figure 6.12.

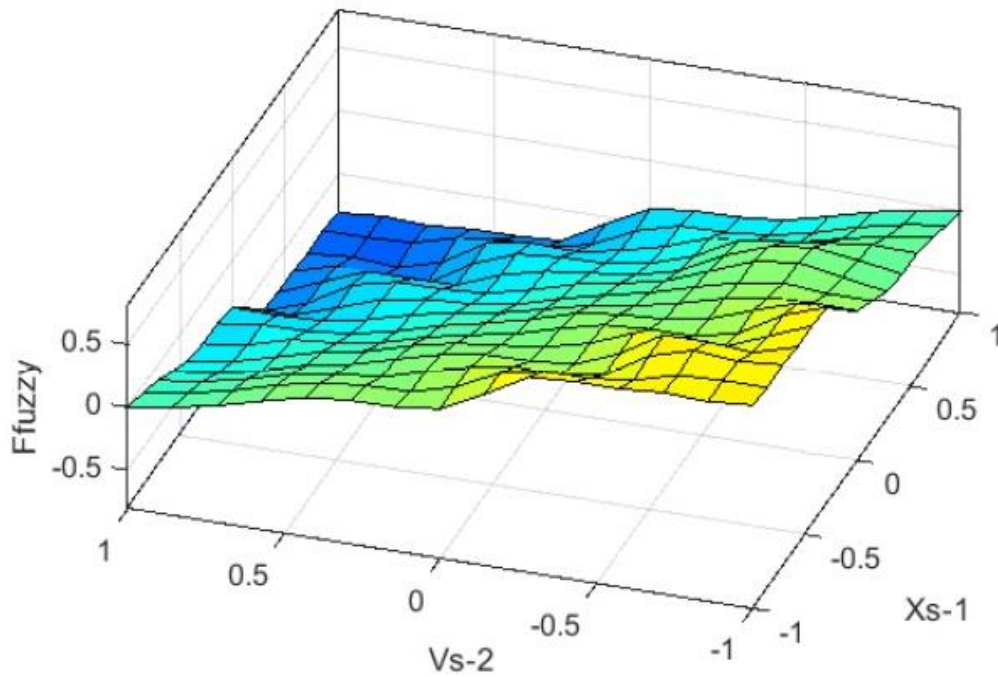


*Figure 6.12: Output Surface of the Fuzzy Logic Controller*

### **6.3 Evaluation of Control Methods**

The evaluation of the proposed controller designs is done using MATLAB/Simulink. To verify our simulation in state-space form, we simulate the passive suspension system on this form to compare it with the results from our initial simulation (Figure 5.3). In fact, a passive suspension system is similar to a semi-active one when there is no controllable damping force. This system is shown in Figure 6.13.

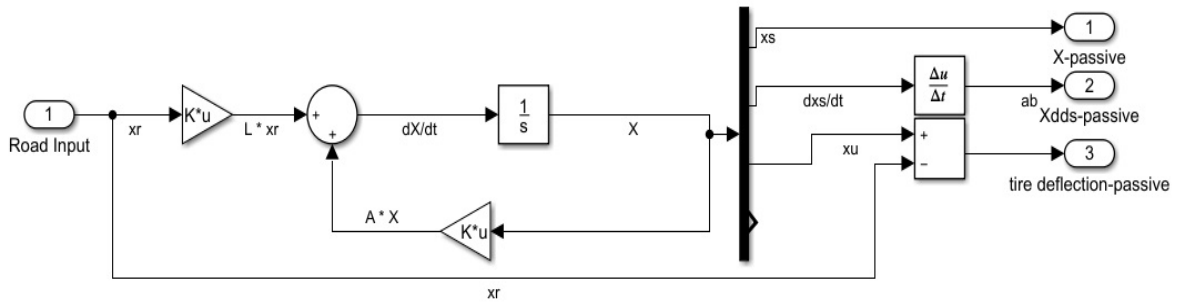


Figure 6.13: Simulink Block of a Passive Suspension System in State-Space Form

Figures 6.14 and 6.15 are the responses of the simulated system in 6.11 which are exactly the same as the responses of the Simulink model shown in Figure 5.3.

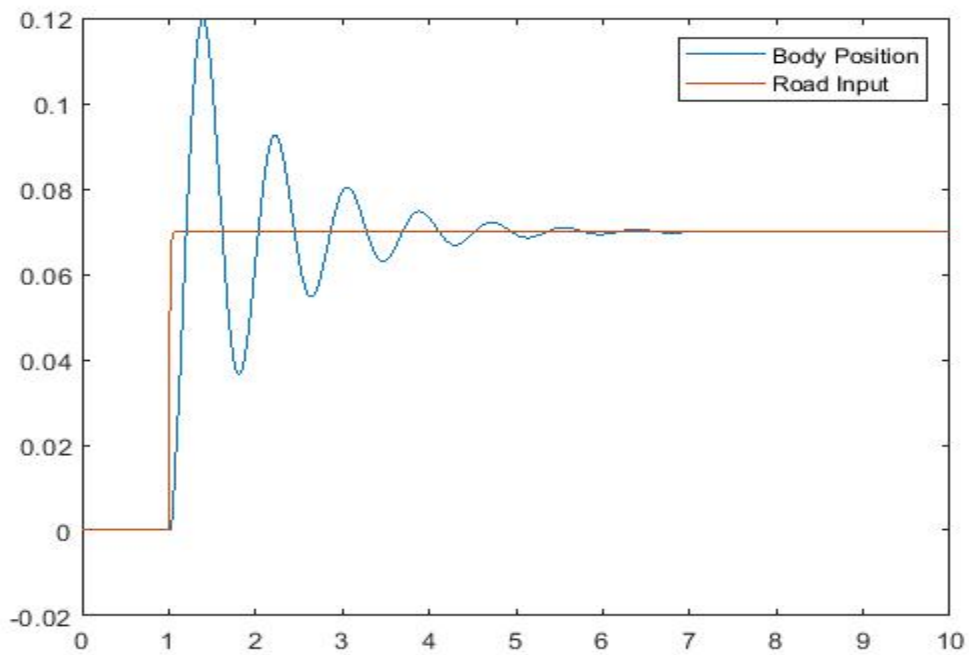
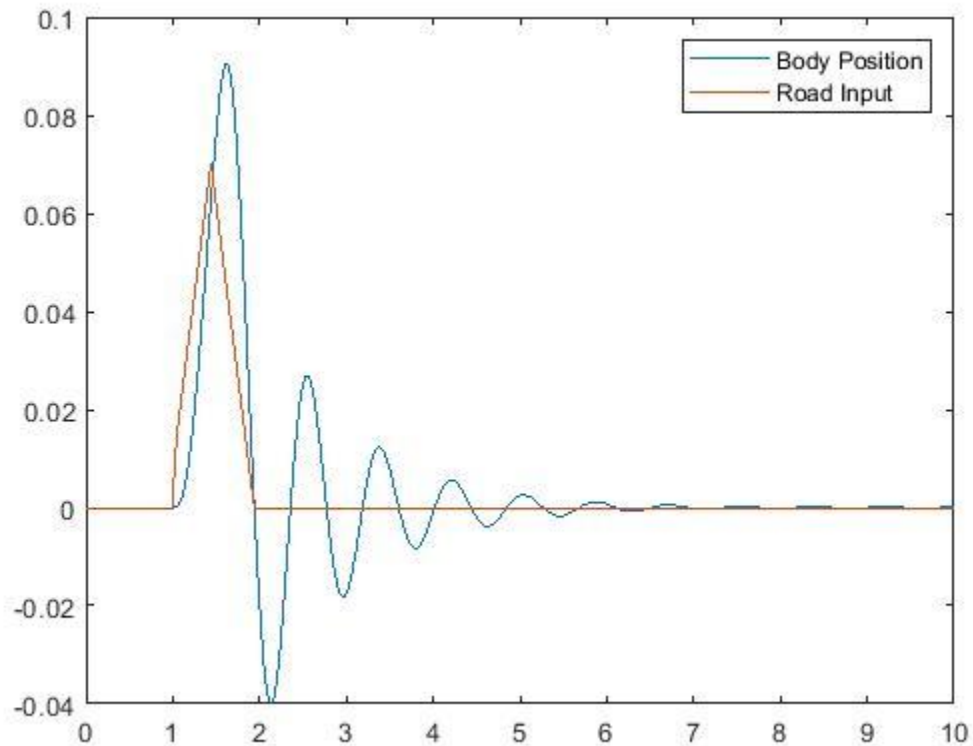


Figure 6.14: Response of Passive Suspension System for Step Input in State-Space Form



*Figure 6.15: Response of Passive Suspension System for Bump Input in State-Space Form*

Following the verification of the Simulink model, models with controllable damping forces are excited by various road inputs to determine the responses of designed controls, LQR, and FLC.

Three designed suspension systems are presented in Figures 6.16, 6.17, 6.18, and 6.19 in response to four types of road inputs, namely step, bump, sine wave, and road type C, where the sprung body position is the output.

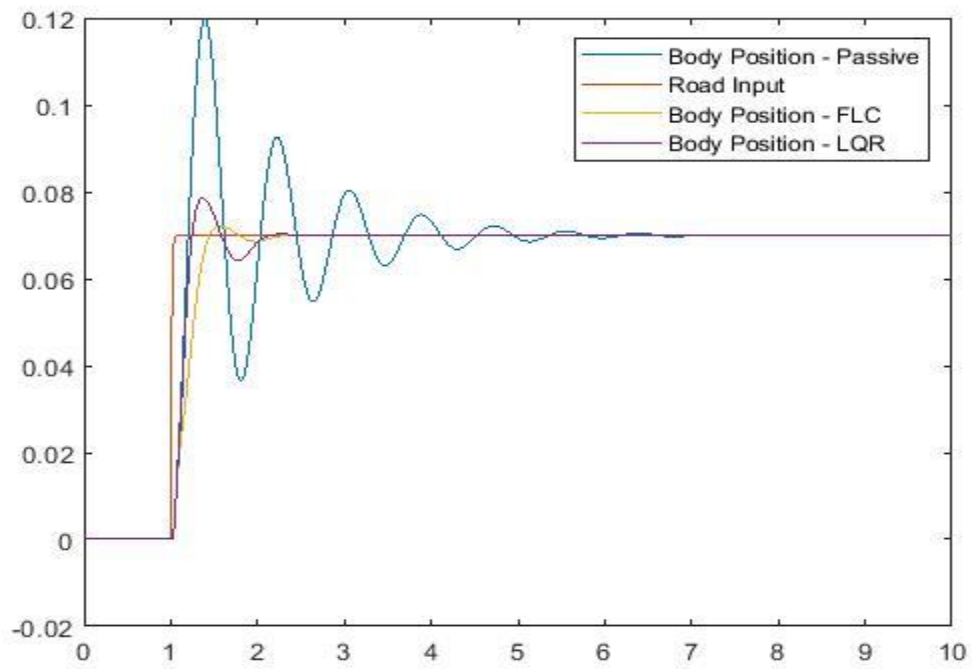


Figure 6.16: Response of Passive, LQR Controlled System, and FL controlled system, excited by a step input

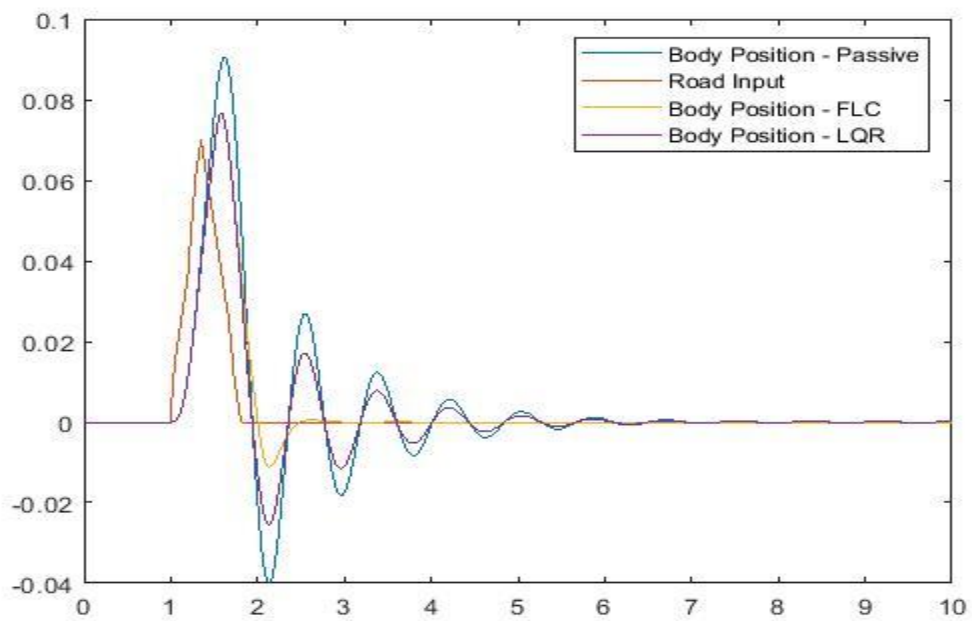


Figure 6.17: Response of Passive, LQR Controlled System, and FL controlled system, excited by a Bump input

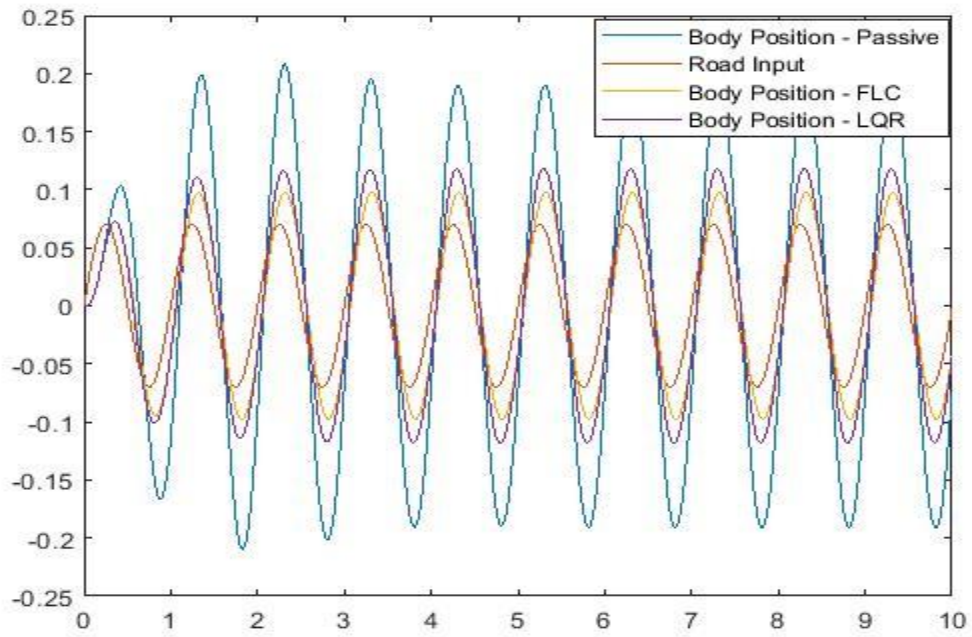


Figure 6.18: Response of Passive, LQR Controlled System, and FL controlled system, excited by a Sine Wave input

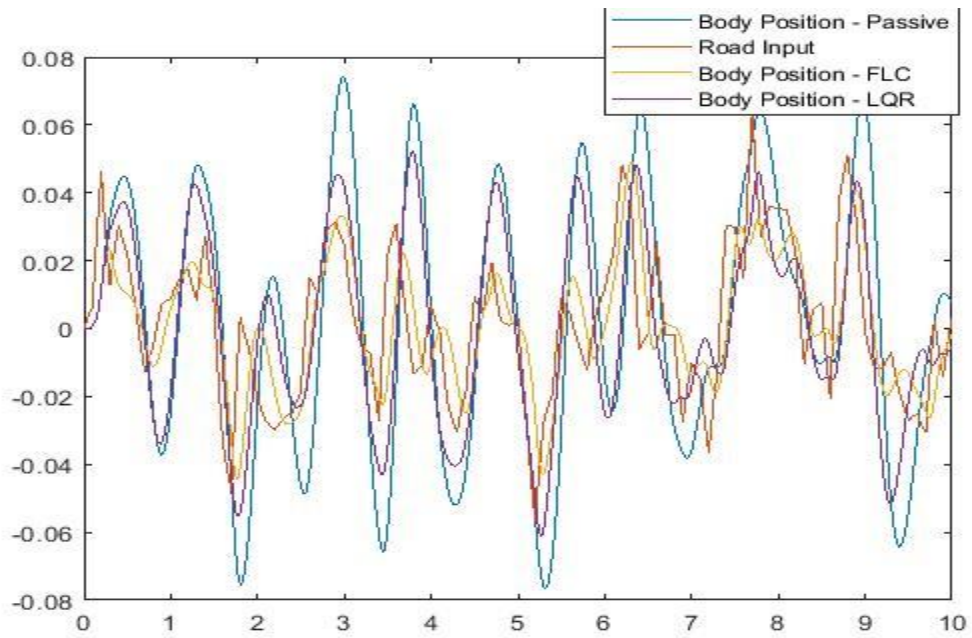
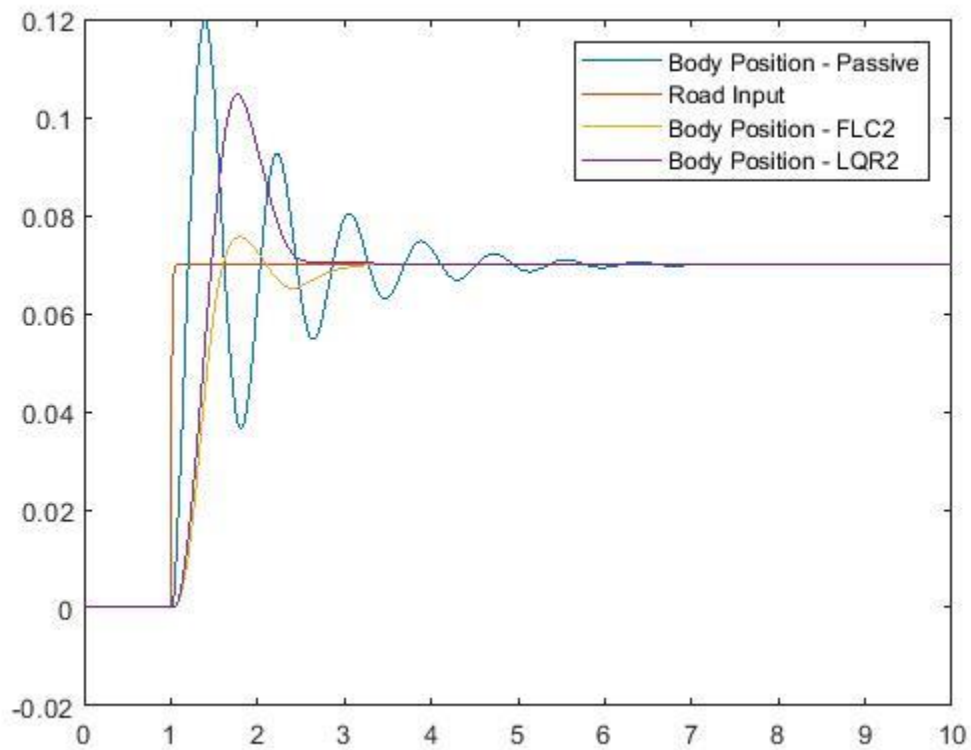


Figure 6.19: Response of Passive, LQR Controlled System, and FL controlled system, excited by Road Type C input

Simulation is performed with an additional suspension system to be used for seats using Equation (5.12), which is shown in Figure 6.3 when it is controlled by the LQR, and in Figure 6.11 when it is controlled by the FL Controller. Presented below are the results for the passive and semi-active suspension systems, including LQR controlled and FL controlled, when excited by four different types of road inputs.



*Figure 6.20: Response of Passive and Three-Degree-of-Freedom Suspension System using LQR and FLC, Excited by Step Input*



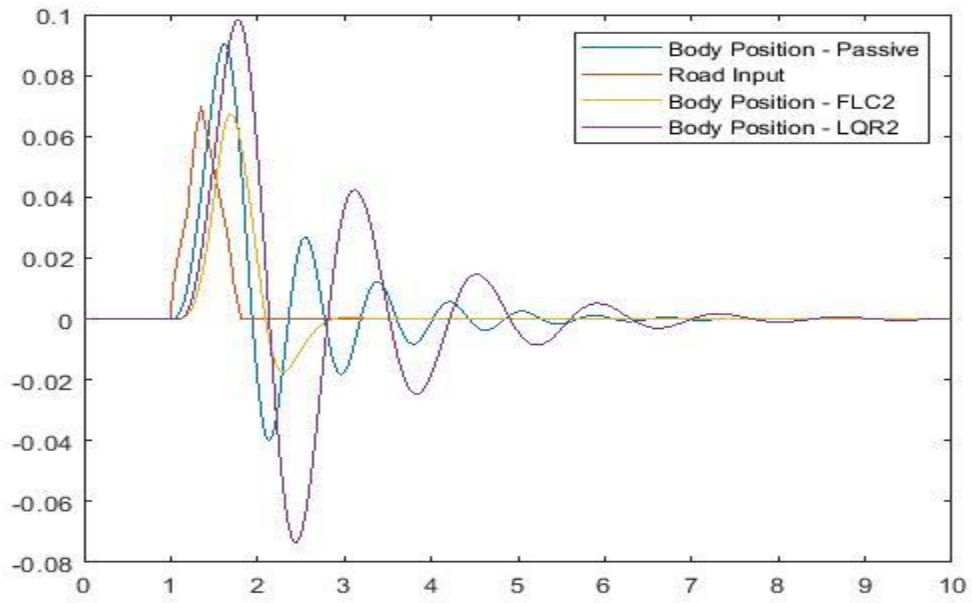


Figure 6.21: Response of Passive and Three-Degree-of-Freedom Suspension System Using LQR and FLC, Excited by Bump Input

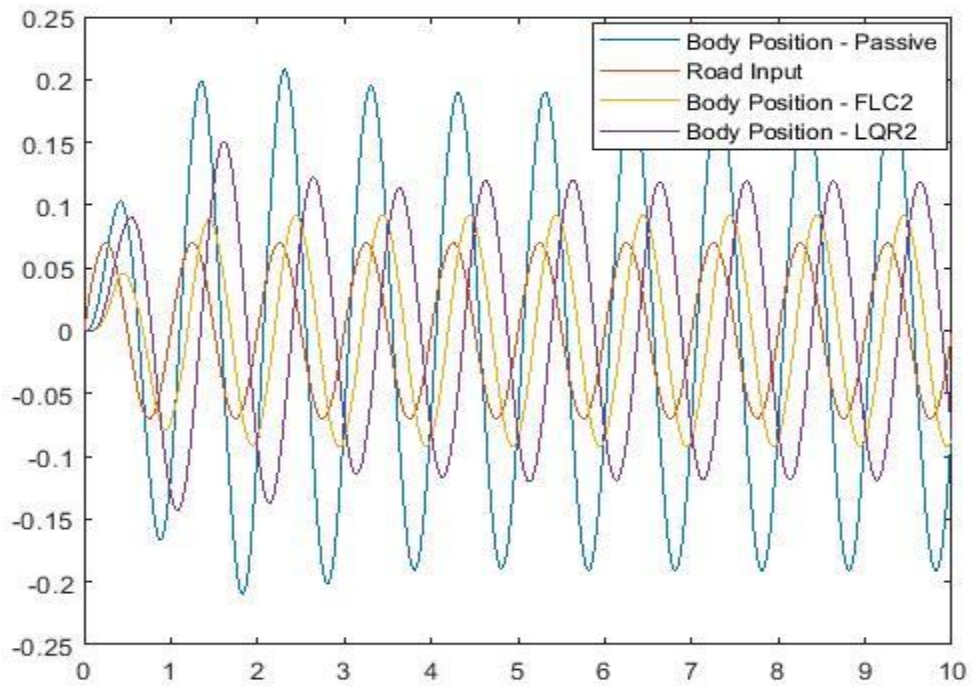
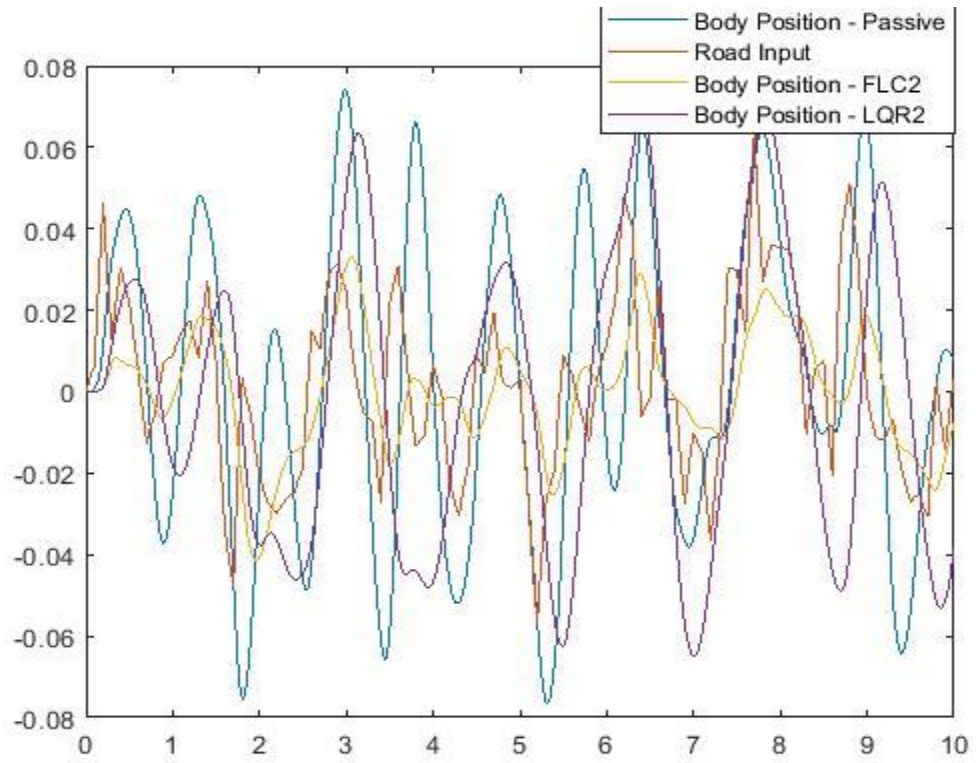


Figure 6.22: Response of Passive and Three-Degree-of-Freedom Suspension System Using LQR and FLC, Excited by Sine Wave Input



*Figure 6.23: Response of Passive and Three-Degree-of-Freedom Suspension System using LQR and FLC, excited by Road Type C input*

## CHAPTER 7

### RESULTS AND CONCLUSION

#### 7.1 Results:

Although the presented figures in Chapter 6 provide insight into the performance regarding the sprung mass displacement, as was discussed in Chapter 1, this thesis compares the performance regarding the acceleration of the sprung mass as well as the tire deflection using RMS values. Ride comfort can be gauged by the RMS value of sprung body acceleration, while road holding can be assessed by the RMS value of tire deflection, which can lead to improved handling stability.

This research's first goal was to develop a semi-active suspension system that provides good ride comfort as well as acceptable handling stability. To determine whether the proposed control systems are effective in terms of ride comfort, the RMS values of body acceleration and tire deflection resulted from the control systems are examined. Reduction in these values can indicate the improvement of the suspension system. These values are shown in Tables 7.1, 7.2, 7.3, and 7.4.

*Table 7.1: RMS Values of Sprung Mass Acceleration and Tire Deflection for Step Input*

Step Input	Passive (Normalized Value)	LQR controller (Normalized Value, LQR/Passive)	FL Controller (Normalized Value, FL/Passive)
Sprung Acceleration (m/s <sup>2</sup> )	8.295 e-1 (1.000)	6.655 e-1 (0.802)	6.851 e-1 (0.826)
Tire Deflection	3.359 e-3 (1.000)	3.170 e-3 (0.944)	2.866 e-3 (0.853)

*Table 7.2: RMS Values of Sprung Mass Acceleration and Tire Deflection for Bump Input*

bump Input	Passive (Normalized Value)	LQR controller (Normalized Value, LQR/Passive)	FL Controller (Normalized Value, FL/Passive)
Sprung Acceleration (m/s <sup>2</sup> )	6.271 e-1 (1.000)	4.492 e-1 (0.716)	3.631 e-1 (0.579)
Tire Deflection	1.565 e-3 (1.000)	1.170 e-3 (0.748)	9.907 e-4 (0.633)

*Table 7.3: RMS Values of Sprung Mass Acceleration and Tire Deflection for Sine Wave Input*

Sine Wave Input	Passive (Normalized Value)	LQR controller (Normalized Value, LQR/Passive)	FL Controller (Normalized Value, FL/Passive)
Sprung Acceleration (m/s <sup>2</sup> )	5.319 (1.000)	3.281 (0.617)	2.687 (0.505)
Tire Deflection	1.274 e-2 (1.000)	8.064 e-3 (0.633)	6.672 e-3 (0.524)

Table 7.4: RMS Values of Sprung Mass Acceleration and Tire Deflection for Road Type C Input

Road Type C	Passive (Normalized Value)	LQR controller (Normalized Value, LQR/Passive)	FL Controller (Normalized Value, FL/Passive)
Sprung Acceleration (m/s <sup>2</sup> )	2.068 (1.000)	1.789 (0.865)	1.761 (0.851)
Tire Deflection	4.949 e-3 (1.000)	4.593 e-3 (0.928)	4.107 e-3 (0.830)

Taking these results into consideration, it is easy to see that a semi-active suspension system incorporating the proposed Fuzzy Logic Controller is superior to two other systems and enhances the performance of the suspension system in terms of ride comfort as well as handling stability. Reduction in the amount of sprung mass acceleration translates into improved ride comfort, while the reduction in tire deflection is an indicator of improved handling stability. These values are presented in Table 7.5 for four types of road inputs.

Table 7.5: Effectiveness of FLC in Ride Quality

Road Input	Step	Bump	Sine Wave	Road Type C
Ride Comfort Improvement (%)	17.4	42.1	49.5	14.8
Handling Stability Improvement (%)	14.7	36.9	47.6	17.0

The other idea which was proposed in this study was considering an additional suspension system for the vehicle's seats which was modelled and simulated. Tables 7.6, 7.7, 7.8, and 7.9 show the RMS values of vehicle's seats vertical acceleration and tire deflection when the proposed suspension systems are excited by four types of road inputs.

Table 7.6: RMS Values of the Vehicle's Seats Acceleration and Tire Deflection for Step Input

Step Input	Passive (Normalized Value)	LQR controller (Normalized Value, LQR/Passive)	FL Controller (Normalized Value, FL/Passive)
Sprung Acceleration (m/s <sup>2</sup> )	8.295 e-1 (1.000)	2.552 e-1 (0.308)	1.668 e-1 (0.201)
Tire Deflection	3.359 e-3 (1.000)	2.879 e-3 (0.857)	2.780 e-3 (0.827)

Table 7.7: RMS Values of the Vehicle's Seats Acceleration and Tire Deflection for Bump Input

bump Input	Passive (Normalized Value)	LQR controller (Normalized Value, LQR/Passive)	FL Controller (Normalized Value, FL/Passive)
Sprung Acceleration (m/s <sup>2</sup> )	6.271 e-1 (1.000)	5.341 e-1 (0.852)	3.323 e-1 (0.530)
Tire Deflection	1.565 e-3 (1.000)	1.073 e-3 (0.685)	9.363 e-4 (0.598)

Table 7.8: RMS Values of the Vehicle's Seats Acceleration and Tire Deflection for Sine Wave Input

Sine Wave Input	Passive (Normalized Value)	LQR controller (Normalized Value, LQR/Passive)	FL Controller (Normalized Value, FL/Passive)
Sprung Acceleration (m/s <sup>2</sup> )	5.319 (1.000)	3.272 (0.615)	2.519 (0.473)
Tire Deflection	1.274 e-2 (1.000)	5.163 e-3 (0.405)	5.480 e-3 (0.430)

Table 7.9: RMS Values of the Vehicle's Seats Acceleration and Tire Deflection for Road Type C Input

Road Type C	Passive (Normalized Value)	LQR controller (Normalized Value, LQR/Passive)	FL Controller (Normalized Value, FL/Passive)
Sprung Acceleration (m/s <sup>2</sup> )	2.068 (1.000)	9.436 e-1 (0.456)	7.655 e-1 (0.370)
Tire Deflection	4.949 e-3 (1.000)	4.809 e-3 (0.971)	4.059 e-3 (0.820)

Presented tables prove that still proposed Fuzzy Logic Controller has the best performance among two other and the additional suspension system leads to providing a better ride quality. The effectiveness of this system is viewed in table 7.10 in terms of improvement percentage in ride comfort and road holding.

*Table 7.10: Effectiveness of FLC with an Additional Suspension System for Seats*

Road Input	Step	Bump	Sine Wave	Road Type C
Ride Comfort Improvement (%)	79.9	47.0	38.5	63.0
Handling Stability Improvement (%)	17.2	40.4	57.0	18.0

## 7.2 Conclusion

A quarter car model is presented in this thesis in state-space form, and two control systems for a semiactive suspension system are developed. The suspension system was designed to reduce the vibrational forces transmitted to the vehicle body and driver regardless of the type of terrain the vehicle is traveling on. The proposed control systems were tested in various types of road inputs and their performance assessed in terms of ride comfort and handling stability.

A balanced LQR control system provided a notable improvement in both ride comfort and handling stability over a passive suspension system; however, the best performance came from the proposed Fuzzy Logic controller. Simulations show that implementing this control strategy can result in up to 49.4% improvement in ride quality and 47.6% improvement in handling stability over a passive system, while these figures are increased when an additional suspension system is considered in the vehicle's seats, increasing ride comfort by 63% and handling stability by 57%.

In conclusion, the designed semi-active suspension system targeted the control problem of vehicle suspension systems and was able to provide a solution to the vehicle ride comfort and handling trade-off problem as it can enhance the suspension performance regarding both the ride comfort and handling stability regardless of the road condition.



### **7.3 Future Work**

Some suggested steps to be taken in furthering the development of the proposed semi-active suspension system are:

- Expand the suspension system model to a half car model and a full vehicle model, to investigate the roll and pitch responses of the system.
- Further investigate the inverse model of MR damper and their effect on whole simulation process.
- Investigate the time delay effects of the variable damper on the actual system response.
- Verify the effectiveness of predetermined control systems in experiments using proposed control methods.

## REFERENCES

- [1] Anubi, O. M., D. R. Patel, and C. D. Crane III. "A new variable stiffness suspension system: passive case." *Mechanical Sciences* 4.1 139-151, 2013.
- [2] Rittenhouse, Jack DeVere. *American Horse-drawn Vehicles: Being a Collection of Two Hundred and Eighteen Pictures Showing One Hundred and Eighty-three American Vehicles, and Parts Thereof*. Bonanza Books, 1948.
- [3] Savaresi, Sergio M., et al. "Semi-active suspension control design for vehicles". Elsevier, 2010.
- [4] Fallah, Mohammad Saber. "New dynamic modeling and practical control design for MacPherson suspension system". Diss. Concordia University, 2010.
- [5] Gillespie T. D., "Fundamentals of vehicle dynamics", Society of Automotive Engineering, Inc., 1992.
- [6] Wong J. Y., "Theory of ground vehicles", Second edition, John Wiley & Sons, 1993.
- [7] Tora, G. "The active suspension of a cab in a heavy machine". INTECH Open Access Publisher, 2012.
- [8] Nariman-Zadeh, N., Salehpour, M., Jamali, A., & Haghgoo, "optimization of a five-degree of freedom vehicle vibration model using a multi-objective uniform-diversity genetic algorithm (MUGA)", *Engineering Applications of Artificial Intelligence*, 543–551, 2.
- [9] Jamali, A., Shams, H., & Fasihozaman, " multi-objective optimum design of vehicle-suspension system under random road excitations". *Multi body Dynamics*, 282- 293, 2014.
- [10] Conde, Esteban Chávez, et al. "Generalized PI control of active vehicle suspension systems with MATLAB." *Applications of MATLAB in Science and Engineering* 16, 2011.

- [11] J. W. Gravatt, "Magneto-rheological dampers for super-sport motorcycle applications," pp. 1–90, 2003.
- [12] Soliman, A. M. A., and M. M. S. Kaldas. "Semi-active suspension systems from research to mass-market—A review." *Journal of Low Frequency Noise, Vibration and Active Control*, 2019.
- [13] Della Santa, A., D. De Rossi, and A. Mazzoldi. "Characterization and modelling of a conducting polymer muscle-like linear actuator." *Smart Materials and Structures* 6.1 , 1997.
- [14] Shen, Y., Golnaraghi, M. F., & Heppler, G. R. "Semi-active vibration control schemes for suspension systems using magnetorheological dampers", *Journal of Vibration and Control*, Volume: 12 (1), pp 3-24, 2006.
- [15] L. Tianye, W. Zhongdong, T. M. Xiang, and Z. Wanling, "Study on Semi-active Secondary Suspension of Railway Vehicle," *International Conference on Transportation, Mechanical, and Electrical Engineering (TMEE)*, pp. 237–253, 2011.
- [16] Tan, CheeFai, Frank Delbressine, Wei Chen, and Matthias Rauterberg. "Subjective and objective measurements for comfortable truck drivers' seat." In *Proceedings of the Ninth International Symposium on Advanced Vehicle Control (AVEC 2008)*, pp. 851-856. 2008.
- [17] Zuo, L., and S. A. Nayfeh. "Low order continuous-time filters for approximation of the ISO 2631-1 human vibration sensitivity weightings." *Journal of sound and vibration* 265.2, 2003.
- [18] Y. Zhiqiang, Z. Baoan, Z. Jimin, and W. Chenhui, "Research on Semi-active Control of High-speed Railway Vehicle Based on Neural Network-PID Control," presented at the *Seventh International Conference on Natural Computation*, 2011.
- [19] Smyth, A., Masri, S., Kosmatopoulos, E., Chassiakos, A., & Caughey, T. "Development of adaptive modeling techniques for non-linear hysteretic systems ", *International Journal of Non-Linear Mechanics*, Volume: 37, pp 1435– 1451, 2002.
- [20] Winslow, W. M. Method and means for translating electrical impulses into mechanical force , U.S. Patent 2,417,850, 1947.

- [21] Jacob, Rabinow. "Magnetic fluid shock absorber." U.S. Patent No. 2,667,237. 26 Jan. 1954.
- [22] Sarkar, Chiranjit, and Harish Hirani. "Effect of particle size on shear stress of magnetorheological fluids." *Smart Science* 3.2 , pages: 65-73, 2015.
- [23] Weiss, K. D. & Nixon, D. A. "Viscoelastic properties of magneto- and electrorheological fluids" , *Journal of Intelligent Material Systems and Structures*, Volume: 5, pp 772-775, 1994..
- [24] Palagi, Stefano, et al. "Micro-and nanorobots in Newtonian and biological viscoelastic fluids." *Microbiorobotics*. Elsevier, pages: 133-162, 2017.
- [25] Fernando, D., Goncalves, J. H. K., & Mehdi, A. "A review of the state of the art in magnetorheological fluid technologies – Part I: MR fluid and MR fluid models", the *Shock and Vibration Digest*, Volume: 38, (3), pp 203–219, 2006..
- [26] Abu-Khudhair, Aws, Radu Muresan, and Simon X. Yang. "Fuzzy control of semi-active automotive suspensions." 2009 International Conference on Mechatronics and Automation. IEEE, 2009.
- [27] Wang, J. & Meng, G. "Magnetorheological fluid devices: principles, characteristics and applications in mechanical engineering", *Proceedings of the Institution of Mechanical Engineers; Part B; Journal of Engineering Manufacture* Volume: 215 (3) pp 165- 174,.
- [28] Lord Corporation Website <http://www.lord.com>.
- [29] Carlson J. D., Catanzarite, D. M., & Clair, K. A. "Commercial magnetorheological fluid devices ", *Proceedings of the 5th International Conference on ER Fluids, MR Fluids and Associated Technology*, Sheffield, UK. Vo. 10, 1995.
- [30] Dyke, S. J. "Acceleration feedback control strategies for active and semi-active control systems: modeling, algorithm development, and experimental verification", PhD Thesis, Department of Civil and Geological Sciences, Notre Dame, Indiana, 1996.

- [31] Marin, L., Nicolae, C. P., Cornel, V., & Ladislau, N. V." Investigations of a magnetorheological fluid damper", IEEE Transactions on Magnetics, Volume: 40, (2), pp 469-472, 2004.
- [32] Choi, S. B., Nam, M. H., & Lee, B. K. "Vibration control of a MR seat damper for commercial vehicles", Journal of Intelligent Material Systems and Structures, Vol. 11 (12), pp 936-944, 2000.
- [33] Yu, M., Dong, X. M., Choi, B. S., & Liao, C. R. "Human simulated intelligent control of vehicle suspension system with MR dampers", Journal of Sound and Vibration, Volume: 319 (3-5), pp 753-767,2009.
- [34] Lee, H. S. & Choi, B. S. "Control and response characteristics of a magnetorheological fluid damper for passenger vehicles", Intelligent Material Systems and Structures, Volume: 11, pp 80-87, 2000.
- [35] Karnopp, D., Crosby, M. J., & Harwood, R. A. "Vibration control using semi- active force generators". ASME Journal, Vol. 96, No. 2, pp. 619-626, 1974.
- [36] Gordon, T. J. "Non-linear optimal control of a semi-active vehicle suspension system", Chaos, Solutions And Fractals, Vol. 5, No. 9, pp. 1603-1617, 1995.
- [37] Tudon-Martinez, Juan-C., Ricardo-A. Ramirez-Mendoza, and Ruben Morales-Menendez. "Control of Automotive Semi-Active MR Suspensions for In-Wheel Electric Vehicles.", 2011.
- [38] Zhang Y. and Alleyne A., "A practical and effective approach to active suspension control", Journal of Vehicle System Dynamics, 43(5), 305-330. 80, 2005.
- [39] Savaresi, Sergio M., Sergio Bittanti, and Mauro Montiglio. "Identification of semi-physical and black-box non-linear models: the case of MR-dampers for vehicles control." Automatica 41.1, pp:113-127, 2005.
- [40] R. M. Goodall, S. Bruni, and T. X. Mei, "Concepts and prospects for actively controlled railway running gear," Vehicle System Dynamics, vol. 44, pp. 60-70, 2006.

- [41] R. Goodall, "Active Railway Suspensions: Implementation Status and Technological Trends," *Vehicle System Dynamics*, vol. 28, pp. 87-117, 1997.
- [42] S. Sun, H. Deng, W. Li, H. Du, Y. Q. Ni, J. Zhang, et al., "Improving the critical speeds of high-speed trains using magnetorheological technology," *Smart Materials and Structures*, vol. 22, p. 115012, 2013.
- [43] Y. Liu, "Semi-active damping control for vibration isolation of base disturbances," PhD thesis, University of Southampton, Southampton, 2004.
- [44] H. Li and R. Goodall, "Distinguishing between Random and Deterministic Track Inputs for Active Railway Suspensions," *Vehicle System Dynamics*, vol. 29, pp. 772-777, 1998.
- [45] Keith D. Weiss, J. David Carlson, Donald A. Nixon, "Visco elastic Properties of Magneto- and Electro-Rheological Fluids," p. 1, 1994.
- [46] R. S. J. & S. N. Stanway, "Non-linear modeling of an electrorheological vibration damper," *Journal of Electrostatics*, vol. 20(2), pp. 167-184, 1987.
- [47] D. S. Pour and S. Behbahani, "Semi-active fuzzy control of machine tool chatter vibration using smart MR dampers," *International Journal of Advanced Manufacturing Technology*, vol. 83, pp. 421-428, 2016.
- [48] T. Smyth, et al., "Development of adaptive modeling techniques for non-linear hysteresis systems," *Journal of Non-linear Mechanics*, vol. 37, pp. 1435- 1451, 2002.
- [49] Shames, I. H., and Cozzarelli, F. A. "Elastic and inelastic stress analysis. Prentice-Hall", Inc., Englewood Cliffs, N.J, 1992.
- [50] Jesus Lozoya-Santos, Jorge, et al. "Hysteresis Modelling for a MR Damper." 7th EUROSIM Congress on Modelling and Simulation (EUROSIM 2010), 2010.
- [51] Spencer Jr, BrnF, et al. "Phenomenological model for magnetorheological dampers." *Journal of engineering mechanics* 123.3 ; 230-238, 1997.

- [52] Al-Holou, Nizar, Dae Sung Joo, and Adnan Shaout. "The development of fuzzy logic based controller for semi-active suspension system." Proceedings of 1994 37th Midwest Symposium on Circuits and Systems. Vol. 2. IEEE, 1994..
- [53] Titli, A., and S. Roukieh. "Design of Active and Semi Active Automotive Suspension Using Fuzzy Logic." In Proceedings of the 12. Triennial World Congress of the International Federation of Automatic Control, vol. 3, pp. 73-77, 2015.
- [54] Jain, Saransh, Shubham Saboo, Catalin Iulian Pruncu, and Deepak Rajendra Unune. "Performance investigation of integrated model of quarter car semi-active seat suspension with human model." Applied Sciences 10, no. 9, pp: 3185, 2020.
- [55] J. Sun and Y. Sun, "Comparative study on control strategy of active suspension system," in Measuring Technology and Mechatronics Automation (ICMTMA), Third International Conference on, vol. 1. IEEE, 2011, pp. 729–732, 2011.
- [56] International Organization for Standardization, et al. Mechanical Vibration--Road Surface Profiles--Reporting of Measured Data. Vol. 8608. International Organization for Standardization, 1995.
- [57] S. S. Rao and F. F. Yap, Mechanical vibrations. Prentice Hall Upper Saddle River, vol 4, 2011.
- [58] A. Aldair and W. Wang, "Design an intelligent controller for full vehicle nonlinear active suspension systems," International journal on smart sensing and intelligent systems, vol. 4, no. 2, pp. 224–243, 2011.
- [59] Biglarbegian, Mohammad, William Melek, and Farid Golnaraghi. "A novel neuro-fuzzy controller to enhance the performance of vehicle semi-active suspension systems." Vehicle System Dynamics 46.8, 2008.
- [60] Anand, Raj R., Saurabh Shrivastava, and M. W. Trikande. "Modelling and analysis of skyhook and fuzzy logic controls in semi-active suspension system." 2015 International Conference on Industrial Instrumentation and Control (ICIC). IEEE, 2015.

- [61] Múčka, Peter. "Simulated road profiles according to ISO 8608 in vibration analysis." *Journal of Testing and Evaluation* 46.1, 2017.
- [62] Gysen, B. L. J., Paulides J. J. H., Janssen, J. L. G., & Lomonova, E. A, "Active electromagnetic suspension system for improved vehicle dynamics:", *IEEE Vehicle Power and Propulsion Conference*, 2008.
- [63] Nguyen, Sy Dzung, Quoc Hung Nguyen, and Seung-Bok Choi. "A hybrid clustering based fuzzy structure for vibration control–Part 2: An application to semi-active vehicle seat-suspension system." *Mechanical systems and signal processing* , vol. 56, pp: 288-301.
- [64] Eneh, Princewill Chigozie, and Innocent Ifeanyichukwu Eneh. "MODELING OF AN ACTIVE SUSPENSION SYSTEM USING STATE SPACE APPROACH.",*International Journal of Engineering and Scientific Research*, volume 3, issue 11, 2019.
- [65] Heidarian, Alireza, and Xu Wang. "Review on seat suspension system technology development." *Applied Sciences* 9.14, 2019.
- [66] Rao, K. Dhananjay, and Shambhu Kumar. "Modeling and simulation of quarter car semi active suspension system using LQR controller." *Proceedings of the 3rd International Conference on Frontiers of Intelligent Computing: Theory and Applications (FICTA)*, 2015.
- [67] Mantaras, Daniel A., and Pablo Luque. "Ride comfort performance of different active suspension systems." *International Journal of Vehicle Design*, vol: 40 ,pp:106-125, 2006.



## VITA AUCTORIS

NAME: Behnam Riazi

PLACE OF BIRTH: Tehran, Iran

YEAR OF BIRTH: 1985

EDUCATION: Sharif University, B.Sc., Tehran, Iran, 2010

University of Windsor, M.Sc., Windsor, ON, 2021